CREEP-RUPTURE AND FATIGUE BEHAVIORS OF NOTCHED OXIDE/OXIDE CERAMIC MATRIX COMPOSITE AT ELEVATED TEMPERATURE

THESIS

Mark A. Sullivan, Captain, USAF

AFIT/GAE/ENY/06-M30

DEPARTMENT OF THE AIR FORCE
AIR UNIVERSITY

AIR FORCE INSTITUTE OF TECHNOLOGY

Wright-Patterson Air Force Base, Ohio

AFIT/GAE/ENY/06-M30

**CREEP-RUPTURE AND FATIGUE BEHAVIORS OF
NOTCHED OXIDE/OXIDE CERAMIC MATRIX COMPOSITE
AT ELEVATED TEMPERATURE**

THESIS

Presented to the Faculty

Department of Aeronautical and Astronautical Engineering

Graduate School of Engineering and Management

Air Force Institute of Technology

Air University

Air Education and Training Command

In Partial Fulfillment of the Requirements for the

Degree of Master of Science in Aeronautical Engineering

Mark A. Sullivan, BS

Captain, USAF

March 2006

APPROVED FOR PUBLIC RELEASE; DISTRIBUTION UNLIMITED.

AFIT/GAE/ENY/06-M30

CREEP-RUPTURE AND FATIGUE BEHAVIORS OF NOTCHED OXIDE/OXIDE CERAMIC MATRIX COMPOSITE AT ELEVATED TEMPERATURE

Mark A. Sullivan, BS
Captain, USAF

Approved:

/signed/

_____   _____
Dr. Shankar Mall (Chairman)   date

/signed/

_____   _____
Dr. Vinod Jain (Member)   date

/signed/

_____   _____
Dr. Theodore Nicholas (Member)   date

AFIT/GAE/ENY/06-M30

Abstract

    Oxide/oxide composites are being considered for use in high temperature
aerospace applications where their inherent resistance to oxidation provides for better
long-life properties at elevated temperature than most other ceramic matrix composites
(CMCs). One promising oxide/oxide CMC is Nextel™720/Alumina (N720/A) which
uses an 8-harness satin weave (8HSW) of Nextel™720 fibers embedded in a porous
alumina matrix. Previous research has shown N720/A to have excellent fatigue and
creep-rupture properties in 1200°C air.

    Possible aerospace applications for N720/A will likely require inserting holes into
the material for mounting and cooling purposes. The notch characteristics must be
understood to ensure designs using the material are sufficient for the desired application.
This research effort examined the fatigue and creep-rupture characteristics of N720/A
with a 0°/90° fiber orientation and notch to width ratio (2a/w) of 0.33. Specifically, 12.0
mm wide rectangular specimens with a 4.0 mm center hole were subjected to axial
fatigue and creep-rupture loads in 1200°C laboratory air environment. Monotonic tensile
tests at 1200°C were performed on notched and unnotched specimens to provide a
baseline for comparison with previous research. Fracture surfaces were examined under
microscope to observe microstructure and damage mechanisms. Comparisons to
previous unnotched research at 1200°C show N720/A to be primarily insensitive to the
notch under monotonic and creep loading conditions. Fatigue loading with maximum
stress equal to 88% the ultimate tensile strength (UTS) caused large reduction in fatigue
life to 8 cycles, though all other fatigue tests loaded at or below 80% of UTS showed
fatigue lives exceeding 300,000 cycles.

Acknowledgments

  I would like to express my sincere appreciation to my faculty advisor, Dr. Shankar Mall for his guidance and support throughout the course of this thesis effort. I am also grateful to Barry Page and fellow student, Captain John Mehrmen, for their frequent assistance with the test equipment. And most importantly I wish to thank my parents and sister for their love and support.

        Mark A. Sullivan

Table of Contents

List of Figures

List of Tables

CREEP-RUPTURE AND FATIGUE BEHAVIORS OF

NOTCHED OXIDE/OXIDE CERAMIC MATRIX COMPOSITE

AT ELEVATED TEMPERATURE

I.   Introduction and Background

During the 20th century rapid advancements were made in the field of composites.

By the 1950s new composite technologies were applied to the aerospace industry in the

form of filament winding in missile applications. Since then the high stiffness, high-

strength, and low-density of composite materials has lead to ever increasing use in

aerospace structures, with the recently designed Boeing 787 being roughly 50%

composite material by weight [12:2-3].

1.1 Propulsion Advancements

This same period also marked tremendous advancements in aircraft propulsion,

starting with the development of one of the first jet engines by Frank Whittle in the late

1930s. Improvements in engine technology would find turbine inlet temperatures

increasing from 600°C in Whittle's engine to over 900°C by the 1970s thanks to the

advent of metallic superalloys [8:66]. Increased operating temperatures are desired as

they result in greater engine efficiency [4:1755; 28:137; 29:275]. Later increases of

turbine inlet temperature would come from more than improved material properties, but

also from forced injection of cooling air along engine component surfaces. The injection of this air directly cools the metal and also creates a low temperature boundary layer that helps insulate the metal surface from the much hotter combustion temperatures [8:67]. In addition to superalloy improvements, computational fluid dynamic (CFD) modeling has allowed further increases in temperature through improved placement of cooling (effusion) holes. While use of cooling air allows temperature increases that improve efficiency, compressing the cooling air takes energy and can cause a net reduction in engine efficiency if overused. As such, it is still desirable to use the most heat tolerant materials available [28:253].

In the 1980's the US government began funding efforts to develop advanced ceramics as a follow-on material to the superalloys [34:31]. Figure 1 shows ceramics offer a temperature limit significantly greater than that of superalloys. While much effort has gone into researching basic ceramic properties and building demonstration components such as ceramic turbine blades, vanes, and combustor liners [21], ceramics have been incorporated into relatively few production engine applications [8:66; 34:1]. This slow acceptance is partly due to cooled superalloys being able to withstand ever increasing temperatures. Engine designers are also reluctant to switch from well characterized metals to a relative newcomer that has many undetermined qualities [34:36].
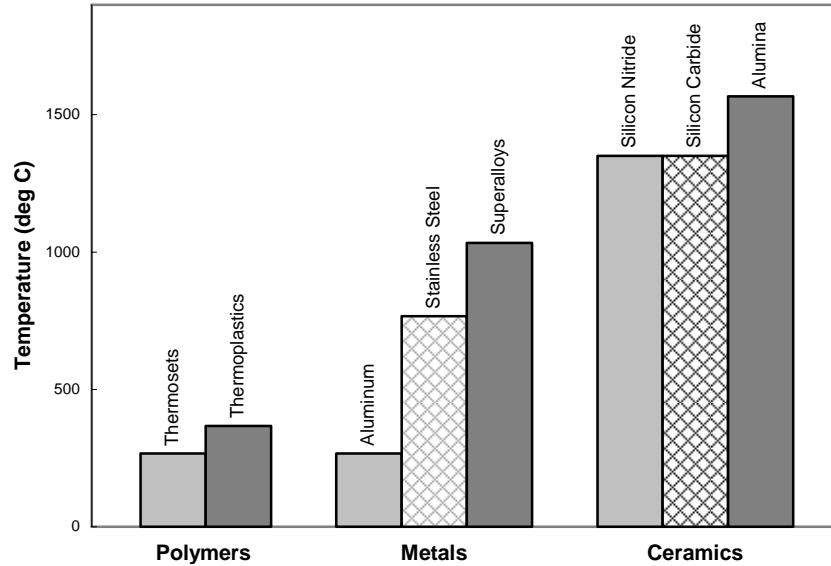
Figure 1. Service temperature limits for several monolithic materials [10:5]

1.2 Ceramic Matrix Composites

A significant amount of the high temperature ceramic research in the aerospace industry is directed toward ceramic matrix composites (CMCs). These composites use ceramic fibers embedded within a ceramic matrix to provide better toughness than monolithic ceramics [10:8]. This improvement comes from the ability of reinforcing fibers to deflect cracks in less harmful directions or to bridge across cracks while continuing to carry a load [12:102; 25:415]. Fiber/matrix debonding and fiber pullout in the wake of a crack exert a closing force that inhibits crack growth [10:315]. Without debonding the crack opening displacement would induce a large local strain on the fiber, often large enough to cause fiber failure. Debonding the fiber and matrix in the vicinity of the crack spreads strain from the crack opening displacement over a longer length of the fiber, decreasing the strain on the fiber.

3

Two methods are commonly used in CMCs to encourage fiber/matrix debonding. The first employs a fiber coating to weaken the bond between matrix and fibers. Examples of coatings include boron nitride (BN), carbon, and monazite ($LaPO_4$) [10:319; 27:8]. Another debonding method involves controlling matrix porosity so the matrix will fracture and release reinforcing fibers prior to fiber failure [3:565; 31].

1.2.1 Oxidation Concerns

Oxidation is a major problem for any material operating within the high temperature environment found within a jet engine. Composites containing carbon are particularly susceptible to this form of degradation. There are two main approaches to protection; the first is using inhibitors to slow the carbon-oxygen reaction rate, the second is to use barrier coatings to inhibit the ability of oxygen to reach the carbon [10:384]. A third alternative is to use fiber and matrix materials that are inherently oxidation resistant, as is the case with oxide/oxide CMCs such as N720/A.

1.2.2 Nextel™720/Alumina (N720/A)

The Nextel™720/A oxide/oxide composite characterized in this study was manufactured by Composite Optics, Inc. (COI) Ceramics of San Diego, California. In 1998 the company was awarded a Small Business Innovative Research (SBIR) contract by the Air Force Research Laboratories (AFRL) to use commercially available fibers to develop a low cost oxide/oxide composite capable of retaining 90% strength over a 100 hr loading at 1200°C [11].

COI's solution employed woven Nextel™720 fibers within a matrix composed entirely of alumina (N720/A) in place of the alumina-silicate matrix used previously

(N720/AS). Both forms of composite rely on porosity in the matrix to facilitate

fiber/matrix debonding in place of fiber coatings [3:5651; 11; 24:1561]. It is suspected

that between 1100°C and 1200°C the silicate in the N720/AS matrix begins sintering [31:

Sec 2, 27]. The coalescing silica grains decrease matrix porosity and reduce the ability of

the matrix to crack. This reduced ability to crack makes the aluminosilicate matrix less

capable of releasing fibers in high stress locations and is likely the reason residual

strength drops 40% following 100 hr exposure to 1100°C compared to residual strengths

following exposure to 1000°C for the same amount of time [11]. The pure alumina

matrix of N720/A remains comparatively stable at 1200°C, resulting in good fatigue and

creep properties at this increased temperature [14; 17].   Properties of the Nextel™720

fiber and alumina matrix are presented along with properties of other fiber and matrix

materials in Table 1 and Table 2.

Table 1. Properties of ceramic matrix materials [10:12]

Material	Density (g/cm^3)	Melting point $(°C)$	Young's Modulus (GPa)	Coefficient of Thermal Expansion $(10^{-6}/K)$	Fracture Toughness K_{1c} $(MPa\ m^{1/2})$
Al_2O_3	3.9	2050	380	7-8	1-3
SiC	3.2	—	420	4.5	2.2-3.4
Si_3N_4	3.1	—	310	3.1	2.5-3.5
MgO	3.6	2850	210	3.6	—
Mullite	3.2	1850	140	5.3	3.0-4.0
Borosilicate glass	2.3	—	60-70	3.5	0.5-2
Soda-lime glass	2.5	—	60-70	8.9	0.5-1

Table 2. Properties and composition of alumina based fibers [8:331]

Manufacturer	Trade mark	Diameter (μm)	Density (g/cm^3)	Strength (GPa)	Strain to Failure (%)	Young's Modulus (GPa)
α-Al$_2$O$_3$ fibers						
Du Pont de Nemours	FP	20	3.92	1.2	0.29	414
Mitsui Mining	Almax	10	3.6	1.02	0.3	344
3M	Nextel™610	10-12	3.75	1.9	0.5	370
Alumina silica fibers						
ICI	Saffil	1-5	3.2	2	0.67	300
Sumitomo	Altex	9 and 17	3.2	1.8	0.8	210
3M	Nextel™312	12-12 or 8-9	2.7	1.7	1.12	152
3M	Nextel™440	10-12	3.05	2.1	1.11	190
3M	Nextel™720	12	3.4	2.1	0.81	260

1.3 Notch Sensitivity

Possible applications for the N720/A CMC will most likely require the presence of mounting and effusion holes. The notch characteristics must be understood to ensure designs using the material are sufficient for the desired application.

The central notch ratio (2a/w) of 0.33 examined in this study has a theoretical elastic stress-concentration factor $K_t = \sigma_{tip}/\sigma_{net} \approx 2.3$, which assumes isotropic and homogenous material properties [30:746]. If the material has no means of redistributing stresses at the notch tip, this stress-concentration factor would result in critical crack growth occurring at 43% of the ultimate tensile strength (UTS). In ductile metals the material in the high stress region at the notch tip will instead deform plastically, redistributing stress to material further from the tip and allowing greater loads before

critical failure [13:289]. Brittle materials, such as ceramics, are unable to redistribute stress concentrations through plastic deformation, though some are instead able to redistribute stress through the formation of a dense region of non-critical microcracks ahead of the notch tip. This behavior is frequently seen in ceramic matrix composites including N720/AS [19:2820-2821; 20:1724-1725; 23:1565-1567; 24:3091]. Other brittle materials of lower fracture toughness, such as monolithic ceramics, are unable to redistribute stress concentrations and instead spawn a single critical crack that results in specimen fracture [10:296; 13:290].

Papers by Heredia et al. [19] and Mackin et al. [20] indicate notched composites with a brittle matrix typically suffer inelastic damage of the types shown in Figure 2. Extension of the matrix cracks formed during the manufacture of N720/A resulted in primarily class II behavior, with possible class I behavior occurring when net-section stresses approached tensile strength, which would have resulted in failure of higher stressed fibers near the hole. Kramb et al. analyzed damage progression in N610/AS, using ultrasonic C-scans to characterize damage regions in monotonically loaded notched specimens (not loaded to failure). Their results showed changes in temperature can impact the mode of damage formation, with class II behavior evident at room temperature and class I behavior evident at 950°C [23:1565,1568]. It appears the greater thermal stability of N720/A did not cause a similar change of damage mechanism during the course of this study.

Class I
Matrix Cracking + Fiber Failure

Class II
Matrix Cracking:
No Fiber Failure

Class III
Shear Damage by Matrix
Cracking

Pull-Out Tractions
Redistribute Stress

Matrix Cracks
Redistribute Stress

Shear Damage Zone
Redistribute Stress
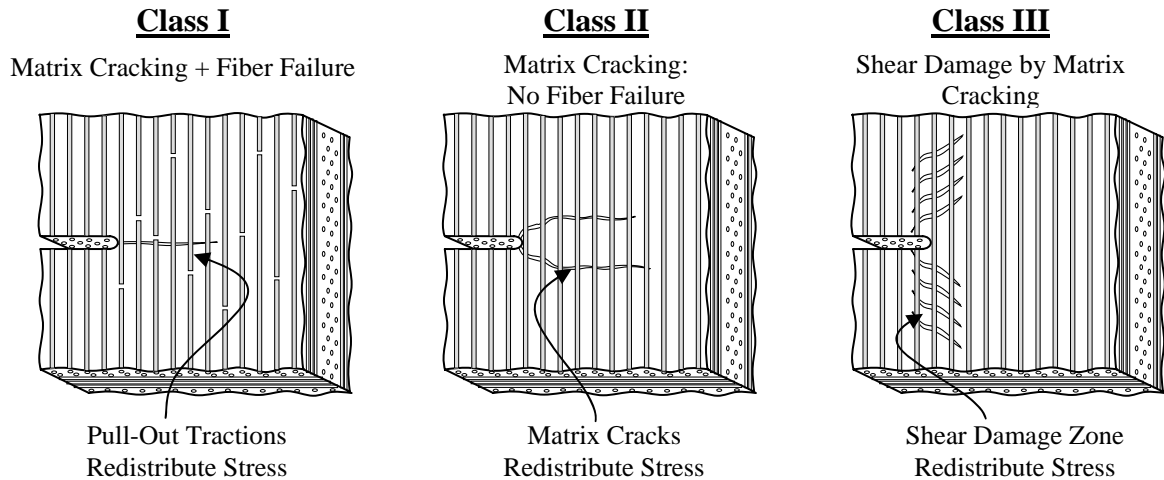
Figure 2. Three damage classes identified for ceramic matrix composites (CMCs) [19; 20]

1.4 Creep and Fatigue Loading

The desire to maximize turbine inlet temperature, increase engine life, and minimize weight forces engineers to push the limits of material properties when designing new components. Creep deformations become large enough to be a concern when a material is exposed to temperatures ranging between 30 and 60% of its melting temperature [13:706]. The Nextel™720/A composite consists of alumina and mullite and has an average melting temperature of ~1950°C (Table 1). This means N720/A is at ~64% of its melting temperature when heated to 1200°C, suggesting moderate increase in temperature beyond this point will result in unacceptably high creep, something which Harlan [17] confirmed during creep testing at 1330°C. Allowable creep strains for engine components are in the neighborhood of 1% over a 1000 hr life [26:289]. This corresponds to a creep rate of 2.8×10^{-9} (1/s) and would require limiting N720/A stresses to ~30 MPa based on the creep rate for N720/A at 1200°C as calculated by Harlan [17:58]. Musil's analysis of N610/Monazite/Alumina suggests temperature would have

to drop to nearly 1000°C to achieve the same creep life at 30 MPa [27:87]. Another study determined the creep rate of N720 fiber is 250 times less than the creep rate of N610 fiber when both are loaded to 170 MPa in 1100°C air [35:1011]. Clearly the combination of alumina and mullite in the N720 fibers outperforms the pure alumina N610 fibers when exposed to creep loads at elevated temperatures.

Situations of fatigue loading are found throughout turbine engines and can also cause significant amounts of damage. Flutter is a particularly destructive fatigue load that occurs when rotating parts reach an RPM corresponding to a natural frequency. The resulting high frequency vibrations (>1000 Hz) can lead to engine failure in a matter of minutes [26:285]. High cycle fatigue can also result from uneven airflow over a turbine face, causing rotating blades to be heavily loaded when passing through regions of dense air and lightly loaded when passing through regions of less dense air. Since a fan blade sweeps through these regions once per revolution, the blade will experience a variable loading at a frequency equal to the engine's rotational speed. In addition to high cycle fatigue, low cycle fatigue caused by changing throttle settings, aircraft maneuvering, and varying engine temperatures and associated thermal strains also have the capacity to cause fatigue damage. As with creep, N720/A has shown excellent fatigue properties during unnotched testing, but research is still needed to determine if the material performs equally well in the presence of notches.

1.5 Previous Work

Several studies have investigated the notch sensitivities of the Nextel™610/AS [23; 24] and Nextel™720/AS [3; 6; 7; 22] oxide/oxide composites. Kramb et al. found N610/AS to be very notch sensitive at 950°C, with a notched section strength only 35% that of an unnotched specimen at roughly the same temperature [24:3095]. This significant notch sensitivity was attributed to minimal formation of matrix cracks within fiber tows at elevated temperature. John et al. analyzed the notch sensitivity of N720/AS at 1100°C, finding both large holes and 0.5 mm effusion holes to be insensitive to notches during tensile tests while creep tests of both geometries *did* show significant notch sensitivity [22:627]. Conversely, Buchannan et al. found little notch sensitivity of similarly sized effusion holes in N720/AS subjected to creep loads at 1100°C, though larger double notched geometries did reduce creep life relative to unnotched tests [7]. Buchanan et al. also tested monotonic notch sensitivities of N720/AS at 1100-1200°C, only finding slight notch sensitivities at temperatures of 1100°C and 1200°C [6]. No studies of notch sensitivity were found for N720/A.

The research of N720/A has thus far analyzed the creep and fatigue behaviors of unnotched specimens exposed to varying environmental conditions. Harlan [17] found N720/A to have good creep resistance when exposed to 1200°C lab air, though increasing temperature to 1330°C resulted in a 40x reduction in creep-rupture life. Exposure to steam also severely reduced the creep resistance of N720/A, with creep rupture lives 1/10th and 1/20th those of non-steam tests at 1200°C and 1330°C, respectively. Exposure to steam is a concern for turbine engines due to the humidity of environmental air and the production of water during combustion. Eber [14] analyzed the effect fatigue loading

had on N720/A when exposed to the same environmental conditions as those of Harlan's study. As with creep, excellent fatigue resistance was found for specimens exposed to 1200°C lab air. These specimens achieved run-out of 100,000+ cycles under all loadings, with maximum stress ranging from 100 MPa to 170MPa. Increasing temperature to 1330°C reduced fatigue life significantly, with the 100 MPa fatigue loading resulting in a much shorter fatigue life of 1,500 cycles. The presence of steam further reduced fatigue life for both elevated temperatures, with maximum fatigue stress of 100 MPa causing failure after a mere 350 cycles in the 1330°C steam environment.

1.6 Objective

This study examined the sensitivity of N720/A to a centrally located circular notch of ratio 0.33 (2a/w) when exposed to monotonic, creep, and fatigue loadings in 1200°C air. Unnotched monotonic tensile tests at 1200°C were performed to provide a baseline for comparison with previous research on unnotched N720/A specimens, using the same constant actuator displacement rate of 0.05 mm/s. Creep and fatigue tests were then performed on notched specimens and compared to unnotched results of earlier research to identify changes in behavior caused by the notch presence. As with monotonic testing, tests of notched specimens used the same parameters as previous unnotched tests, with initial loading of creep specimens occurring at 25 MPa/s up to the desired creep load and fatigue specimens being exposed to a 1.0 Hz sinusoidal load with a 0.05 stress ratio $\left(R = \sigma_{min}/\sigma_{max}\right)$.

II.   Material and Specimen

This chapter describes the material properties of the Nextel™720/A ceramic matrix composite (CMC) investigated in this study. The following section will cover particulars on the specimen geometries tested.

2.1. Material Description

As stated in the introduction, the Nextel™720/A plate used in this study was manufactured by Composite Optics, Inc. (COI) Ceramics of San Diego, California. COI Ceramics uses the same general sol-gel manufacturing process to make N720/A and N720/AS CMCs. Specifically, Nextel™720 eight harness satin weave (8HSW) fabric is prepregged in a viscous slurry and laid up with the desired fiber orientation of [0°/90°]. The lay-up is then cured at low temperature (less than 180°C) and pressure (less than 0.7 MPa), followed by a pressureless sinter at 1150°C that is halted when the composite reaches the desired density [11].

As with most sol-gel processes, this manufacturing process frequently produces macroporosity and matrix cracking [10:153; 31: Sec 2, 8, Sec 4,1-4]. Macroporosity results when the slurry is unable to fully infiltrate the woven fibers, while matrix cracking occurs during sintering [10:19]. The N720/A plate examined in this study showed both forms of defects, with macroporosity being visible in a side view of the

laminate shown in Figure 3 and fine matrix cracks visible in the top lamina shown in

Figure 4.
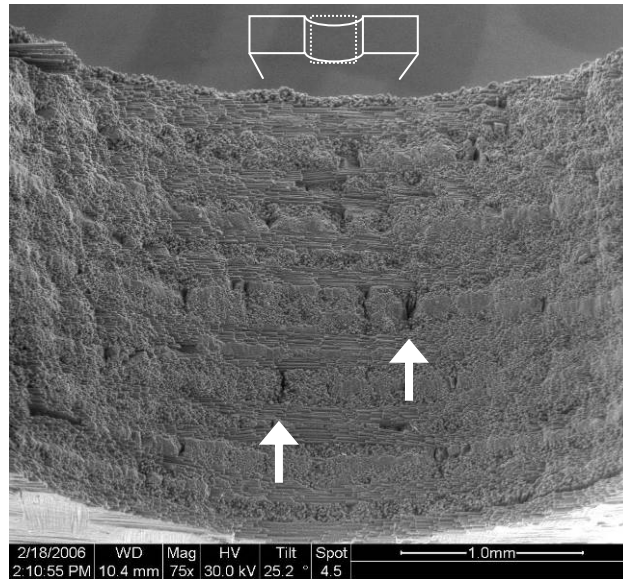
Figure 3. Surface condition of machined hole (inside view), visible macroporosity
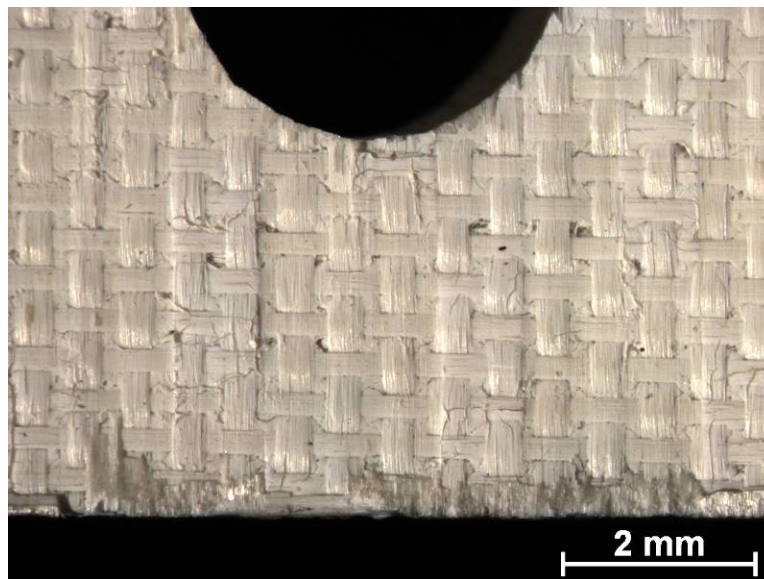
Figure 4. Surface condition of notched specimen; fine matrix cracks present

2.2. Specimen Geometry

Test specimens were machined from a single panel of N720/A (#WI4569), containing 12 plies of 8HSW fabric oriented at 0°/90° and having an approximate thickness of 2.8 mm. Values of porosity and fiber volume were approximately 24% and 44% respectively.

One specimen was cut into a dogbone shape for monotonic testing at 1200°C to determine the unnotched ultimate tensile strength of this plate. Comparison of these results with those of similar unnotched monotonic tests performed at 1200°C by Harlan and Eber [14; 17] will allow comparing notched creep and fatigue tests of this study with the unnotched creep and fatigue tests performed in their research.

Specimens were machined to lengths of approximately 150 mm to allow cutting two specimens from the width of 30.7 x 30.8 cm plate. A small amount of material around the perimeter of the plate was first trimmed away to remove uneven ply overlaps and heavier matrix cracking that occurred at the edges. In the grip region, both notched and unnotched specimens were 12.0 mm wide. A 50.0 mm radius was used to taper the dogbone specimen from the 12.0 mm width at the grips to the 8.0 mm width for the gage section, as shown in Figure 5. Length of the gage section was made 18.0 mm to allow room for extensometer rods with 12.7 mm spacing.

The notched specimen, also shown in Figure 5 was a simple rectangular shape with a centrally located 4.0 mm circular hole. This corresponds to a diameter to width ratio (2a/w) of 0.33. The patterned circles in each image indicate fiber tows are oriented in the 0° and 90° directions.
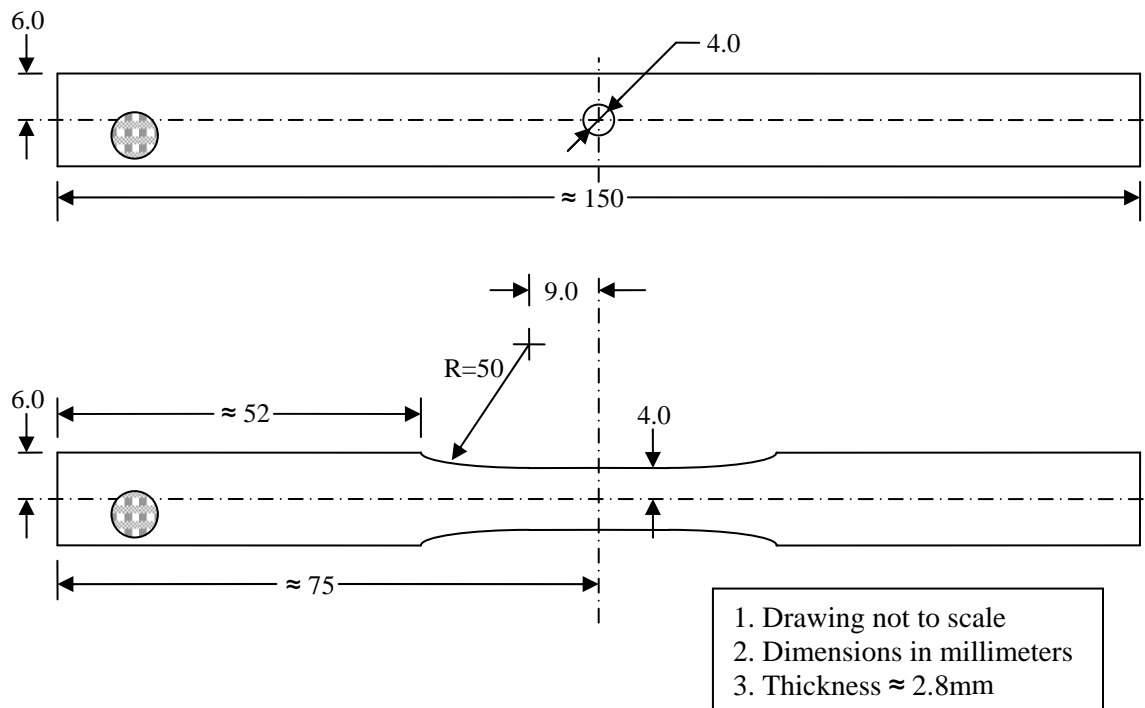
Figure 5. Geometry of centrally notched and dogbone specimens

1. Drawing not to scale
2. Dimensions in millimeters
3. Thickness ≈ 2.8mm

III. Experimental Equipment and Procedures

This section describes the equipment used to characterize the notched Nextel™720/A ceramic matrix composite. Details of test and post-test procedures are also described.

3.1 Equipment

The equipment used falls into three major categories: the mechanical test apparatus, the high temperature equipment, and the imaging devices.

3.1.1 Mechanical Test Apparatus

All tests were performed on the horizontally oriented Material Test Systems (MTS) Corporation axial servo-hydraulic machine shown in Figure 6. While this machine is rated for 25 kN (5600 lbs), testing never exceeded 4.5 kN (1000 lbs).
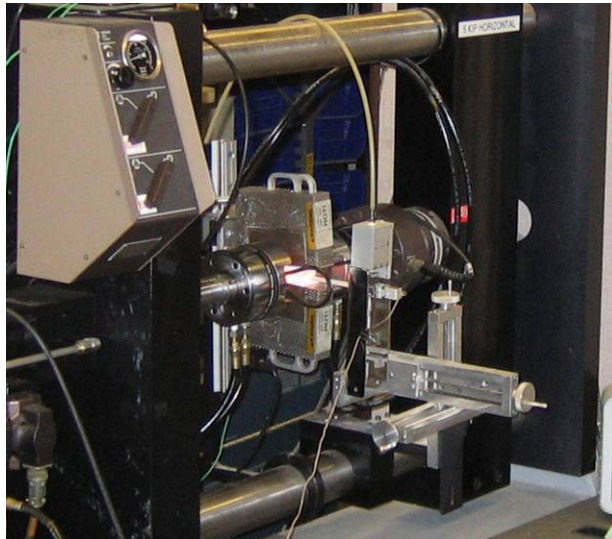
Figure 6. MTS servo-hydraulic machine (25 kN capacity)

Specimens were gripped by a pair of water-cooled MTS 647.02A Hydraulic Wedge Grips with a grip pressure of approximately 3 MPa (440 psi). Prior to testing, the grip alignment was verified using a strain gauged alignment fixture to ensure no bending or torsional forces were exerted on the specimens. Throughout testing A NESLAB HX-75 Recirculating Chiller pumped 15°C distilled water through the grips at a total rate of 20 gallons per hour. This kept the grips at a constant low temperature and prevented heat damage to the attached hardware.

During tests, both load and extension data were collected. An MTS model 661.20E-01 load cell with 25 kN capacity measured the axial load generated by the hydraulic piston. Extensometry data were measured with an MTS high temperature extensometer (model number 632.53E-14). Two 3.5 mm diameter ceramic rods with 12.7 mm (0.5 in) gage length and cone tips extended from the extensometer to the specimen. Spring tension held the extensometer and ceramic rods against the specimen. The extensometer assembly shown in Figure 7 includes a three axis positioning system, a heat shield, and a compressed air diffuser to lightly blow cooling air over the extensometer. While the extensometer is capable of measuring strains between +20 and -10%, the failure strain of N720/A is quite small and required setting the extensometer to its highest sensitivity range of ±5.0%. The extensometer calibration was verified prior to testing with a model 650.03 MTS Extensometer Calibrator.
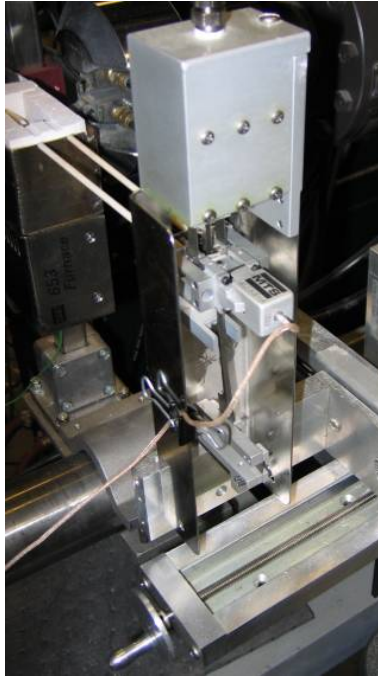
Figure 7. Extensometer assembly

Closed loop test control, signal conditioning, and data acquisition were performed by an MTS TestStar IIs Digital Controller connected to a personal computer running MTS Station Manager software (version 3.4B). The Multi Purpose TestWare feature was used to create programs controlling temperature, load, and data acquisition for monotonic, creep, and fatigue tests. The Basic TestWare feature was used to tune the servo control loop. While gripping a specimen, 1.0 Hz sinusoidal and step load commands were generated and control loop settings adjusted until actual loads closely matched the commanded loads.

3.1.2 High Temperature Equipment

Elevated temperature tests were conducted at 1200°C through the use of a 1150 Watt, single zone, Amteco Hot Rail Furnace (Figure 8) that exposed 15 mm of specimen to the desired temperature. The furnace consisted of two rail mounted halves,

each containing a silicon carbide heating element and an S-type thermocouple. Furnace insulation consisted of a removable fibrous alumina insert with carved gaps to provide room for the specimen and the extensometer rods to protrude when the two halves of the furnace closed together. Since larger specimens were previously used in this furnace, a gap of 1-2 millimeters existed between the insulation and the tested specimens. Left unfilled, this gap resulted in a 120°C temperature difference between the top and bottom of specimens. Placing high temperature cloth insulation in the gap before closing the furnace caused the temperature difference between specimen top and bottom to drop below 23°C, or in other form, ±0.8% of 1200°C.

Furnace temperature was controlled by a single zone MTS 409.83 Temperature Controller. The controller supplied power to both upper and lower heating elements equally, and received temperature feedback from an S-type thermocouple mounted in the upper half of the furnace. A thermocouple in the lower furnace half connected to a temperature display and was not part of the control loop.
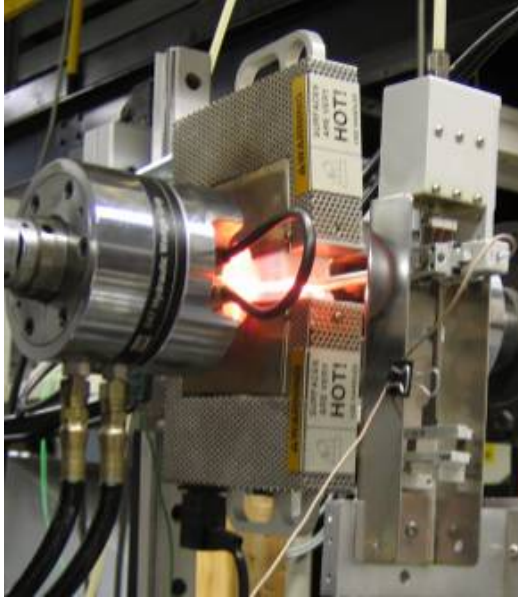
Figure 8. Amteco furnace assembly

Figure 9. Temperature controller

In preparation for calibrating the furnace chamber temperature, two Omega Engineering Inc P13R-015 0.38 mm diameter R-type thermocouples were attached to a notched test specimen. The leads were plugged into a dual input / dual display Omega HH202A Digital Thermometer. R-type thermocouples were chosen for their ability to operate accurately at high temperatures. As Figure 10 shows, a thermocouple was mounted off center on each side of the specimen. The offset allowed the thermocouple leads, running through ceramic insulators, to pass through the gaps in the furnace insulation meant for the extensometer. High temperature wire held the ceramic insulation to the specimen and Zircar Alumina Cement used to bond the thermocouple tips to the specimen surface. After drying several hours the temperature specimen was baked for an hour at 90-95°C to further remove moisture and cure the cement.
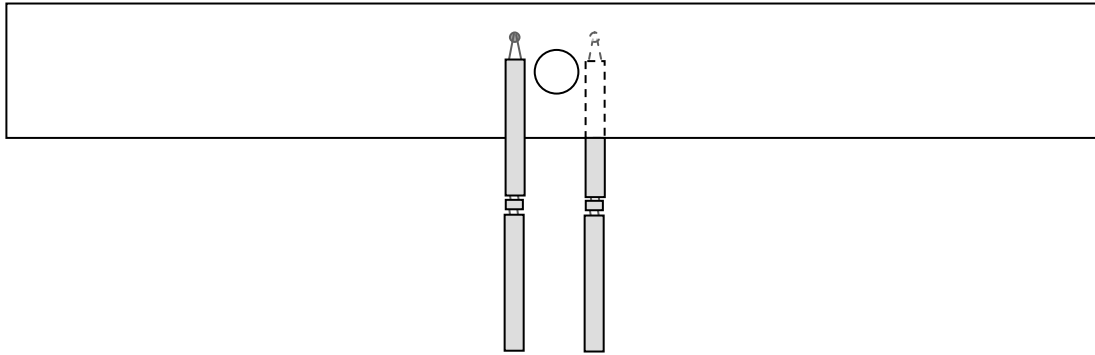
Figure 10. Schematic of temperature specimen (not to scale)

Furnace temperature was calibrated by placing the temperature specimen in the

grips with no load applied. The command temperature was ramped up at a rate of 1°C/s

while monitoring the temperature of the specimen. As the specimen neared 1200°C, the

temperature ramp was stopped to allow furnace and specimen temperatures to reach

equilibrium. The command temperature was then adjusted by small increments until the

average of top and bottom specimen temperatures equaled 1200°C. This command

temperature set point was recorded and used in following tests of specimens without

thermocouples. Periodically heating elements burned out and were replaced. The

furnace was recalibrated after all such replacements and at other times to ensure the set

point still produced the desired specimen temperature.

3.1.3 Imaging Equipment

Images of fracture surfaces were made using both an optical microscope and a

scanning electron microscope (SEM). The optical microscope was a Zeiss

Discovery.V12 with a Zeiss AxioCam HRc to capture images and the SEM used was a

FEI Quanta 200, shown respectively in Figure 11 and Figure 12.

Figure 11. Zeiss Discovery.V12 microscope

Figure 12. Quanta 200 SEM

The optical microscope was used to take low magnification images of the specimens before and after testing. Pre-test images were used to measure hole diameter and observe surface condition of the specimens. Post-test optical micrographs were also taken to record side views of the fracture surface and fiber pullout.

End views of fracture surfaces were made using the SEM. This particular type of SEM generates an image by scanning a primary electron beam in a raster fashion over the specimen and measuring the number of secondary electrons excited off the surface. Unfortunately, the poor conductivity of the ceramic specimens makes it difficult for electrons from the primary electron beam to travel to ground after impacting the specimen surface. This creates regions of charge buildup that deflect the electron beam and distort the image.

To work around this problem most images were taken using Environmental SEM (ESEM) mode. This mode works by introducing a small amount of water vapor to the

low pressure specimen chamber. As before, primary electrons excite secondary electrons off the specimen surface, only now the secondary electrons hit water molecules, which emit even more secondary electrons, repeating in a cascade fashion until the electrons are collected at the positively charged electron detector. The now positively charged water molecules are attracted to the negatively charged specimen surface where they neutralize any charge buildup.

An alternate method of reducing specimen charging is to coat the specimen with a conductive layer of carbon. The benefit of using a coated specimen in high vacuum mode (no water vapor) versus ESEM mode is that smaller regions can be imaged without creating a charge buildup, which allows for higher magnification.

A carbon coating was applied using the SPI-MODULE 11428 Carbon Coater. Specimens were inserted into a vacuum chamber along with a carbon thread held between two electrodes. After evacuating the chamber current was passed through the carbon thread to preheat it, followed by a pulse of current at higher voltage to vaporize the carbon and form a deposit over the specimen. Figure 13 shows a carbon coated specimen on the left and an uncoated specimen on the right. Prior to SEM imaging specimens were cut to a short length and fixed to a conductive base using carbon paint.
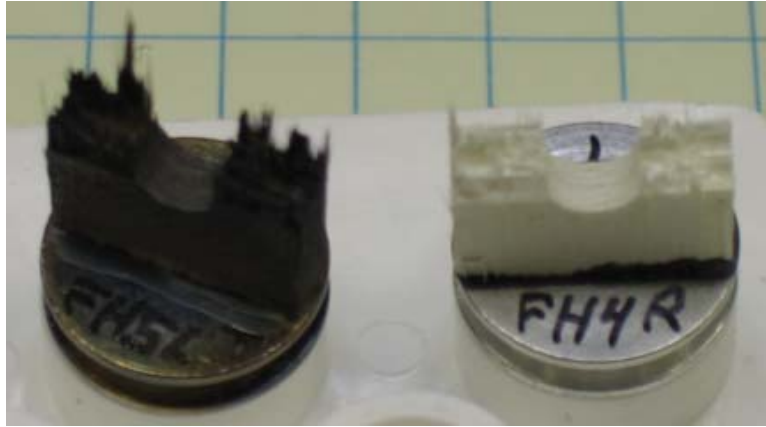
Figure 13. Carbon coated and uncoated fracture specimens

3.2 Test Procedures

Details about equipment preparation along with specific testing procedures for monotonic, creep, and fatigue tests are provided in the following section. After tests were complete, collected data were plotted and analyzed using the Microsoft Excel 2003 spreadsheet program.

3.2.1 Specimen Processing

Specimens were cut to shape on a CNC controlled water-jet cutter with abrasive particles added to the water. A thin sheet of Aluminum covered the upper surface of the composite to keep the water-jet from rounding off the upper corners. Once specimens were cut to their rectangular outer shape a 2.0 mm starter hole was mechanically drilled into the center. The specimens were then returned to the water-jet cutter to expand the started hole to the desired 4.0 mm.

When all cuts were complete, residual abrasive material and other particles remaining on the specimens were removed by an ultrasonic water bath. The specimens were then soaked for 20 minutes in alcohol to displace water that may have soaked into

the specimen. Finally, the specimens were heated in a 250°C oven for 60 minutes for further drying and then allowed to cool.

Tabs were applied to all specimens to minimize stress concentrations on the ceramic surface when gripped [9:45]. Tabs were cut to shape from a sheet of 1.6 mm thick glass-fabric/epoxy and bonded to the specimens using 3 drops of M-Bond 200 adhesive. Edges of the tabs were then filed to the same width as the underlying ceramic. This ensured specimens were not off angle when placed against the grip guides of the servo-hydraulic machine.

The gage region dimensions of each specimen were measured with a digital micrometer (Mitutoyo Solar, model CD-S6" CT). Width and thickness were each measured six times in the net-section region and averaged. Hole diameter was measured using a Zeiss Discovery.V12 optical microscope. The PlanS 1.0x lens was calibrated for distance measurement at two magnification levels. Specimens were then imaged, front and back, and hole diameter measured at the two zoom levels. The four diameter measurements were then averaged and, with the average thickness and width, used in Equation 1 to calculate the minimum cross-sectional area perpendicular to the axis of loading:

$$A = t \cdot (w - d) \tag{1}$$

Where t is *thickness*, w is *width*, and d is *hole diameter*. The net-section stress was then computed using:

$$\sigma_{net} = \frac{P}{A} \tag{2}$$

where *P* equals *axial load*. The net-section stress was based only on cross-sectional area and did not include any stress concentration factors.

3.2.2 Equipment Preparation and Specimen Loading

Before all tests the servo-hydraulic machine was warmed up to ensure hydraulic fluid, valves, and piston components were at a steady operating temperature. A function generator in the Basic TestWare control software was used to command a sinusoidal piston displacement with fully reversed magnitude of 2.5 mm at a frequency of 0.7 Hz for a minimum of 30 minutes. During this time the chiller was also powered on and cooling water allowed to flow to the grips.

Following warm-up, specimens were placed against the grip guides in the open grips and positioned to center the hole in the furnace. While in displacement control mode the right grip would be clamped followed by a switch to force control mode and prompt clamping of the left grip. The switch to force control mode reduced the compressive force exerted on the specimen as a result of the grips clamping.

Once gripped, the extensometer was positioned so the rods would be centered around the specimen hole and fine adjustments made until measured strain neared 0.1%. The spring tension would then be increased and strain zeroed in the Station Manager software.

The two halves of the furnace were then closed around the specimen and the test procedure set to execute. All test procedures at elevated temperature ramped to 1200°C over 25 minutes, followed by a 15 min dwell time to allow furnace and specimen to reach thermal equilibrium. At the conclusion of the dwell time, no-load strain data were collected for 1.0 sec and averaged to determine the thermal strain. This thermal strain

was then subtracted from strain measurements taken under load to determine the mechanical strain.

3.2.3 Monotonic Tension Tests

Monotonic tension tests were conducted in laboratory air at 1200°C for both notched and reduced gage section specimens (eg. dogbone). Both tests were performed in displacement control at a rate of 0.05 mm/sec. Measurements of time, displacement, load, strain, and temperature were recorded every 0.05 sec during the test.

3.2.4 Creep-Rupture Tests

Creep tests were performed only on notched specimens in 1200°C laboratory air. Specimens were loaded to the desired creep stress at a rate of 25 MPa/s, followed by a constant load at the desired creep stress up until specimen failure or runout of >500,000 sec. Time, displacement, load, strain, and temperature data were recorded every 0.05 sec when ramping to the creep stress, while times between recordings while at creep stress ranged from 0.25 sec to 15 sec. The sampling rates were varied so sufficient numbers of data points would be recorded for tests at high creep stress and short duration, while keeping data files a manageable size for low creep stress and long duration tests.

3.2.5 Fatigue Tests

Tension-tension fatigue tests were conducted only on notched specimens in 1200°C laboratory air subjected to a 1.0 Hz sinusoidal loading with a stress ratio of 0.05 $\left(R = \sigma_{\min}/\sigma_{\max}\right)$. PVC adaptive compensation was used to ensure applied loads very nearly matched the command loads. Fortunately the tuning of the servo-hydraulic machine was such that little compensation was needed. Figure 14 shows the measured

load very closely follows the command load even during the initial cycles before adaptive compensation has had time to make adjustments.
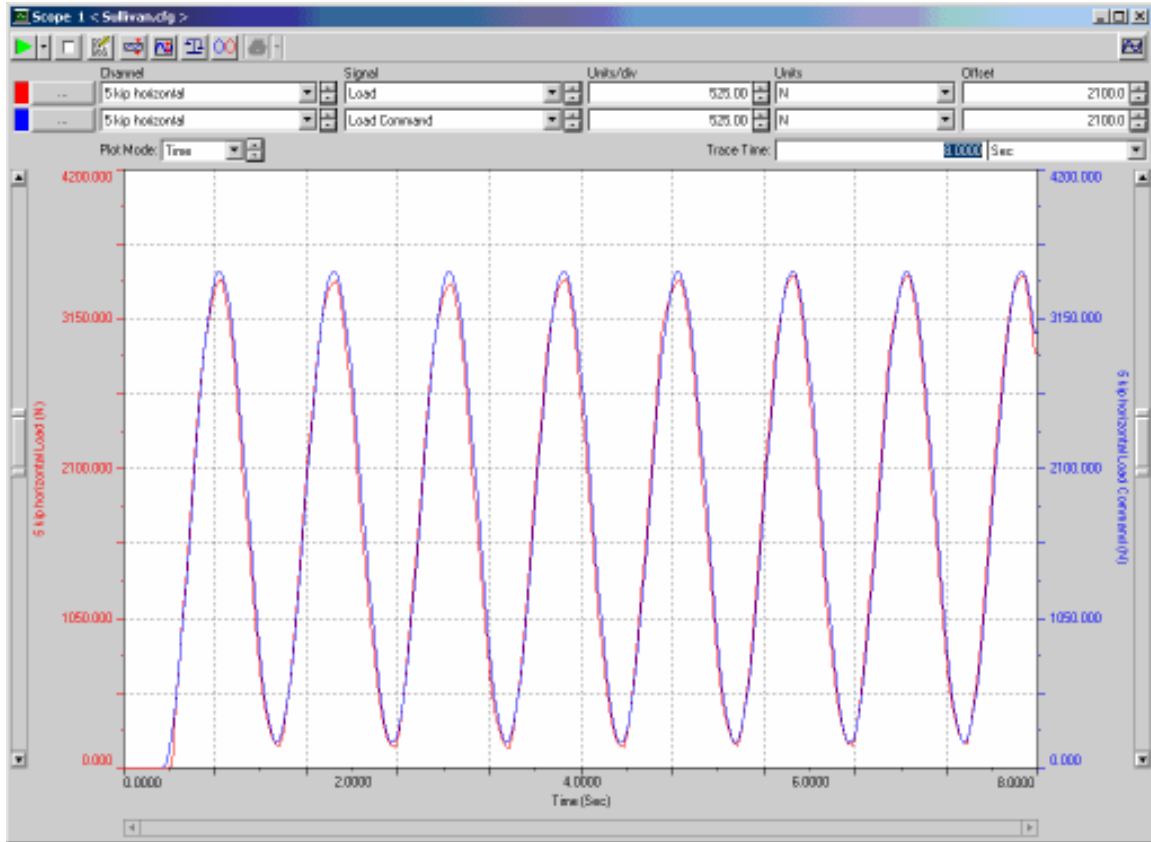
Figure 14. Measured load compared to command load at fatigue test start

Time, segment number (1 segment = ½ cycle), displacement, load, strain, and temperature data were recorded at the peak and valley of every cycle. The same information was also recorded at a rate of 200 Hz for cycles 1, 2, 5, 10, 20, 50, 100, 200, 500, 1000, 2000, 5000, 10000, 20000, 30000, 40000, 50000, 60000, 70000, 80000, 90000, 100000, 200000, 300000, 400000, and 500000. Fatigue run-out was defined as survival up to $5x10^5$ cycles.

3.3 Test Matrix

The following table summarizes all monotonic, creep, and fatigue tests performed

with the Nextel™720/A composite during this research effort.

Table 3. Test Matrix

Specimen Number	Type of Loading	Specimen Geometry	Temperature (°C)	Maximum Stress (MPa)
MS2	Monotonic	Unnotched	1200	200
MH1	Monotonic	Notched	1200	190
CH3	Creep	Notched	1200	100
CH1	Creep	Notched	1200	125
CH2	Creep	Notched	1200	150
CH5	Creep	Notched	1200	175
FH4	Fatigue	Notched	1200	150
FH6	Fatigue	Notched	1200	160
FH5	Fatigue	Notched	1200	175

IV. Results and Discussion

The following chapter presents the results of this investigation and discusses what impact a center notch has on the mechanical behavior of Nextel™720/A CMC at 1200°C. The results of notched monotonic tension tests, creep-rupture tests, and fatigue tests are compared to unnotched behavior under similar conditions as reported in previous research. Lastly, observations of the fracture surfaces are presented and analyzed.

4.1 Monotonic Tensile Tests

Monotonic tension tests were performed on unnotched (dogbone) and notched specimens at 1200°C, the results of which are summarized in Table 4. The unnotched ultimate tensile strength (UTS) of 200 MPa and failure strain of 0.35% closely match values of 192-218 MPa and 0.38-0.43% found in previous research efforts (Table 5).

Notched ultimate tensile strength, based on the net-section area at the hole, was 5% less than the unnotched UTS. Failure strains between notched and unnotched specimens cannot be compared directly as the strain measurements were produced by dividing the displacement of the extensometer rods by the gage length. Since the notched specimens deform unevenly over the gage length, with greater deformation near the hole, it is not surprising the notched failure strain appears less than for unnotched.

This characteristic of the strain measurement for notched specimens also makes it impossible to calculate the modulus of elasticity ($E = \Delta\sigma_{net} / \Delta\varepsilon$) since the net-section stress corresponds only to the minimum cross-section while strain is averaged over the

gage length containing the hole. Instead, net-section stress divided by strain will be

referred to as specimen stiffness ($S = \Delta\sigma_{net} / \Delta\varepsilon$).

Table 4. Summary of Monotonic Test Results at 1200°C

Specimen Number	Specimen Geometry	Stiffness (GPa)	Ultimate Tensile Strength (MPa)	Failure Strain (%)	Location of Failure
MS2	Unnotched	85	200.2	0.35	Just outside gage section at taper
MH1	Notched	93	189.6	0.30	Gage section, hole

Table 5. Unnotched Tensile Data Reported in Previous Studies

Source	Temperature (°C)	Elastic Modulus (GPa)	Ultimate Tensile Strength (MPa)	Failure Strain (%)
COI[1]	23	71.7	175.7	0.31
COI[1]	1200	76.1	218.7	0.43
Eber[2] / Harlan[3]	1200	74.7	192.2	0.38

Sources: Data from [1][11], [2][14:20], [3][17:40]

Stress-strain plots for typical continuous fiber-reinforced CMCs show linear

behavior up to a yield point when microcracks begin forming in the matrix [10:238-239].

The stress-strain curves plotted in Figure 15 show no such yield point since the matrix

already contains extensive microcracking due to the sol-gel manufacturing process. In

the unnotched specimens the pre-existing matrix cracks result in slightly nonlinear

stress-strain curves up to the point of failure as stable crack growth occurs under the

increasing load.

The notched specimen also exhibited slightly nonlinear behavior up to 175 MPa,

at which point the stress-strain curve hooked more noticeably down. This hook is most

likely a result of fiber fracture in the region of concentrated stress near the hole. As these

fibers break, the load they once carried is transferred by the matrix to lower stressed fibers further from the hole. This increased load on the remaining fibers causes increased strain, which accounts for the greater stiffness reduction just before failure [23:1567]. This behavior is analogous to necking that occurs in ductile metals, where plasticity results in reduced load carrying area and also results in a hooked stress-strain curve. This sort of relaxation is not apparent in the unnotched specimens since their longitudinal fibers are nearly equally loaded, meaning loads from fibers stressed to failure will transfer to neighboring fibers that are themselves on the verge of failing, meaning fewer fibers can fail before critical crack growth is achieved.

The initial stiffnesses found in this study (Table 4) and by Eber and Harlan (Table 5) were calculated from the slope of a best fit line through stress-strain data between the initial loading and the 35 MPa loading. The initial unnotched stiffness of 85 GPa found in this study exceeds the 75-76 GPa elastic modulus found in previous research. This increased stiffness might indicate lesser amounts of initial matrix cracking within the N720/A plate examined in this study, but could also result from other factors such as better alignment of the N720 fabric layups during manufacturing.
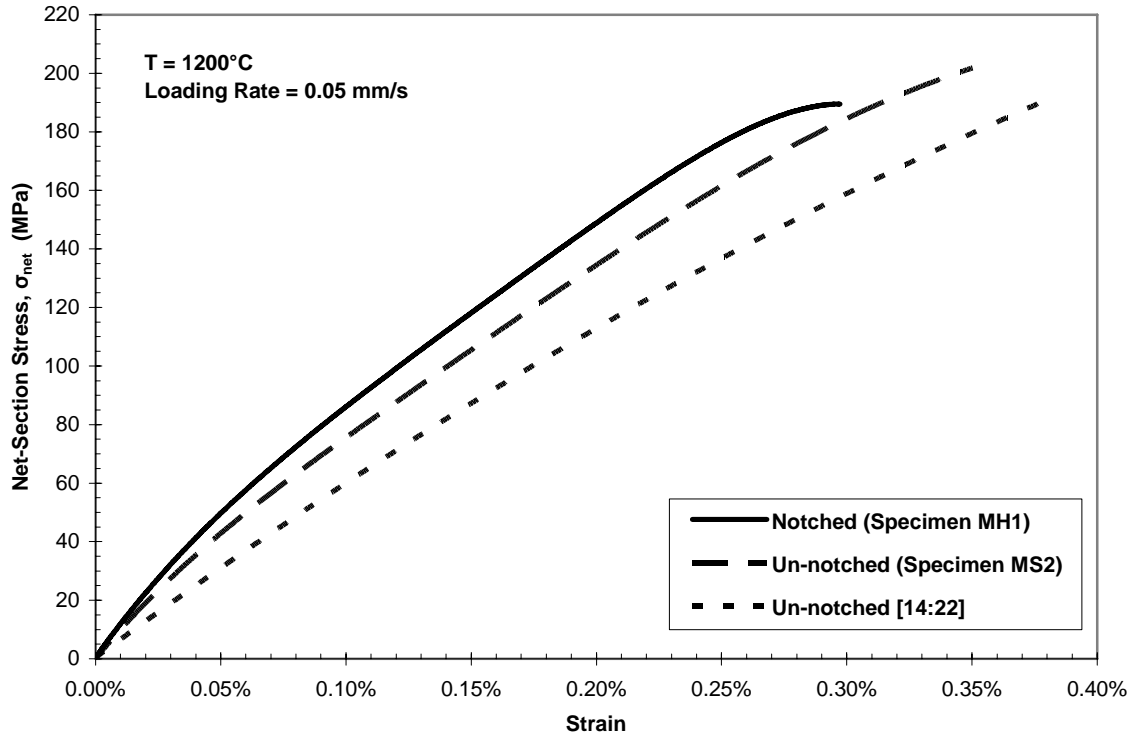
Figure 15. Tensile stress-strain curve for N720/A at 1200°C

Extensometer data was collected during the temperature ramp up for all tests. The thermal strain measured at the end of the temperature ramp was subtracted from strain values measured during testing to provide the mechanical strain. Thermal strain was also used to calculate coefficients of thermal expansion, for each specimen using the equation $\alpha_t = \varepsilon_t / \Delta T$, where ε_t is the *thermal strain* and ΔT is the *temperature difference* between room temperature and test temperature. The coefficients of thermal expansion listed in Table 6 vary little from the average value of $5.7 \times 10^{-6}/°C$ and compared closely to the coefficient of thermal expansion of $6.0 \times 10^{-6}/°C$ of a bare fiber [1:16].

Table 6. Thermal Expansion of Nextel™720/A between 23°C and 1200°C

Specimen Number	Specimen Geometry	Thermal Strain (%)	α_t (10^{-6}/°C)
MS2	Unnotched	0.658	5.60
MH1	Notched	0.705	5.99
CH3	Notched	0.670	5.69
CH1	Notched	0.665	5.65
CH2	Notched	0.671	5.70
CH5	Notched	0.665	5.65
FH4	Notched	0.679	5.77
FH6	Notched	0.655	5.57
FH5	Notched	0.659	5.60
		Average	5.69
		Standard Deviation	0.128

4.2 Creep-Rupture Tests

Creep-rupture tests were performed on notched specimens at 1200°C, at stress

levels of 100, 125, 150, and 175 MPa. Time to rupture and failure strain data are

presented in Table 7 along with creep-rupture data from previous research performed on

unnotched specimens. As mentioned for the monotonic test results, the strains measured

on the notched specimens represent the average strain over the gage length. Since a large

portion of the gage length is below the net-section stress, it is not surprising to find

failure strains over the notched gage length significantly lower than those values recorded

for unnotched.

The notched and unnotched geometries did exhibit similarities in failure strains

relative to monotonic failure strains in specimens of the same shape. The highest creep

stress values for notched and unnotched geometries produced failure strains much closer

to their respective monotonic failure strains than did lower creep stresses. At these lower

stresses, failure strains for notched creep specimens were 40% larger than the notched

34

monotonic failure strain, while unnotched geometries exhibited failure strains 8 times those of the monotonic tests.

Table 7. Creep Results at 1200°C

Specimen Number	Creep Stress		Strain at Failure (%)	Time to Rupture (sec)	Time to Rupture (hrs)	Location of Failure
	(MPa)	% UTS				
Notched (UTS = 190 MPa)						
CH3	100	53	>0.54	>847,575	>235.44	Runout
CH1	125	66	0.43	69,750	19.37	Gage section, hole
CH2	150	79	0.51	5,726	1.59	Gage section, hole
CH5	175	92	0.31	106	0.03	Gage section, hole
Unnotched[1] (UTS[2] = 192 MPa)						
14-1	80	42	1.11[3]	917,573	254.88	Gage section, near taper
7-2	100	52	3.04	147,597	41.00	Gage section, center
9-2	125	65	3.40	15,295	4.25	Gage section, center
5-2	154	80	0.58	968	0.27	Gage section, center

Sources: [1,2][17:47, 40]   Note: [3]Hydraulic system restart during this test may have contributed to failure.

The creep stress and rupture times plotted in Figure 16 suggest a constant logarithmic relation between stress and rupture time at stresses at and below 80% of the UTS. At similar creep stresses the notched geometry resulted in rupture lives 5 times greater than lives for unnotched geometry. An explanation is that notched specimens concentrate stress in the minimum cross sectional area, making any defects away from the hole grow cracks at a much slower rate due to lower stresses away from the net-section. The slower rate of growth reduces the likelihood these defects will reach critical crack length before cracks in the net-section reach critical length. Even distribution of

stress throughout unnotched specimens allows defects anywhere along the gage length to grow to critical values.
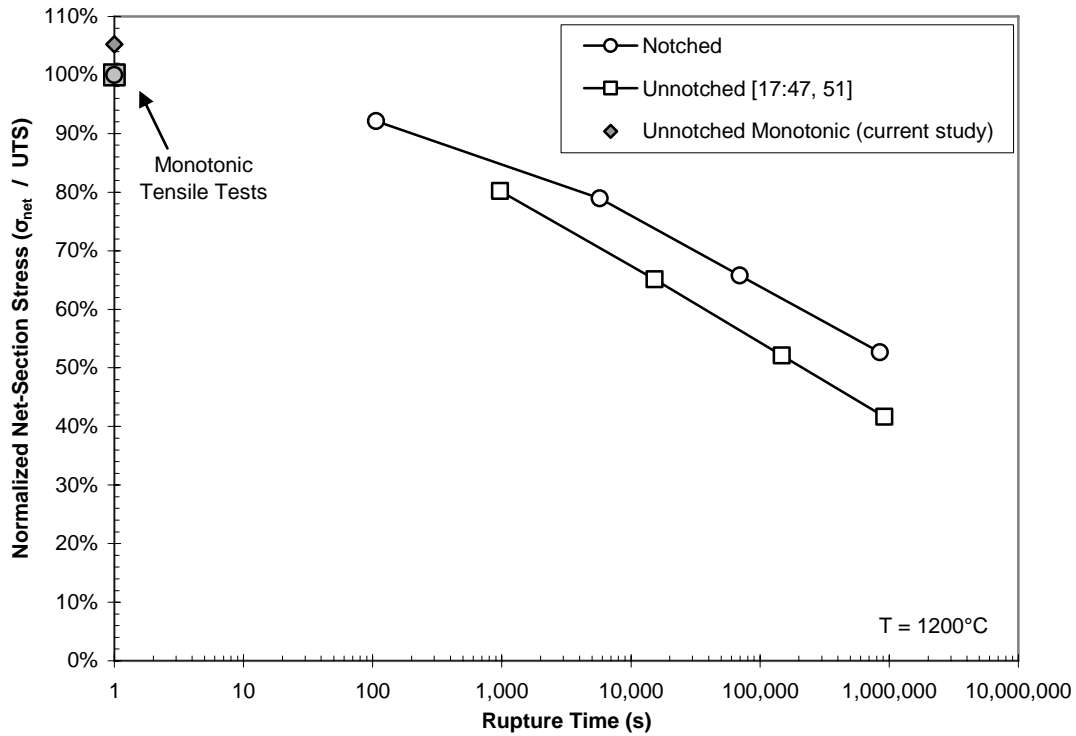

Figure 16. Creep stress vs. time to rupture for N720/A at 1200°C

The increase of creep strain as a function of time in the notched specimens is presented in Figure 17, Figure 18, Figure 19, and Figure 20. While each figure includes time-strain plots for all four notched stress levels, separate figures were used to allow adjustment of the timescale so regions of primary, secondary, and tertiary creep could be easily identified for each test.

When loaded to 100 MPa, notched N720/A exhibited both primary and secondary regions of strain increase, as apparent in Figure 17. Unexpected maintenance to the hydraulic system required halting and restarting this test mid run. Unfortunately the

strain gage exhibited slipping during the latter half of the test. Despite this slipping, it is apparent the secondary region extends to 800,000 s. However, it is impossible to determine whether or not tertiary strain growth occurred during the last period of the test.
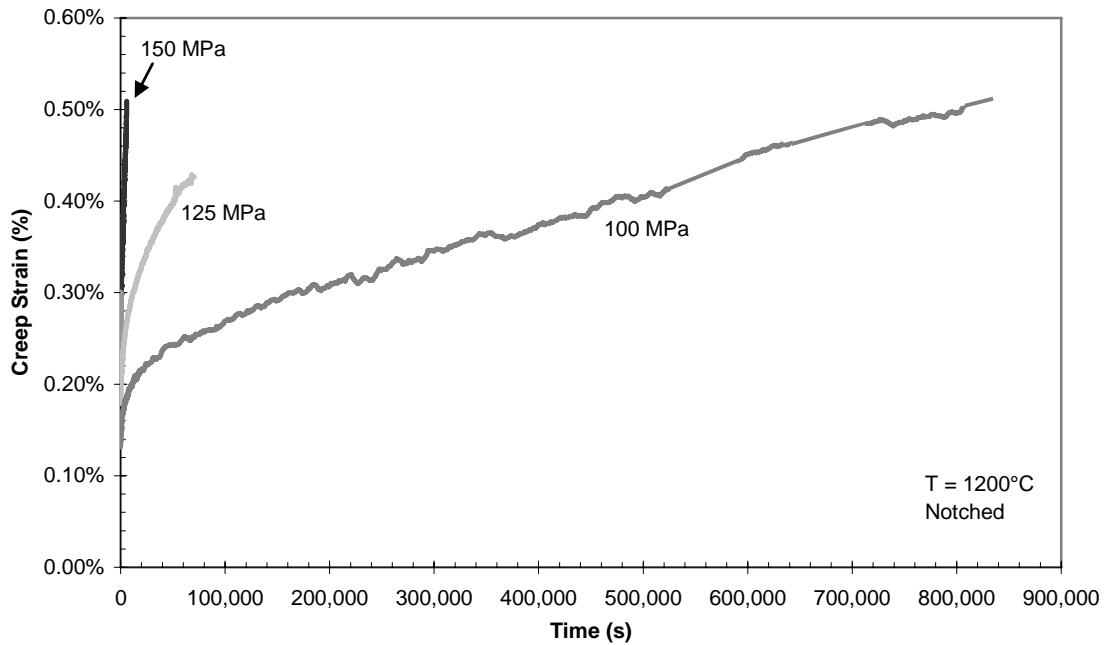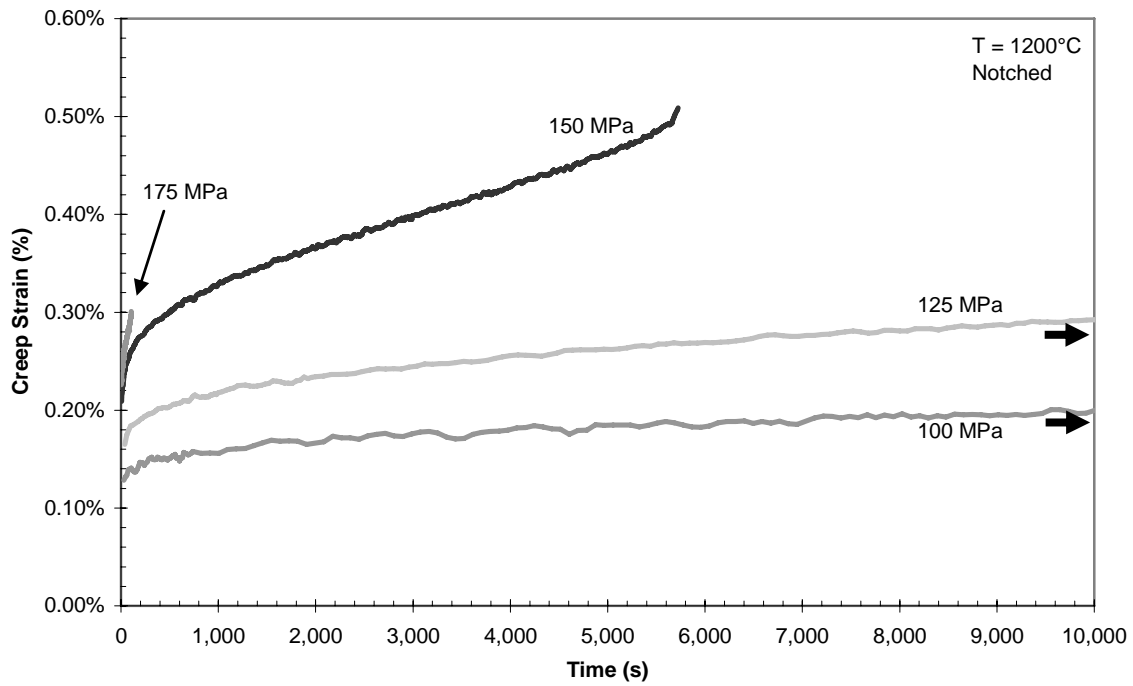

Figure 17. Creep strain vs. time for notched N720/A at 1200°C

The strain-time plot for 125 MPa is shown in Figure 18. In this case the curve appears to remain concave down up to failure, suggesting the specimen remained in the region of primary strain growth for the entire test. Calculation of creep rate was based on a linear curve fit of the last 10,000 seconds.
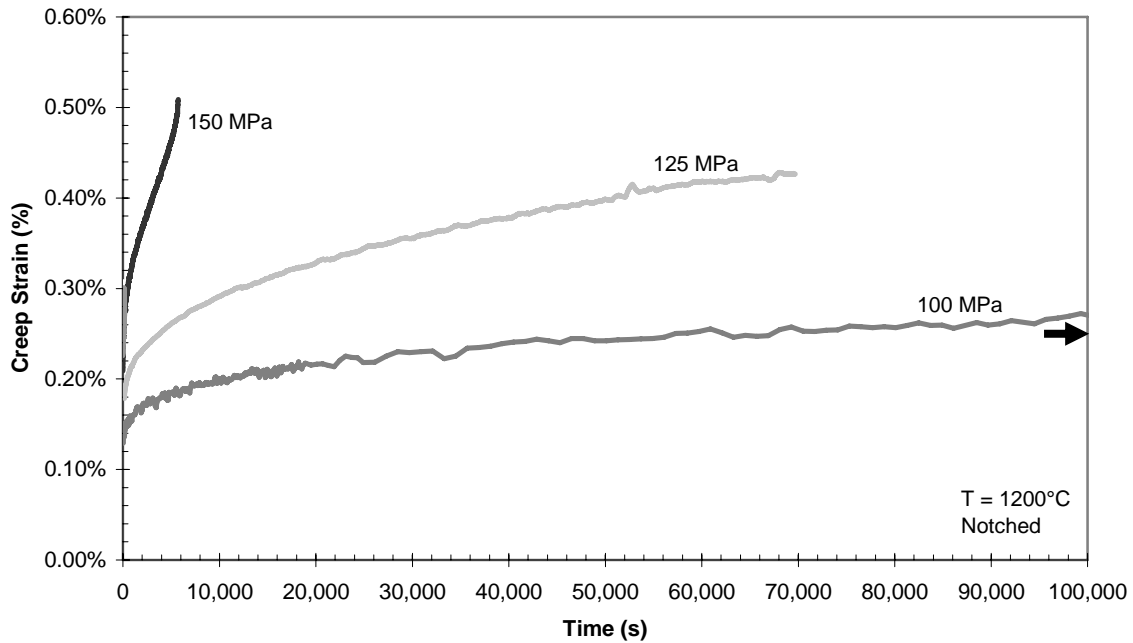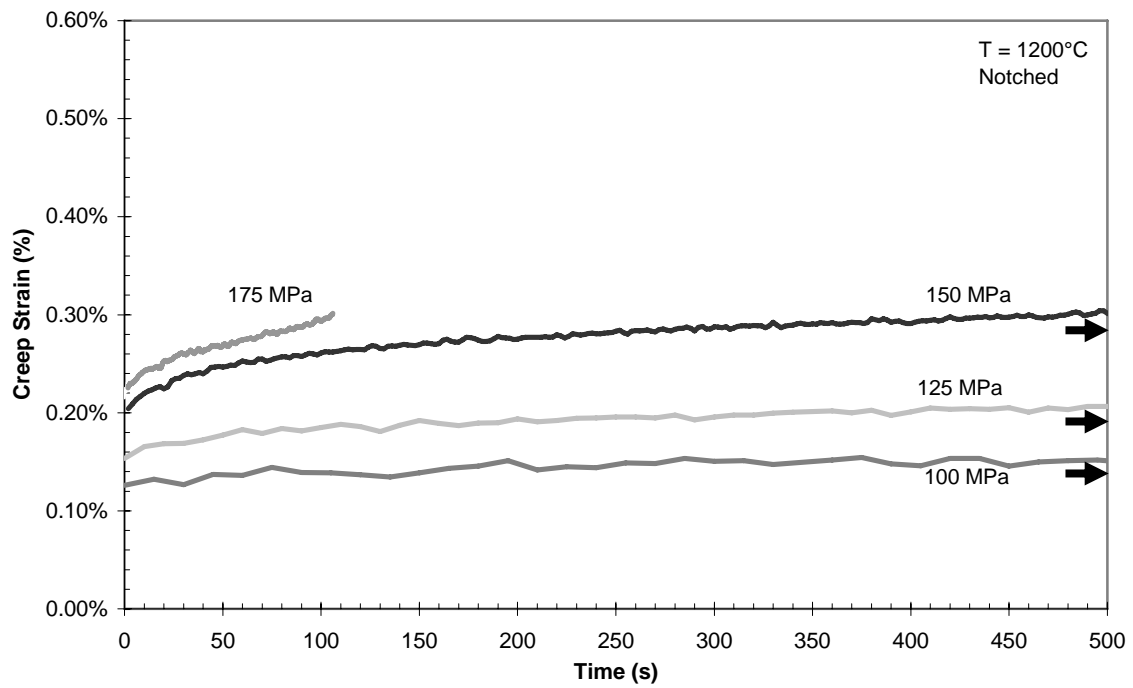
Figure 18. Creep strain vs. time for notched N720/A at 1200°C (truncated time scale)

Figure 19 and Figure 20 show the presence of primary, secondary, and tertiary creep for notched specimens at 150 MPa and 175 MPa. The 0.31 failure strain for the 175 MPa test is only slightly greater than the 0.30 failure strain of the notched monotonic test, suggesting the initial ramp of load to the creep stress is causing a similar damage mechanism.

Figure 19. Creep strain vs. time for notched N720/A at 1200°C (truncated time scale)

Figure 20. Creep strain vs. time for notched N720/A at 1200°C (truncated time scale)

Data from the previous plots were used to calculate the minimum creep rates shown in Table 8. Creep rates in the unnotched geometry ranged from 20 to 100 times greater than the rates calculated for notched samples. But again, directly comparing strain is misleading as the creep rate in the region of the hole is certainly greater than the rate averaged over the gage length.

Table 8. Creep Rate Results at 1200°C

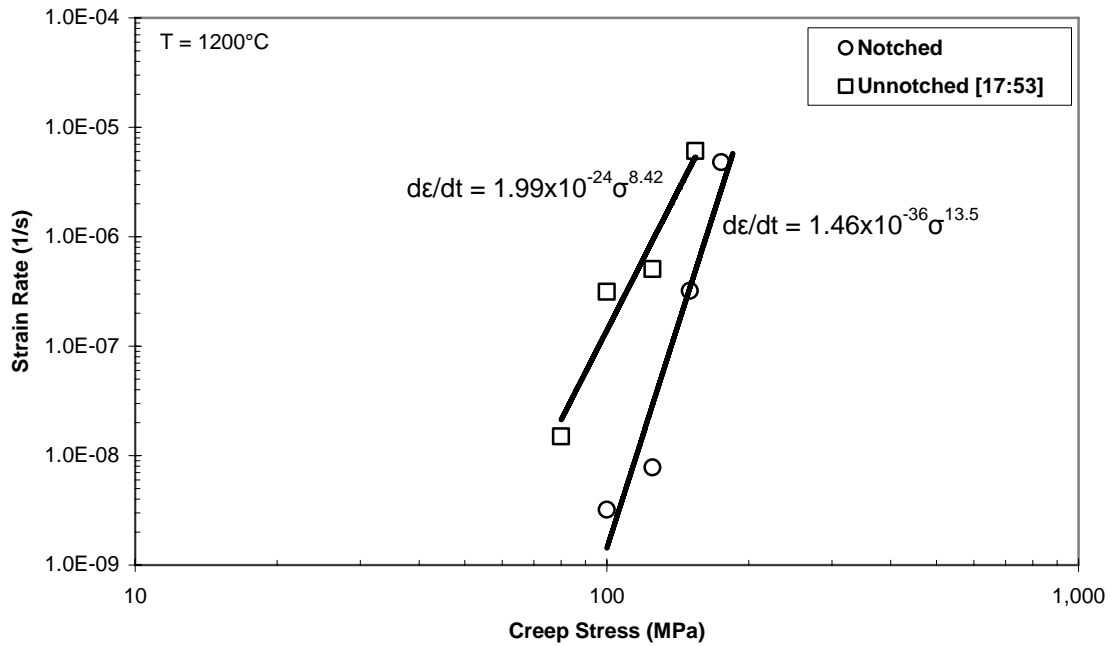| Specimen | Creep Stress | | Creep |
Number	(MPa)	% UTS	Rate (1/s)
Notched (UTS = 190 MPa)			
CH3	100	53	3.2E-09
CH1	125	66	7.8E-09
CH2	150	79	3.2E-07
CH5	175	92	4.8E-06
Unnotched[1] (UTS[2] = 192 MPa)			
14-1	80	42	1.5E-08
7-2	100	52	3.1E-07
9-2	125	65	5.1E-07
5-2	154	80	6.1E-06

Sources: [1,2][17:53, 40]

Creep strain rates were plotted as a function of stress with power regressions then used to generate the best fit curves shown in Figure 21. Coefficients of these curves represent constants of the Norton-Bailey equation:

$$d\varepsilon / dt_{min} = A\,\sigma^n \qquad (3)$$

Where $d\varepsilon/dt_{min}$ is the *minimum creep rate*, A is a *temperature dependant constant* encompassing activation energy and other constants, σ is the *applied stress*, and n is the *stress exponent* [13:740; 18:6]. Once again, the method for relating net-section stress to

average strain for the notched specimens makes it impossible to directly compare

constants for the two curves. The lower strain rate for the notched specimen is a

byproduct of stresses dropping at increasing distance from the net-section.

Figure 21. Minimum creep rate vs. creep stress for N720/A at 1200°C

4.3 Tension-Tension Fatigue Tests

Tension-tension fatigue tests were performed on notched specimens at 1200°C

with a stress ratio, *R,* of 0.05 for maximum stresses of 150 MPa, 160 MPa, and 175 MPa.

Data on failure strain and cycles to failure are presented in Table 9 for notched and

unnotched, the latter coming from previous research [14]. The 0.41% failure strain of the

160 MPa test fell between the notched monotonic failure strain of 0.30% and the 150

MPa notched creep failure strain of 0.51%. Interestingly, the 0.28% failure strain of the

175 MPa fatigue test fell slightly below the notched monotonic failure strain of 0.30%.

As with the notched monotonic specimen, it is likely stress concentration at the hole exceeded the ultimate tensile strength during a portion of the fatigue cycles, causing fibers in the high stress region to fail. With each progressing cycle more and more fibers are broken, resulting in increasing crack propagation rate that leads to a much shorter life.

Table 9. Fatigue Results at 1200°C

| Specimen Number	Maximum Stress		Strain at Failure (%)	Cycles to Failure	Location of Failure
	(MPa)	% UTS			
Notched (UTS = 190 MPa)					
FH4	150	79	>0.43	>500,992	Run-out
FH6	160	84	0.41	301,292	Gage section, hole
FH5	175	92	0.28	8	Gage section, hole
Unnotched [1] (UTS [2] = 192 MPa)					
6	100	52	0.44 [3]	>120,199	Run-out
7	125	65	0.45 [3]	>146,392	Run-out
8	150	78	0.53 [3]	>167,473	Run-out
9	170	88	0.51 [3]	>109,436	Run-out

Sources: [1,2][14:20-24]   Note: [3]Failure strain found by monotonically testing run-out specimens.

Previous tests on unnotched geometries all exceeded the prescribed run-out time and were halted between 100,000 and 160,000 cycles. The specimens were then monotonically loaded to failure while still heated to 1200°C [14:34]. The residual stress values ranged from 192 to 199 MPa, exceeding even the monotonic tensile strength.

An S-N plot of the data (Figure 22) shows both notched and unnotched geometries of N720/A have excellent fatigue resistance when maximum stresses remain below 80% of the UTS. In the notched tests only the 150 MPa fatigue load achieved run-out, defined in this effort as exceeding 500,000 cycles. When attempting to manually

stop the test the applied load spiked and broke the specimen. Fortunately the control software was recording maximum and minimum loads, allowing the computation of an approximate residual stress of 177 MPa. While this was closer to impact loading than monotonic loading methods used previously, it does show fatigue damage accumulated during the test.
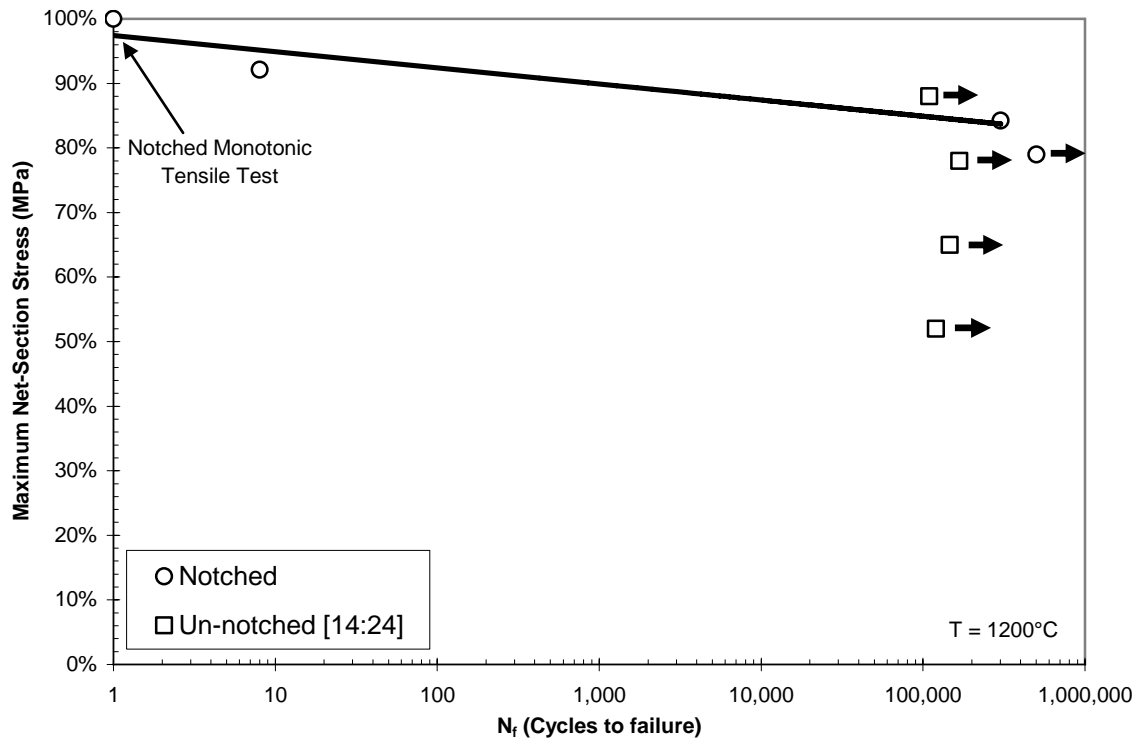

Figure 22. Fatigue stress vs. cycles to failure for N720/A at 1200°C

Unlike lower stressed specimens, the presence of a notch greatly reduced the fatigue resistance of the 175 MPa specimen. With only 8 cycles before failure, this specimen accumulated significantly more fatigue damage per cycle than the 170 MPa unnotched specimen that had a run-out life exceeding 109,000 cycles [14:24]. The notched monotonic stress-strain curve (Figure 15) shows stiffness reduction starting to

occur at 175 MPa, making it likely the 175 MPa fatigue test accumulated damage in a similar manner. This would involve concentrated stresses adjacent to the hole exceeding the ultimate tensile stress and causing some of the $0°$ fibers in the stress concentration region to fail. Each additional cycle propagated the crack further, with a critical crack length eventually reached during the eighth cycle.

One method of monitoring the accumulation of fatigue damage is to plot maximum and minimum strains for each cycle. The notched data are presented in such a fashion in Figure 23, with the reminder that notched strains values are a measure of strain averaged over the gage length and not local strain values. The strains for 150 and 160 MPa tests closely follow each other and suggest there is little difference in the damage accumulation between the two stresses. The 175 MPa test displayed markedly different behavior. Over the first four cycles the specimen experienced higher maximum strains than the other tests, but the rate of strain increase differed little. Once beyond the fourth cycle maximum strain began accumulating at a much faster rate, leading to failure at the eighth cycle.
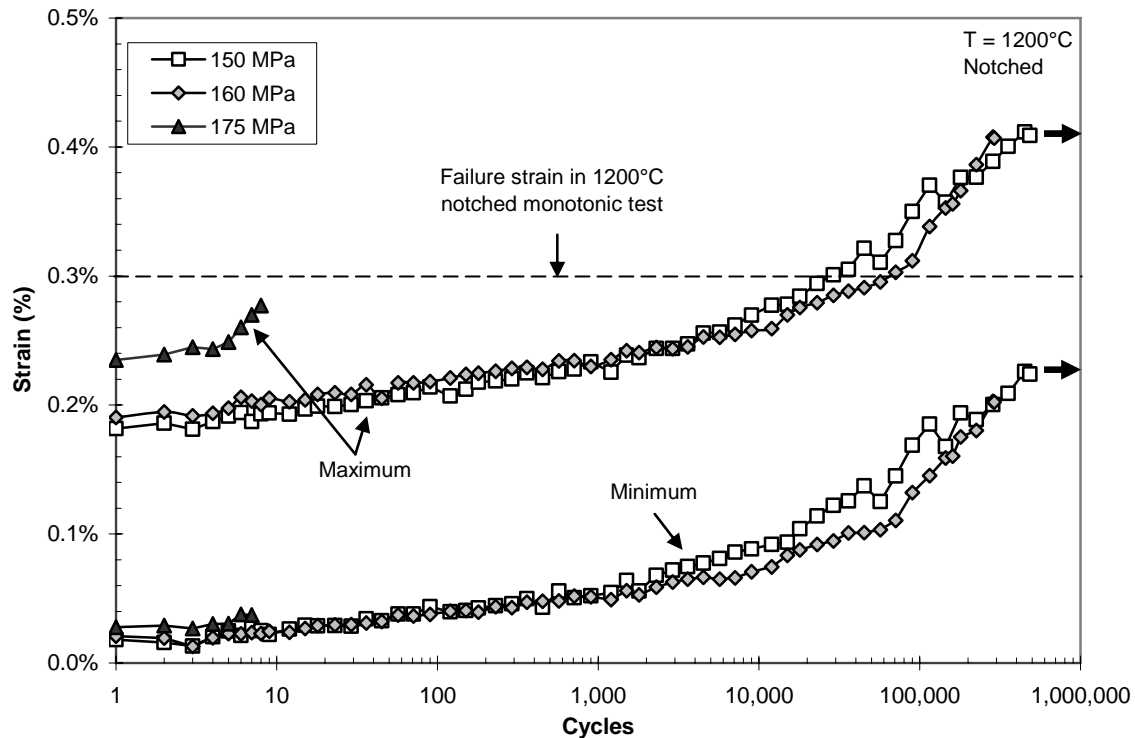
Figure 23. Maximum and minimum strain vs. fatigue cycles for notched N720/A at 1200°C

Another method of visualizing damage accumulation is to subtract the minimum strain from the maximum strain for a cycle and plot this $\Delta\varepsilon$ over the life of the specimen. In Figure 24 it appears the 150 and 160 MPa tests both accumulate damage at roughly the same low rate. The $\Delta\varepsilon$ values for 160 MPa are approximately 6% larger than the values for 150 MPa, which matches the 6% difference in maximum stress between the two tests. While the rate of strain increase remains the same between the specimens, the higher loaded specimen will be the first to reach a high enough strain to start causing significant numbers of fiber failures. Once this starts happening, more fibers will fail on each subsequent loading, causing $\Delta\varepsilon$ to grow at an ever increasing rate until the specimen fails completely. This trend is evident in the upwardly concave curve for 175 MPa and the increasing $\Delta\varepsilon$ for cycles preceding the failure point of the 160 MPa specimen.

45
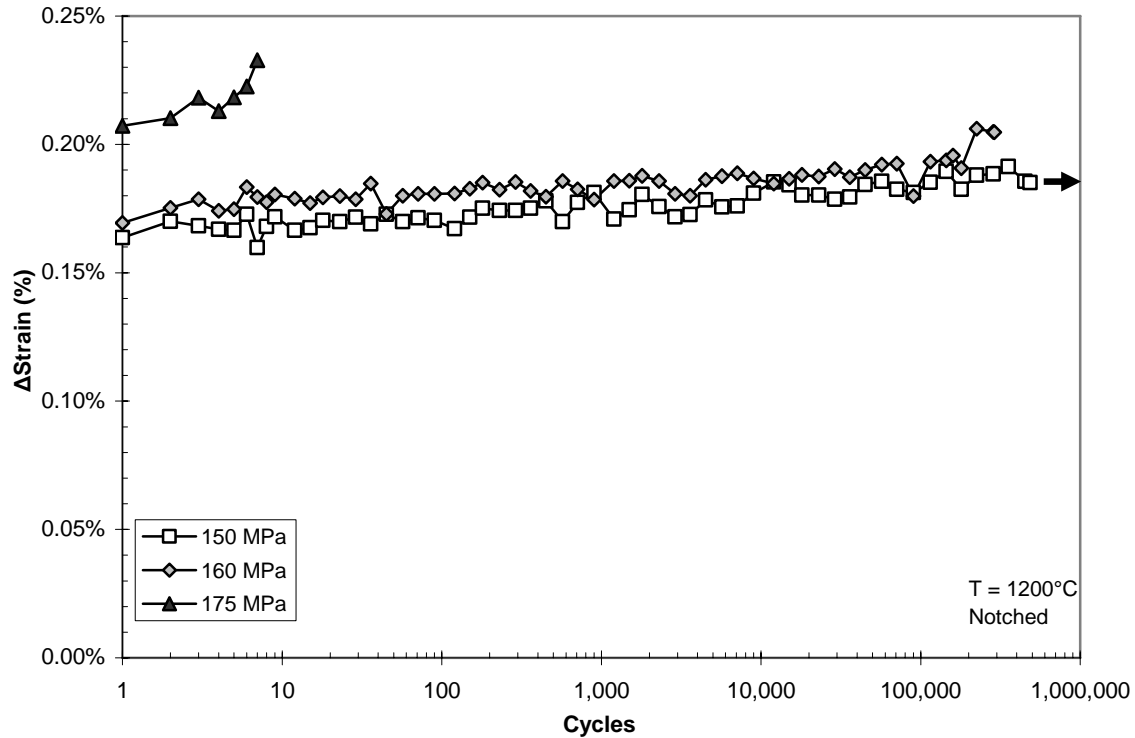
**Figure 24. Delta strain vs. fatigue cycles for N720/A at 1200°C**

Plots of stress-strain behavior during the course of a cycle are presented next. These hysteresis loops show how strain varies during the course of loading and unloading the specimen. The area within a hysteresis loop is a measure of the amount of energy dissipated per unit volume during a cycle [32:99]. In ductile materials this energy represents the plastic work performed during a cycle. In brittle materials, like CMCs, this energy is dissipated through the formation and extension of cracks and by internal friction.

A misunderstanding of the servo-hydraulic control software resulted in hysteresis data acquisition starting half a cycle early, with the result of all hysteresis loops beyond the second cycle starting and ending at their maximum stresses instead of the minimum

stresses intended. With data recorded for both the 1st and 2nd cycles it was possible to plot the initial hysteresis loop starting from zero stress.

Hysteresis loops for 150 MPa and 160 MPa fatigue stresses are presented in Figure 25 and Figure 26. As expected, there was little difference between the two stress levels. Both show larger hysteresis for the first cycle, indicating cracking within the specimen. Cycles following the first showed linear-elastic loading and unloading behavior with minimal energy dissipated during the cycle. This suggests the cycling of the load itself causes little damage, but that creep might be the primary cause of increasing strain with increasing cycles.
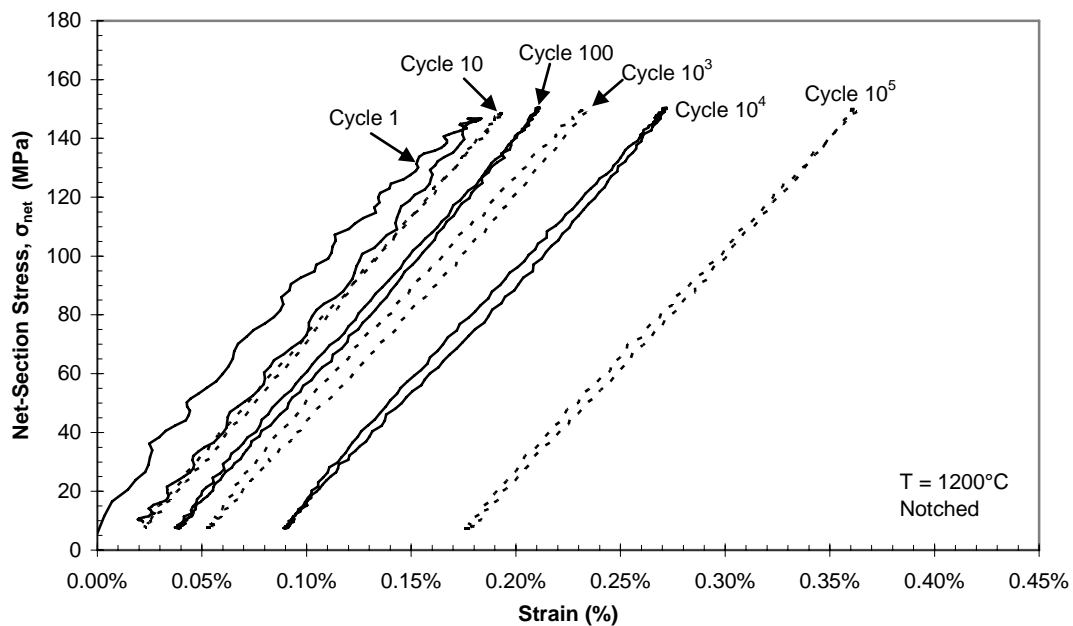
Figure 25. Hysteresis loops for N720/A at 1200°C, 150 MPa stress level
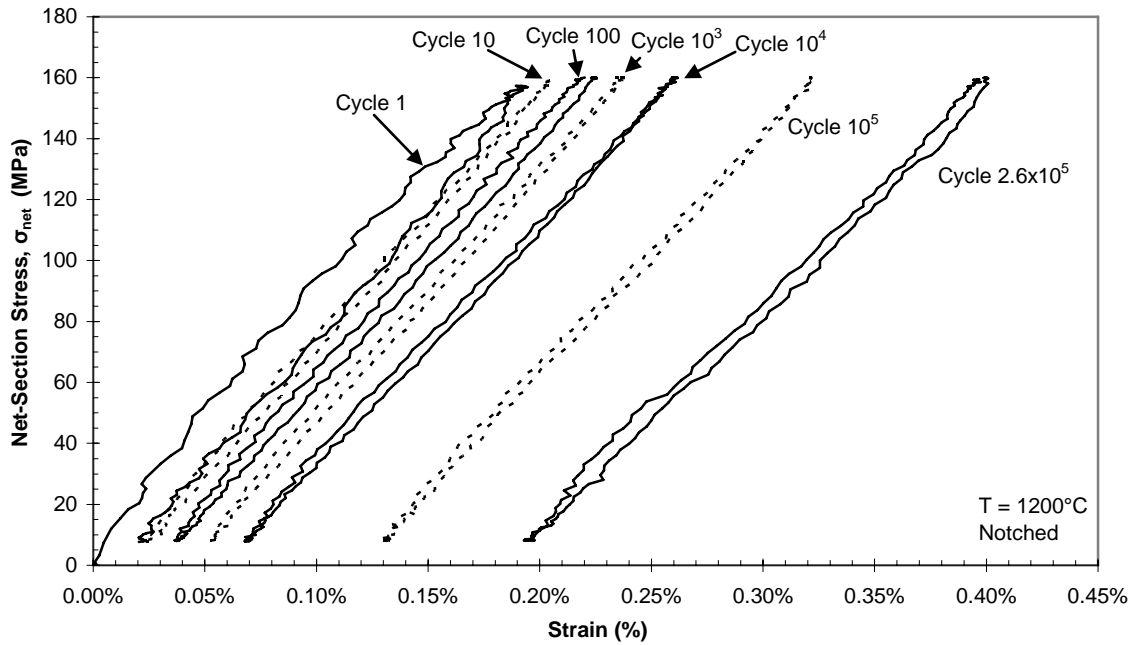
Figure 26. Hysteresis loops for N720/A at 1200°C, 160 MPa stress level

Figure 27 shows hysteresis loops for the 175 MPa fatigue specimen. The higher

maximum stress value for this test resulted in a larger hysteresis for the first cycle,

indicating a greater amount of damage to the specimen. While the hysteresis for the fifth

cycle indicates less damage occurred than during the first cycle, it is still greater than the

typical amount of damage found in fatigue cycles at lower maximum stresses.
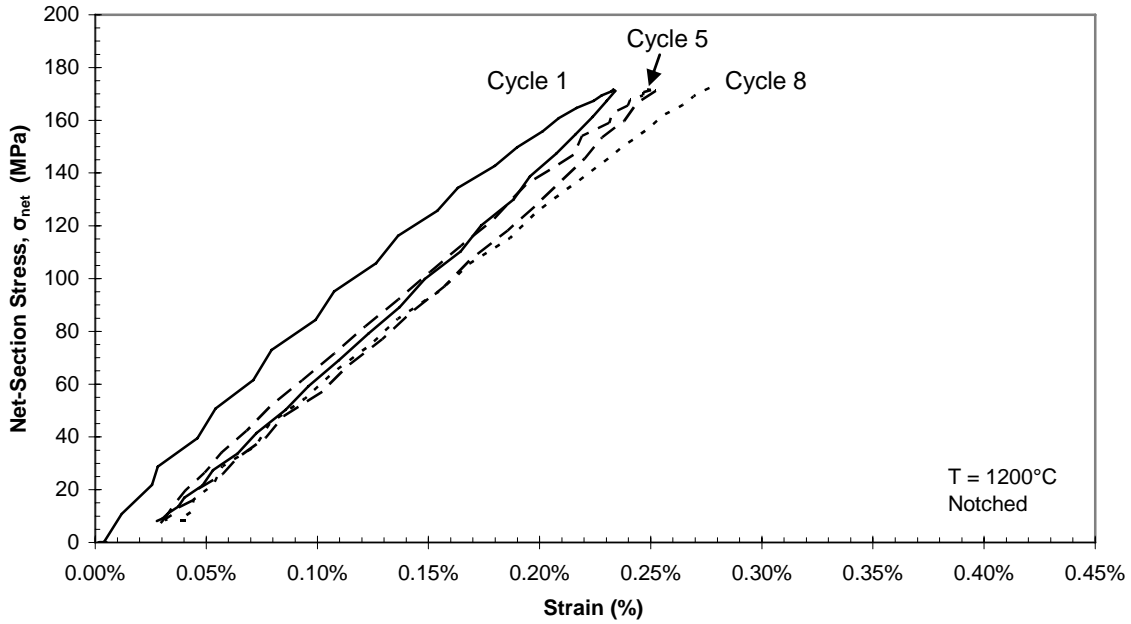
Figure 27. Hysteresis loops for N720/A at 1200°C, 175 MPa stress level

Finally, the reduction in stiffness of the fatigue specimens was examined over the course of testing. Specimen stiffness equals the slope of the linear elastic portion of a hysteresis curve. The narrowness and linearity of the hysteresis curves allowed stiffness to be closely approximated by the secant modulus, which is the slope between the low and high points of a hysteresis loop:

$$S_{sec} = \frac{\sigma_{max} - \sigma_{min}}{\varepsilon_{max} - \varepsilon_{min}} = \frac{\Delta\sigma}{\Delta\varepsilon} \tag{4}$$

Again, the presence of a notch within the gage section makes it more appropriate to refer to this value as *stiffness* instead of *modulus*. The stiffnesses for cycles of each test were normalized by dividing by the stiffness of the first cycle. These values, plotted in Figure 28, show a nearly linear rate of stiffness reduction when compared to the logarithm of the number of cycles. Near the ends of their lives, both the 160 MPa and

175 MPa tests showed greatly increasing rates of stiffness reduction, with final stiffnesses of 83% and 89% respectively.
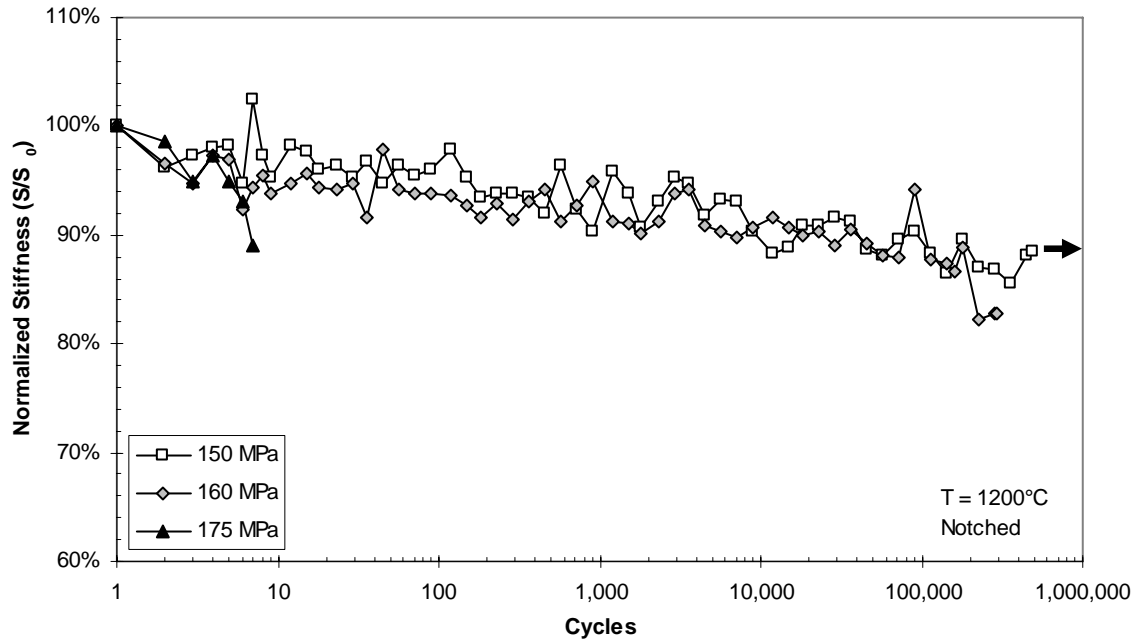

Figure 28. Normalized stiffness of notched N720/A at 1200°C

4.4 Comparison of Creep and Fatigue Tests

The relatively small increases in $\Delta\varepsilon$ and reductions in stiffness over time suggest the primary damage mechanism from the fatigue loading results from creep. Figure 29 shows a comparison of creep strains and mean fatigue strains ($(\varepsilon_{max}-\varepsilon_{min}) / 2$) during the course of testing. The increases in strain of the 150 MPa and 160 MPa tests closely follow the stress-time curve of the 100 MPa creep test. In fact, the mean stress of the 150 MPa and 160 MPa fatigue tests are 79% and 84% of the 100 MPa loading of the creep test. At initial loading the mean strains of the 150 MPa and 160 MPa tests are also

79% and 84% of the initial strain for the 100 MPa test, showing the initial fatigue loading caused no more damage than the load ramp-up for the creep test.

After 10,000 seconds of testing the 150 MPa and 160 MPa fatigue tests had strains 93% and 85% those of the 100 MPa creep test, showing average fatigue strain increases at a slightly faster rate than strain from a steady load. The higher strains for the 150 MPa fatigue test compared to the 160 MPa fatigue test occurring after 1,000 seconds might be a result of fiber straightening or some other non-damaging, strain increasing occurrence in the lower stressed specimen. Despite the lower strain, the 160 MPa fatigue specimen still fails before the 150 MPa fatigue specimen.
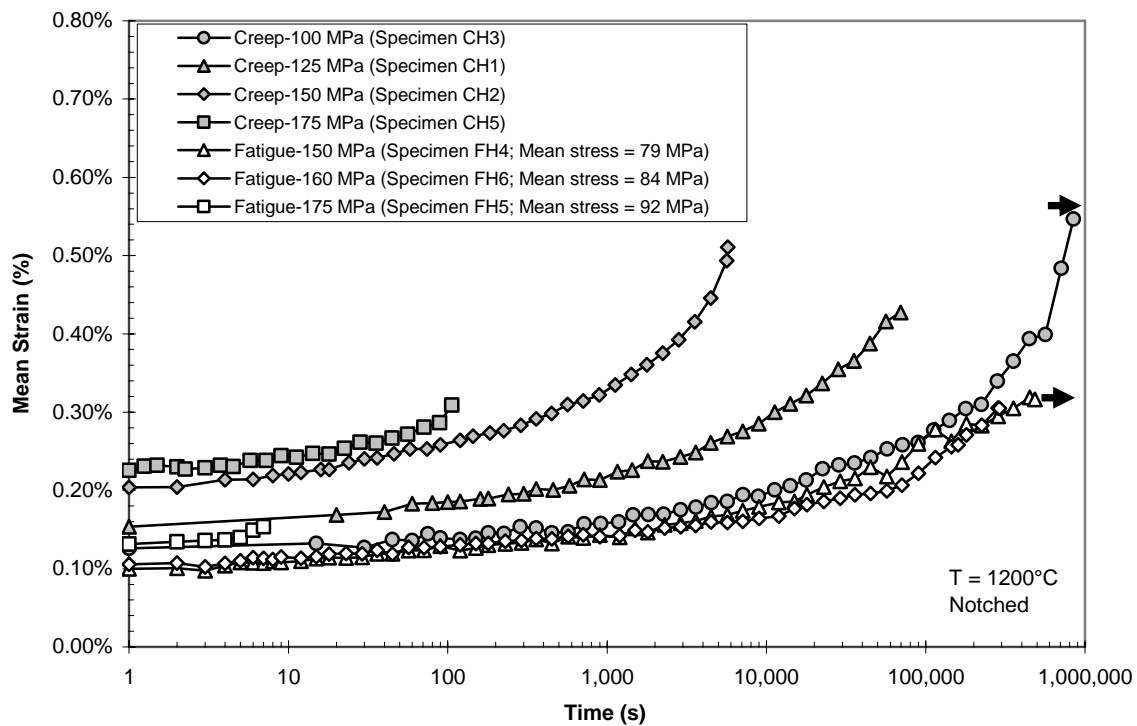
Figure 29. Mean fatigue and creep strains vs. time for notched geometry

Figure 29 also shows the 175 MPa fatigue test, with mean stress of 92 MPa, having higher average strains than the 100 MPa creep test. This shows fatigue loadings with maximum stress at 92% of the UTS incorporate notable damage mechanisms besides creep. The plot of mean stress versus time to failure shown in Figure 30 indicates this additional damage results in a significant reduction in life. The log-scale plot also shows mean fatigue stresses below 45% UTS having approximately the same slope as the S-t curves for notched and unnotched creep. This same region also indicates mean fatigue stress for notched specimens must be 25% less than the creep stress of a similarly notched specimen to achieve the same lifespan.
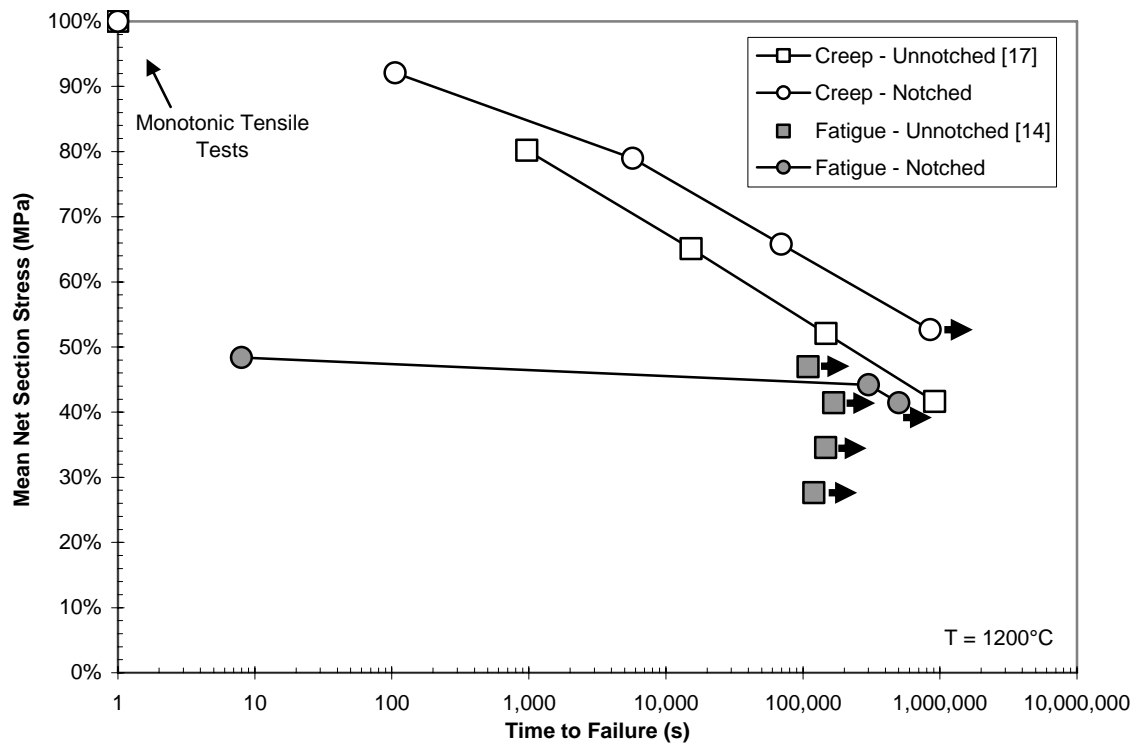
Figure 30. Mean fatigue and creep stress vs. time to failure for N720/A at 1200°C

4.5 Microstructural Analysis

Following the completion of testing, specimens were imaged under microscopes to determine if micro-structural damage could provide clues about the modes of damage mechanism and failure. Low magnification side views of fiber pullout were made with an optical microscope, while end views of the fracture surface were observed with a scanning electron microscope (SEM).

Optical micrographs for monotonic notched and unnotched tests at 1200°C are presented in Figure 31. Both specimens show significant pullout of fiber bundles and individual fibers at random positions across the fracture face. Fracture of the unnotched specimen occurred just outside the gage length at the start of curvature. The small size of the furnace required the tapers to start at the edge of the furnace chamber, making thermal gradients a possible contributor to failure in this region. Use of a larger furnace would be the best solution, but it is expected that this failure just outside the gage length had minimal effect on the calculated ultimate tensile strength.
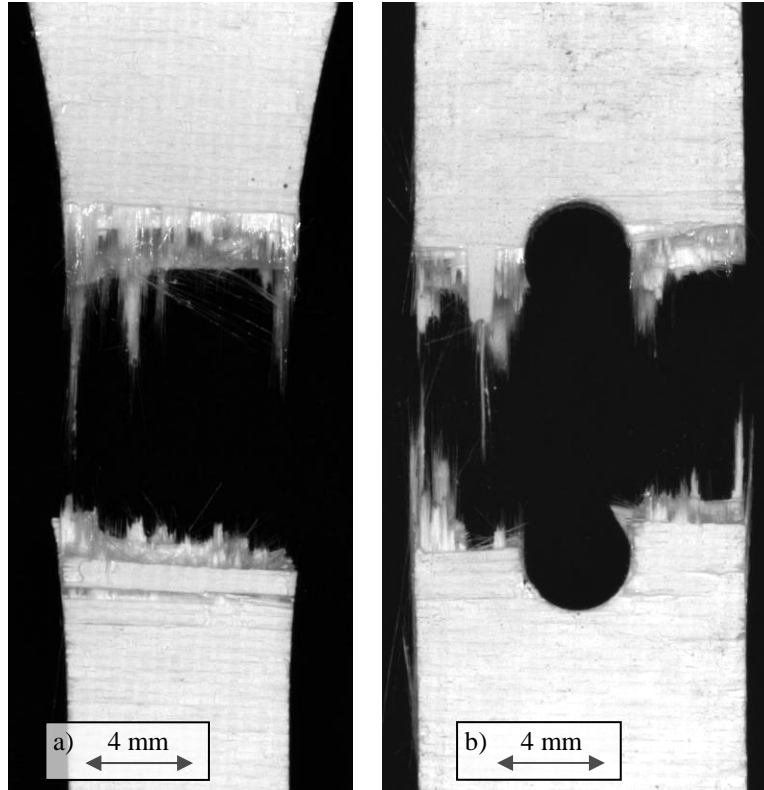
Figure 31. Monotonic tensile tests of (a) unnotched and (b) notched specimens

The creep-rupture specimens of Figure 32 also showed significant amounts of bundle and fiber pullout across the entire fracture surface. Increasing creep stress from 125 MPa to 175 MPa did not cause any apparent changes in fracture appearance. The run-out specimen for 100 MPa creep loading was never tested to failure.
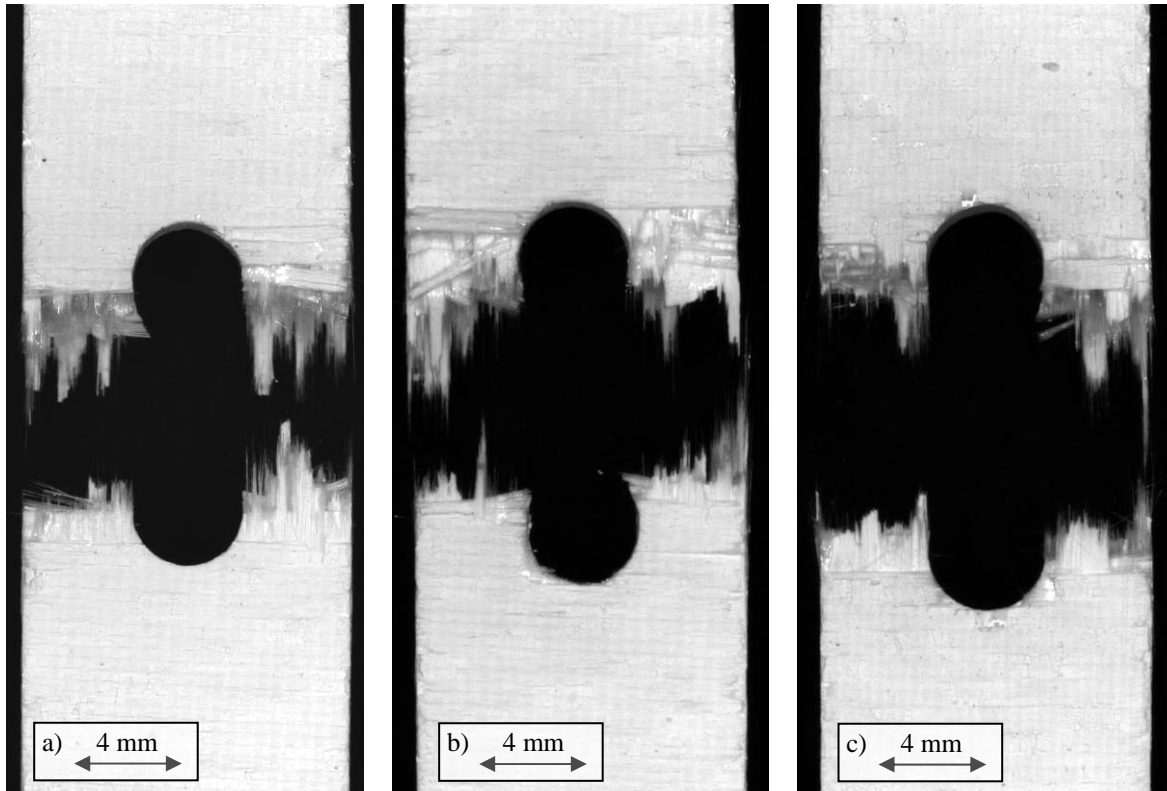
Figure 32. Creep-rupture specimens for (a) 125 MPa (b) 150 MPa and (c) 175 MPa

The 150 MPa tension-tension fatigue specimen, shown in Figure 33a, also exhibits the same amount of fiber pullout as other tests, despite reaching a run-out condition followed by monotonic loading to failure. The 175 MPa test specimen also shows a similarly uneven and fibrous fracture plane. Unexpectedly, the specimen loaded to 160 MPa (Figure 33) shows slightly different behavior. The largest region of failure for this specimen occurred slightly offset from the hole. As viewed in the micrograph, the minimum cross-sectional area bordering the left side of the hole is intact for at least the top lamina. Additionally, 90° tows on the opposite surface fanned out during the course of failure. Other specimens pulled out 90° tows, but none did so to a distance beyond the hole.
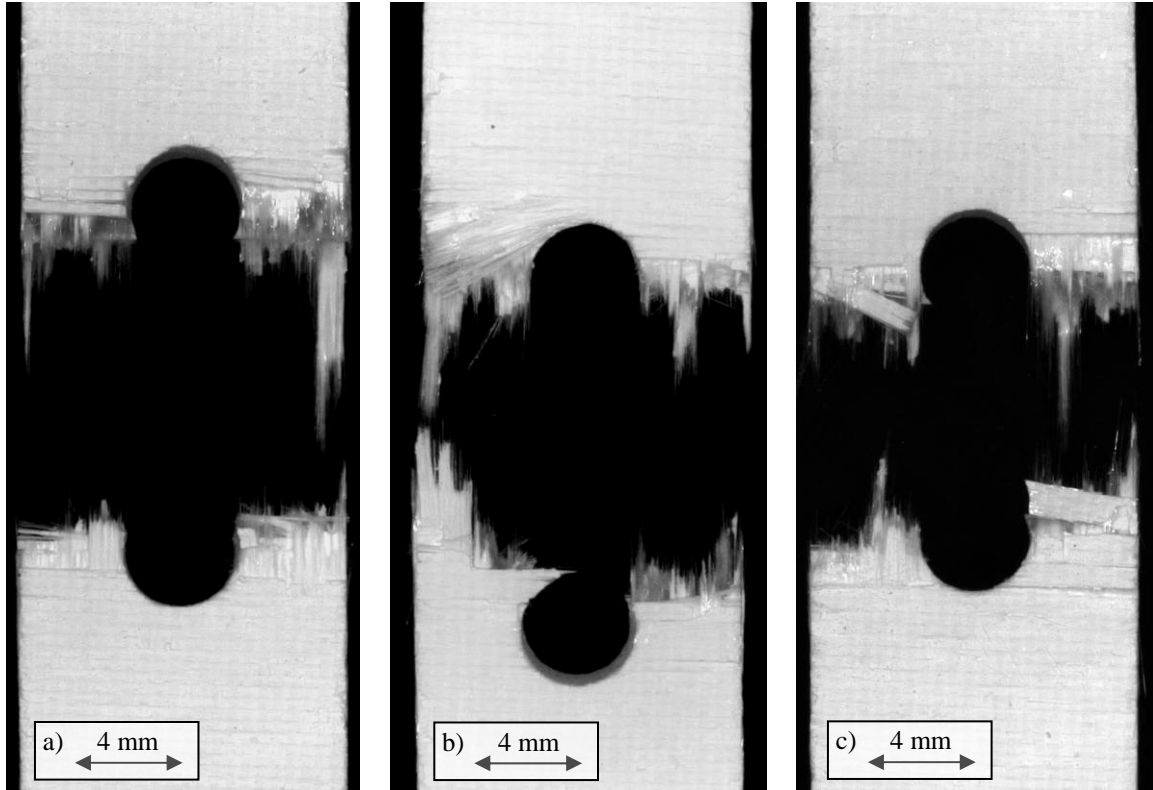
**Figure 33. Tension-tension fatigue specimens for maximum stresses of:
(a) 150 MPa (b) 160 MPa and (c) 175 MPa**

Low magnification end views of the fracture surfaces were made using an SEM.

Figure 34 shows the fracture surface of the unnotched monotonic tensile test at 1200°C.

The surface is characterized by pullout of individual fibers and entire tows, with very

similar appearance to unnotched N720/A specimens tested by previous researchers

[14; 17].
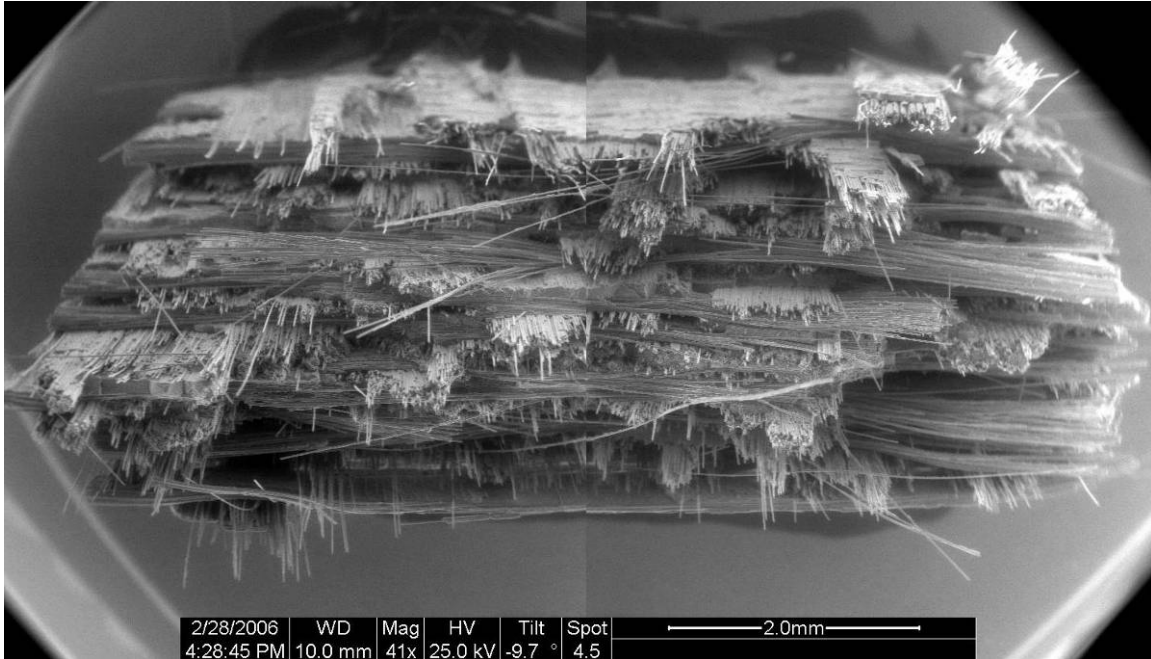
Figure 34. Fracture surface of unnotched monotonic tensile specimen (two images overlapped to show entire fracture surface)

Past research found varying the loading method of N720/A between monotonic, creep, and fatigue to have no discernable impact on the appearance of the fracture surfaces. This research effort also found changing methods of loading caused no apparent change to the fracture surfaces. However, there was a trend in notched specimens for a portion of the 90° tows and regions of un-reinforced matrix to share a common plane of fracture, usually corresponding to the minimum cross-sectional area. This behavior is visible for the notched monotonic and notched creep specimens shown in Figure 35.
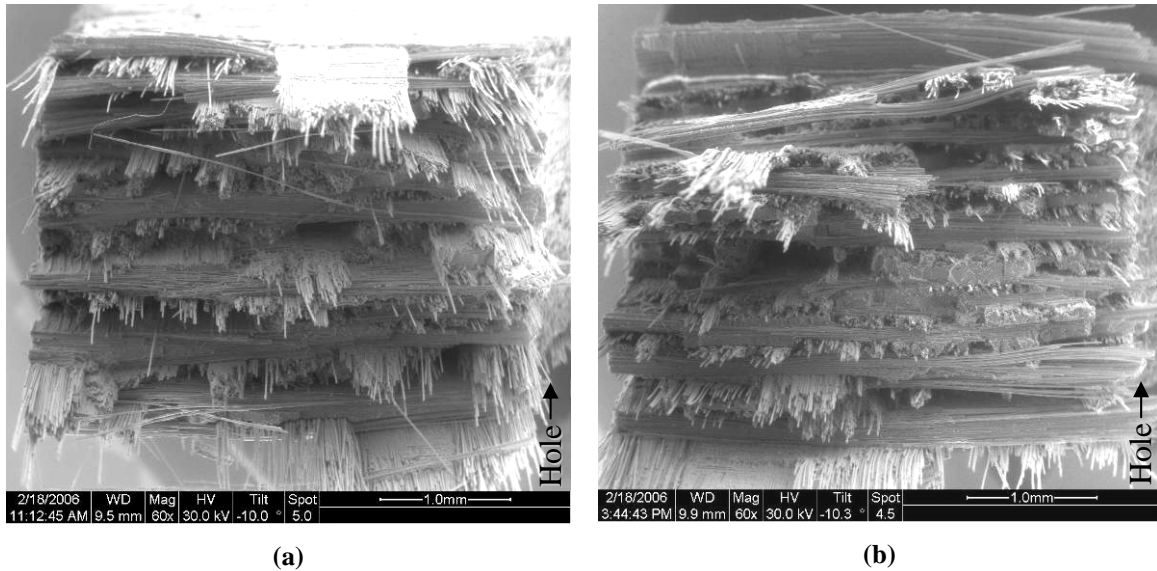
Figure 35. Notched fracture surfaces for (a) monotonic and (b) 150 MPa creep tests

Due to their similar fracture surfaces, micrographs from various notched specimens will be used to show common features. The previously mentioned trend of 90° tows often sharing a common fracture plane suggests cracking of the primary failure plane begins at the edge of the hole or in a nearby defect, then advances along the 90° tows and matrix rich areas [24:3091]. The frequent presence of pores and other inherent cracks [31:Sec 4, 1] also makes possible the growth of several large crack planes in the high stress region around the hole. Figure 36 shows the planes of failure on the left and right side area at slightly offset. When the 0° fibers failed catastrophically, the offset crack planes resulted in several 90° tows being sheared in half as the specimen pulled apart.
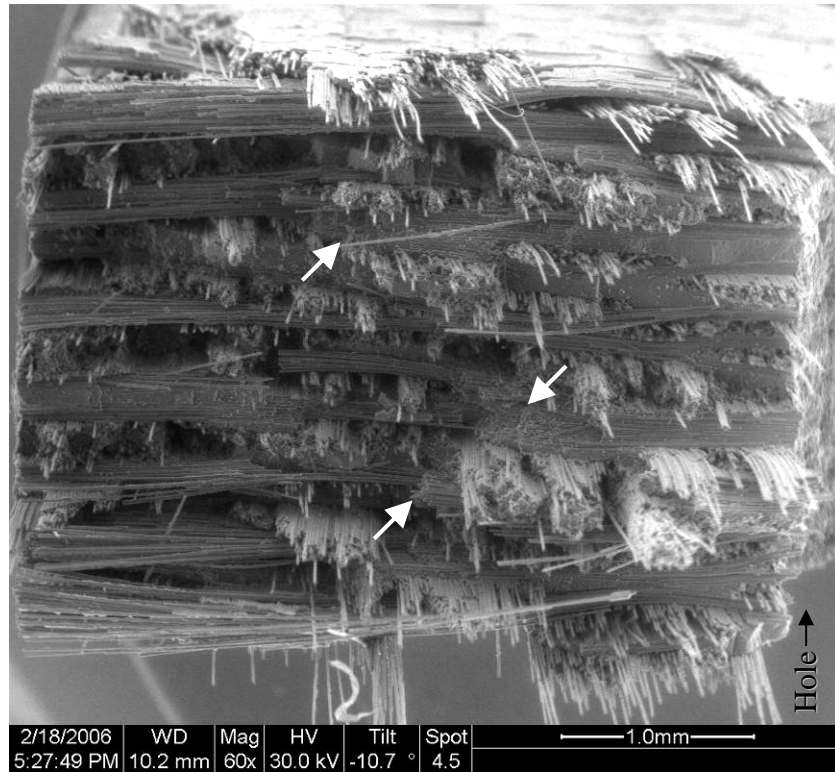
Figure 36. Offset crack planes and resultant shearing of 90° tows (identified with arrows) (notched, 150 MPa fatigue)

The porosity of the alumina matrix allowed cracks propagating along the 90° fibers to deflect into 0° fiber bundles. This behavior dispersed stress and reduced the local strain exerted on the 0° fibers, allowing for varying amounts of crack bridging. Greater amounts of matrix cracking around the 0° fibers resulted in increased individual fiber pullouts of varying length as visible in the upper regions of Figure 37. Lesser amounts of cracking within the 0° tows would result in fibers remaining bonded together and pulling out as a bundle, with bundles often having a relatively planar transverse fracture surface. Lastly, regions with minimal crack propagation along 0° fibers resulted in these fibers failing on nearly the same plane as the primary fracture surface as shown in Figure 38.
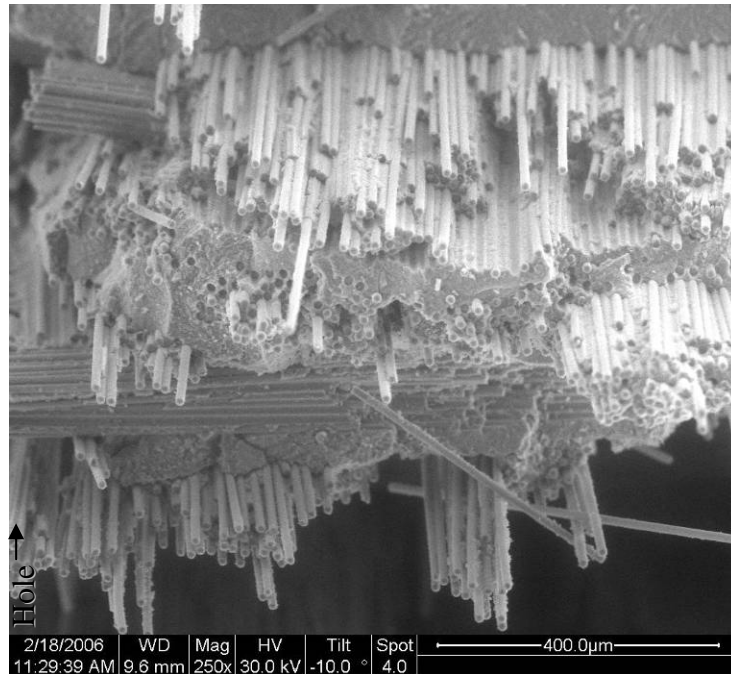
Figure 37. Individual and bundled fiber pullout (notched, monotonic)
**(edge of hole runs along left edge of image)**
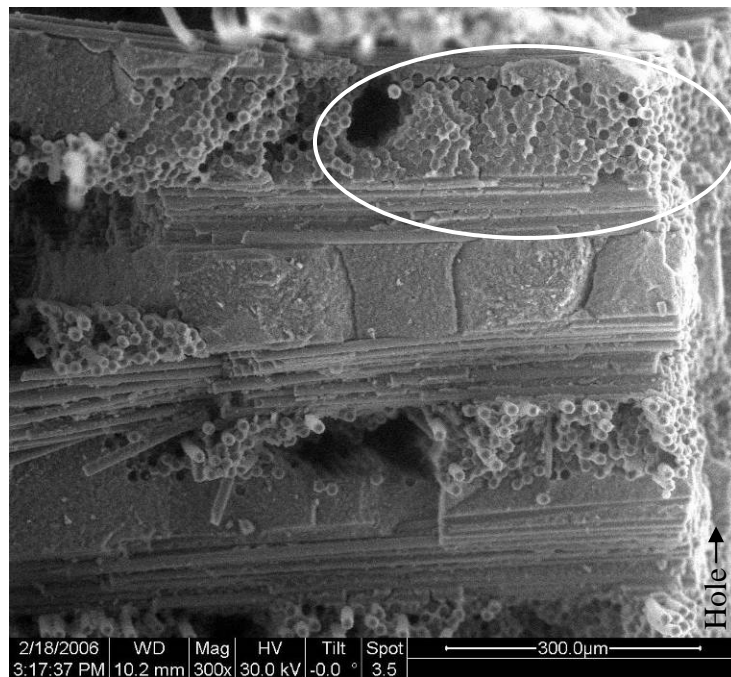
Figure 38. Common fracture plane through 0° fibers (notched, 125 MPa creep)

Figure 39 shows the planar fracture surface of a 0° fiber bundle. While cracking is visible within the matrix, the amount proved insufficient to release the fibers from the strain concentration resulting from the transverse crack.


| 2/18/2006 | WD | Mag | HV | Tilt | Spot | �————50.0μm———— |
| 4:18:46 PM | 9.0 mm | 1800x | 30.0 kV | -5.7 ° | 4.0 | |
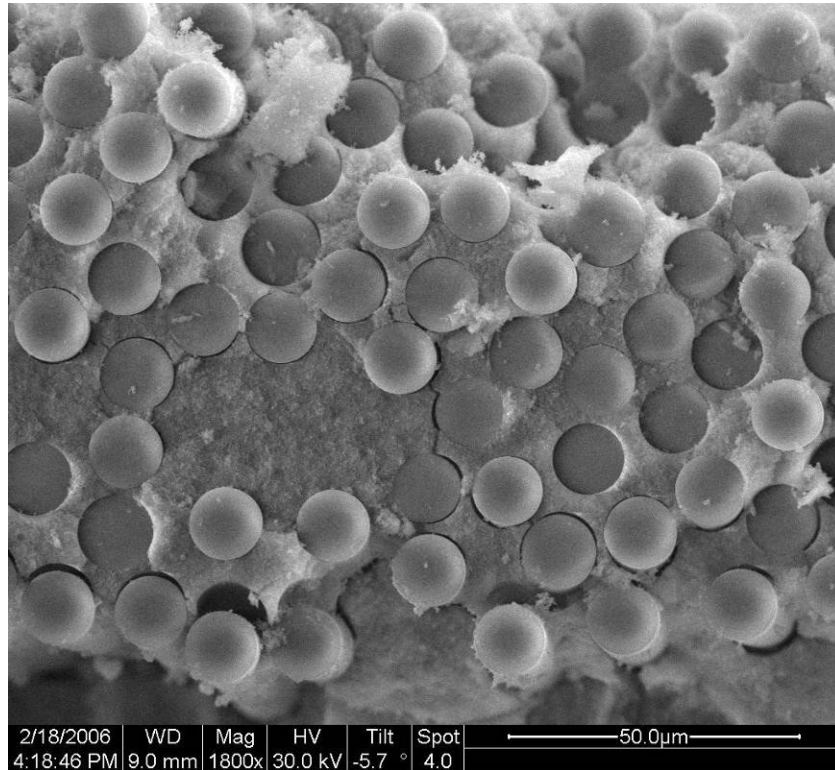
Figure 39. Slight matrix cracking along 0° tows (notched, 150 MPa creep)
(edge of hole 2.0 mm left of image)

A more typical bundle pullout fracture surface is shown in Figure 40. A greater level of matrix cracking along the length of the 0° bundle allowed fibers to fail independent from each other.
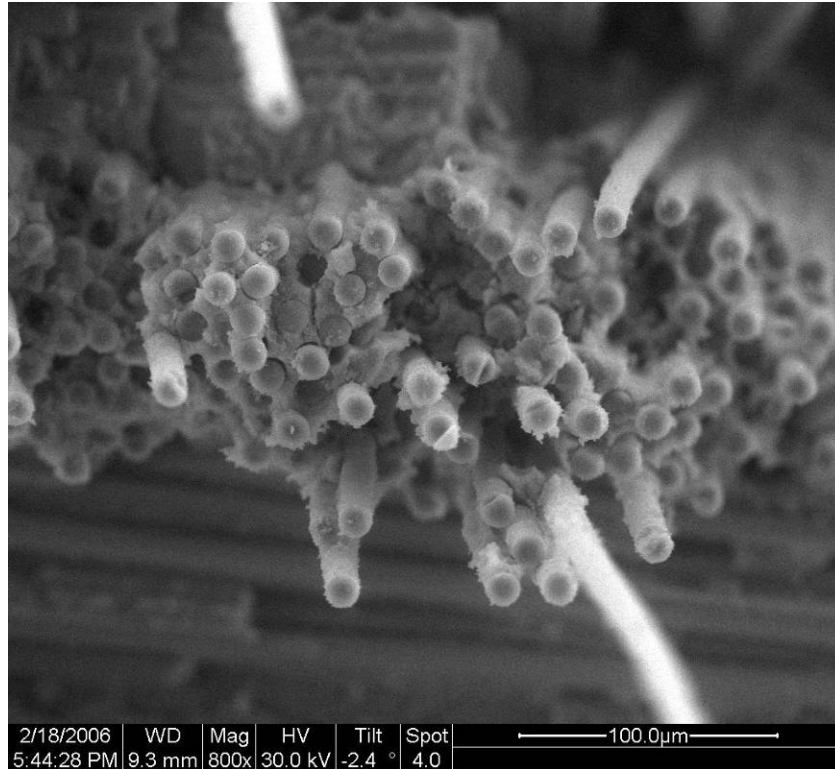
Figure 40. Extensive matrix cracking within fiber bundle (notched, 150 MPa fatigue)
(edge of hole 0.5 mm left of image)

As mentioned before, the specimen loaded to 160 MPa displayed much longer fiber pullouts than other notched specimens. End views of the specimen (Figure 41) also show much larger amounts of matrix cracking within the 90° tows. The cracking is so severe that little matrix remains within these tows, leaving the individual fibers to hang loosely.   Figure 42 shows that even 90° tows at away from the minimum cross-sectional area suffered fracturing and displacement as the 0° fibers pulled out.
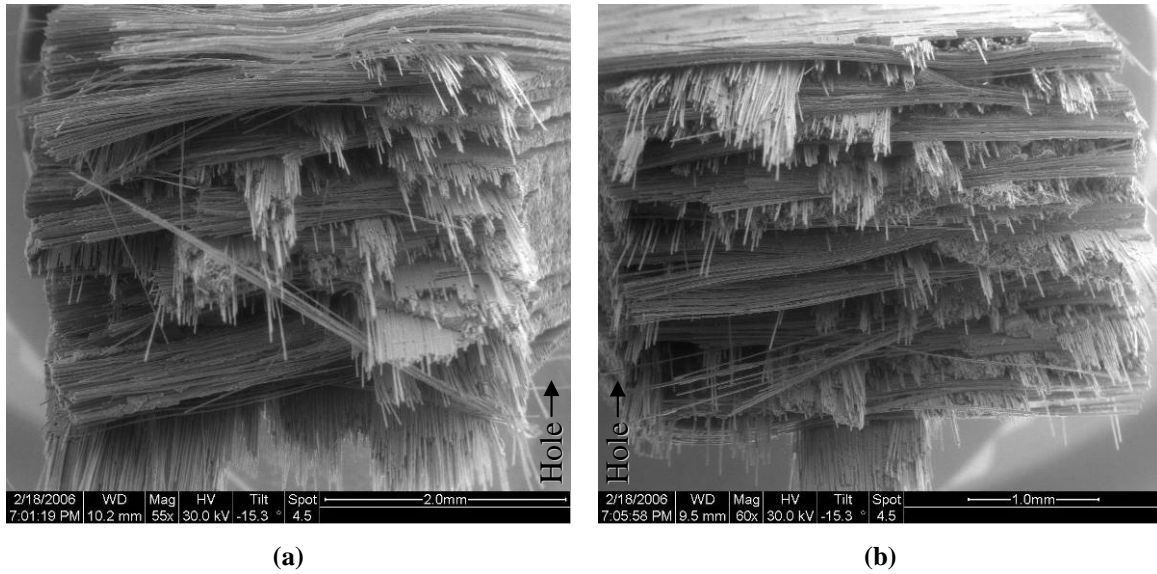
Figure 41. Fracture surfaces for 160 MPa fatigue test (a) left and (b) right of the hole
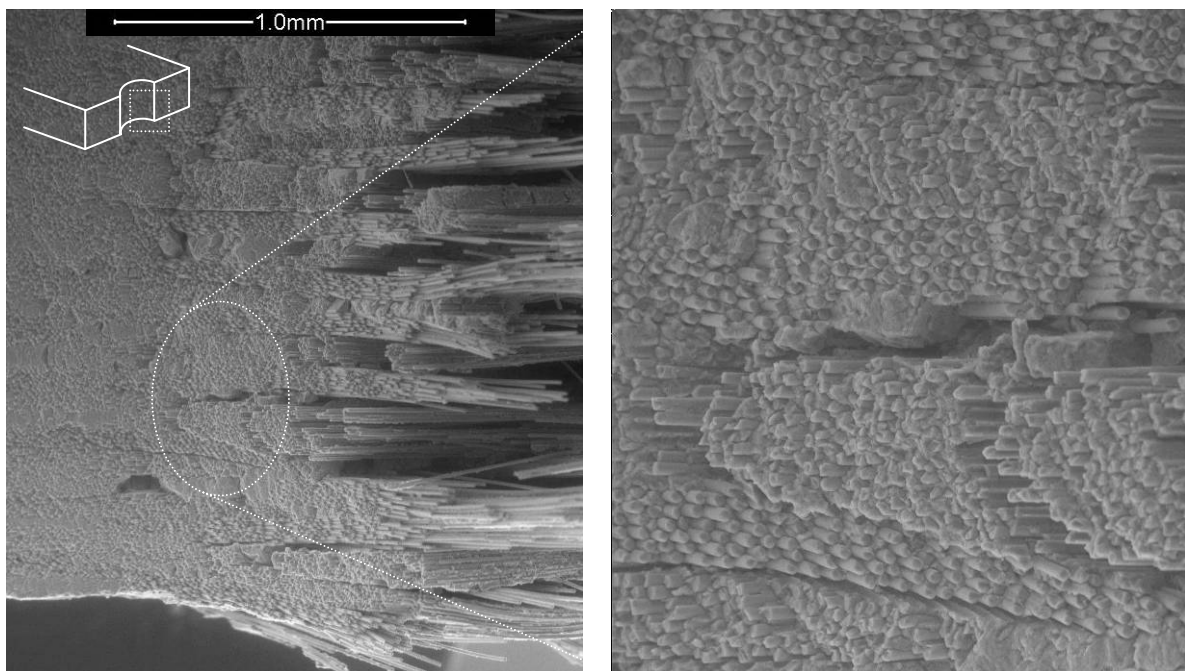
Figure 42. Cracking within 90° tows in 160 MPa fatigue specimen

A possible cause for this behavior is that a second large crack growth plane grew around a defect distant from the crack plane at the minimum cross-sectional area. During catastrophic failure a portion of the 0° tows failed at this distant crack plane, while the

remaining tows failed at the net-section crack plane. As the 0° tows pulled apart, the interlaced 90° tows were pulled in both directions with deflections eventually causing matrix on one end of the 90° tow to disintegrate. If this is indeed the failure mechanism that occurred in the 160 MPa fatigue specimen, it suggests that had no material defects been present in the region near the hole, the 160 MPa fatigue specimen would have had a fracture surface like the other specimens.

4.6 Summary

In summary, the notched specimens behaved in largely the same fashion as the unnotched specimens. In monotonic testing the ultimate tensile strengths between notched and unnotched remained nearly identical, even though the notched specimen displayed a slight reduction in stiffness near the ultimate strength. Notched creep tests actually outperformed the unnotched test results with failure lives 5 times greater than those of unnotched geometry. Fatigue loading did show notch sensitivity with maximum stress of 175 MPa, but aside from this test the notched fatigue lives were consistent with those of unnotched specimens.

Comparisons between the notched fatigue and creep tests suggest the dominant damage mechanism during fatigue loading is in fact creep. The presence of a notch does appear to require mean notched fatigue loads be 25% less than notched creep loads to achieve the same life, but to reach the same life of an unnotched specimen only requires a 4% reduction in mean stress from the unnotched specimen loading. The exception is the 175 MPa fatigue test which showed significant accumulation of fatigue damage that caused a large reduction in life.

Micrographs show indistinguishable fracture surfaces between monotonic, creep, and fatigue specimens of the same geometry. It does appear notched specimens tend to have one or two planes of fracture for the 90° tows. Unnotched specimens instead showed fracture surfaces with no common fracture plane, suggesting flaws at different positions among the different plys were able to grow to significant size. The quick drop in stress away from the notch of notched specimens results in cracks growing primarily within the net-section. This seems not to always be the case, as demonstrated by the unusually long fiber pullout of the 160 MPa fatigue test that hints at significant defect growth slightly away from the net-section, but this sort of behavior was not seen in the other tests and appears to have had minimal impact on fatigue life of the 160 MPa specimen.

V. Conclusions and Recommendations

Even with the presence of a center hole with notch ratio (2a/w) of 0.33, the Nextel™720/Alumina oxide/oxide composite evaluated in this study showed excellent material properties in 1200°C laboratory air. Notable notch sensitivity was only observed in fatigue tests with maximum stress of 175 MPa.

High temperature (1200°C) monotonic testing of notched and unnotched specimens from the same plate showed tensile strengths of 200 and 190 MPa respectively. The 5% reduction of strength in the notched specimen might indicate slight notch sensitivity. Notched monotonic failure strain was 14% lower than for the unnotched specimen. This reduction is misleading since the notched failure strain is based on average strain over the entire gage length, when it is clear larger local strains will occur in the vicinity of the notch. Overall, the reduction in ultimate strength for the notched monotonic test is fairly minor and of the same magnitude as variations resulting from differing quality between N720/A plates.

Creep-rupture loading also showed outstanding behavior with rupture lives of notched specimens actually exceeding those of unnotched specimens by a factor of five. A likely reason for this difference is that even distribution of stress through unnotched specimens allowed defects anywhere along the gage length to spawn large cracks. Conversely, notched specimens concentrate stress around the hole, reducing the probability that distant defects will grow to critical lengths. Creep stresses less than 80% of the UTS show a constant logarithmic relation between stress and rupture life for both

notched and unnotched geometries. This relation proves less accurate as creep stress

approaches the ultimate tensile strength and additional damage mechanisms are

introduced.

Tension-tension fatigue loading also showed notched Nextel™720/Alumina to

have generally good fatigue resistance at 1200°C when cycled at 1.0 Hz with a stress

ratio of R = 0.05. Cycles to failure in notched specimens exceeded 300,000 when

maximum stress was kept at or below 160 MPa.   Notched testing at 175 MPa resulted in

a fatigue life of only 8 cycles, a tremendous reduction from the run-out life of 109,000

cycles for a 170 MPa unnotched specimen. As with the notched monotonic specimen, it

is likely stress concentration at the hole exceeded the ultimate tensile strength of the

material, leading to larger crack propagation and a much shorter life. The long lives for

fatigue tests at or below 160 MPa suggests the concentrated stress in these specimens

remains low enough to not cause significant amounts of fiber fracture prior to failure.

Optical and scanning electron microscopy of fracture surfaces showed similar

amounts of fiber pullout between notched and unnotched specimens. Monotonic, creep,

and fatigue loadings caused no discernable trends in fracture surface characteristics.

Pullout of 0° bundles and fibers were similarly random between notched and unnotched

geometries. There was a trend in notched specimens for 90° tows and matrix rich regions

to fracture in the net-section area along one or two planes transverse to the direction of

loading. Fracture surfaces of unnotched specimens showed no such trend toward a

common fracture plane among the 90° tows [14; 17]. The 160 MPa fatigue specimen had

a unique fracture surface that suggested an additional crack propagation plane formed

away from the net-section, likely forming around a material defect. The following fiber

pullout caused the disintegration of matrix within numerous tows along the fracture surface, resulting in a "hairy" appearance not seen in other specimens.

Overall, the Nextel™720/Alumina oxide/oxide composite showed excellent creep and fatigue properties with generally minimal notch sensitivity. The only exception is for fatigue testing where maximum stress should not exceed 160 MPa if a long cycle-life is desired. While many studies have analyzed the high temperature properties of Nextel™720/Aluminosilicate (N720/AS) [2; 5] and specifically its notch characteristics [5; 6; 22], no research was found characterizing the impact of notches on N720/A. Future efforts could evaluate the effects of additional notch ratios (2a/w), different notch geometries, and also different temperatures. Another possible research avenue is to investigate notch behavior of N720/A with different fiber orientation.
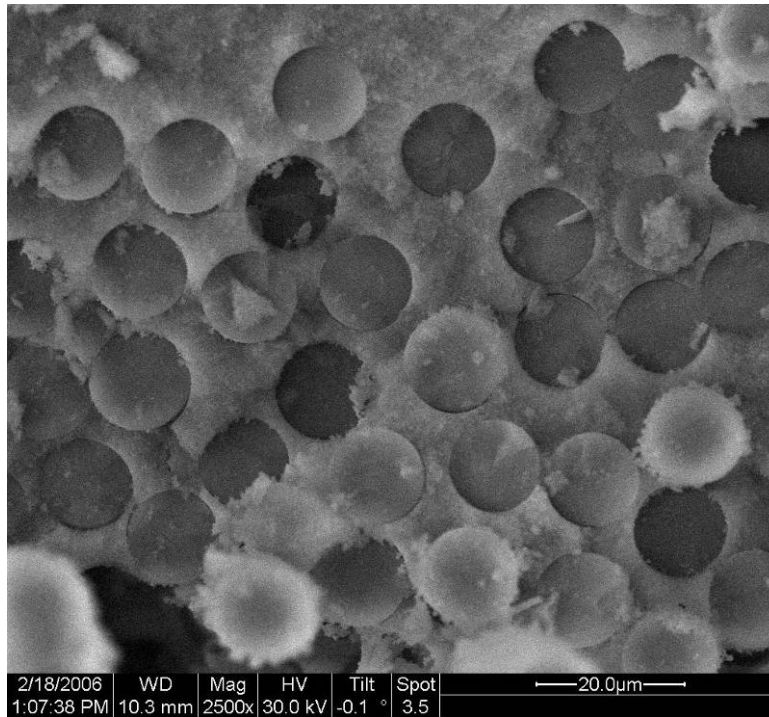
Figure 43. Specimen MS2 (unnotched, tensile, 1200°C), 2500x (center of fracture surface)
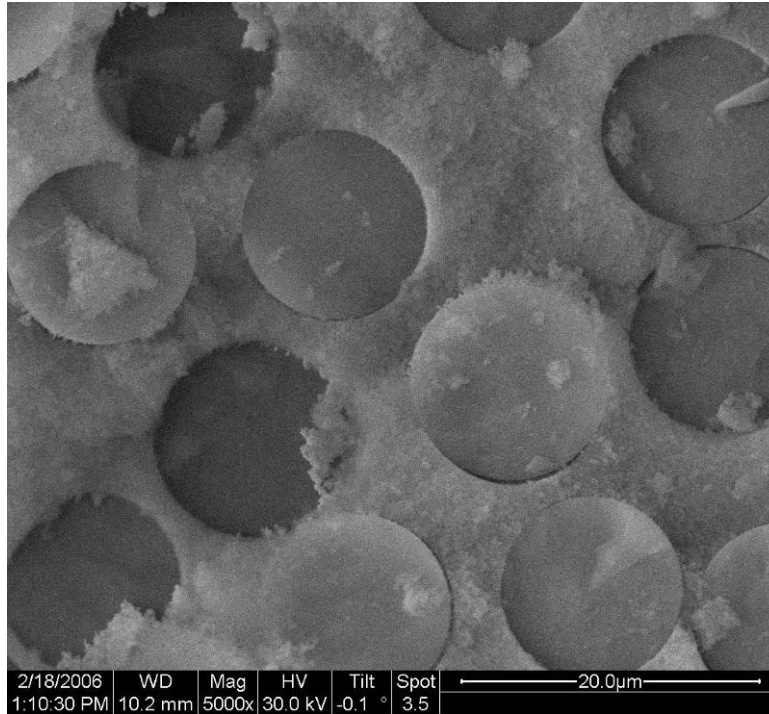
**Figure 44. Specimen MS2 (unnotched, tensile, 1200°C), 5000x
(center of fracture surface)**
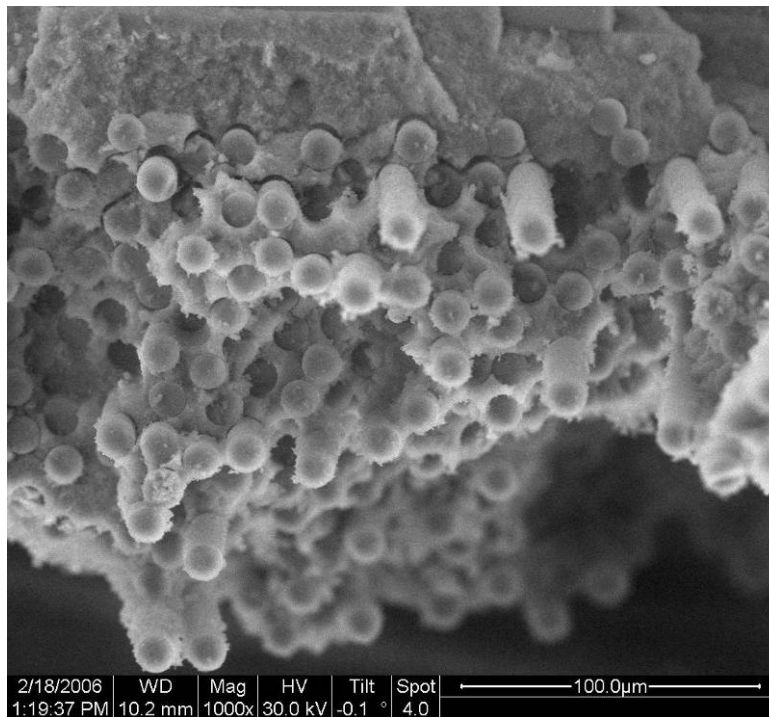
**Figure 45. Specimen MS2 (unnotched, tensile, 1200°C), 1000x
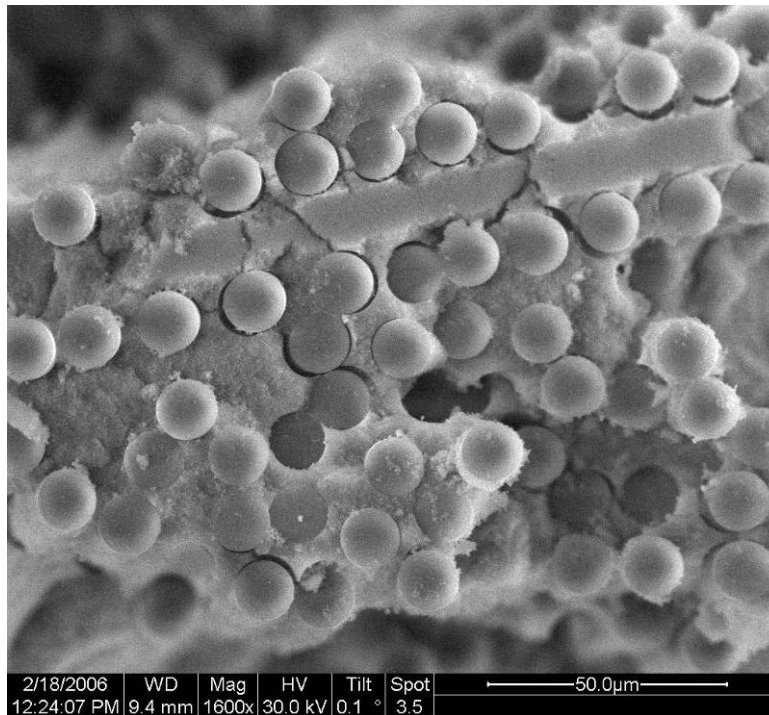(near center of fracture surface)**
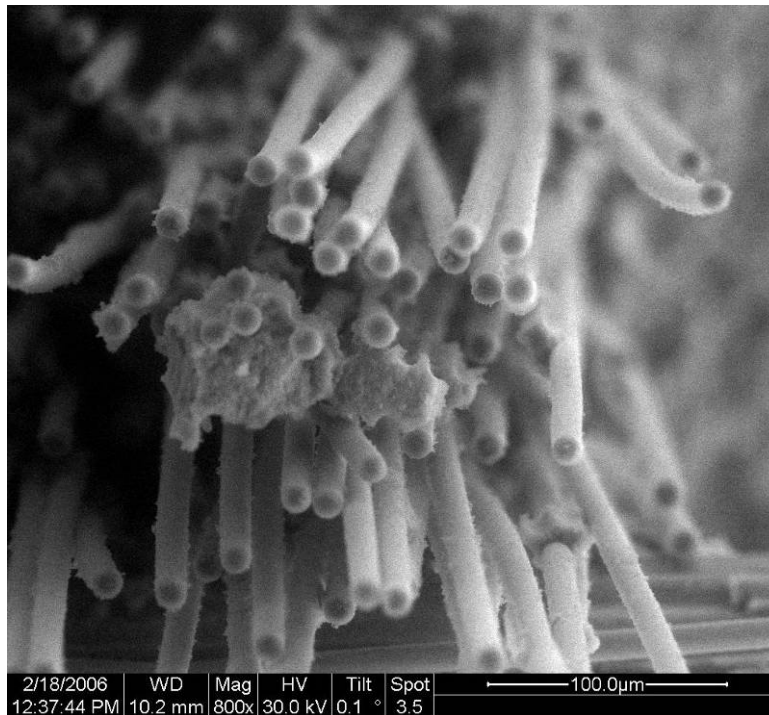
Figure 46. Specimen MH1 (notched, tensile, 1200°C), 800x
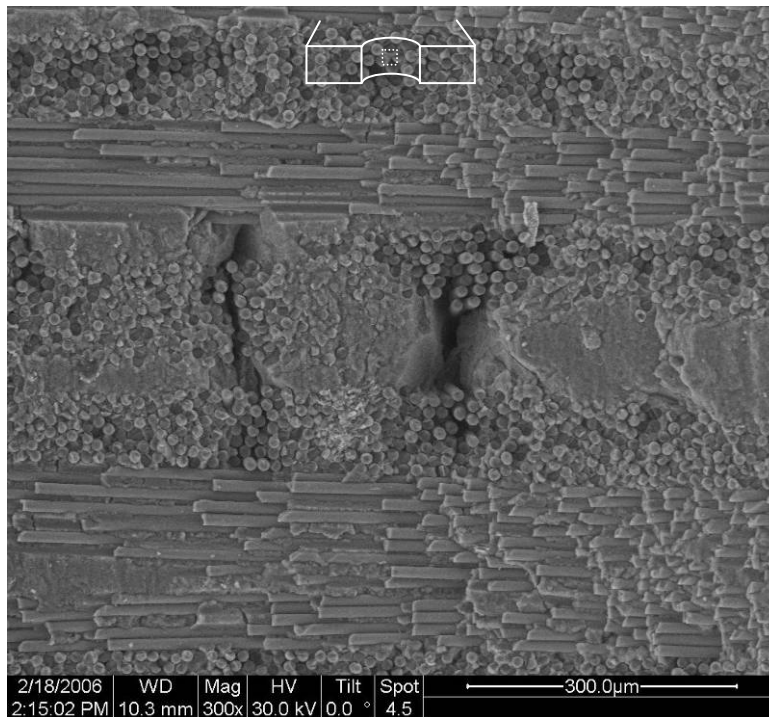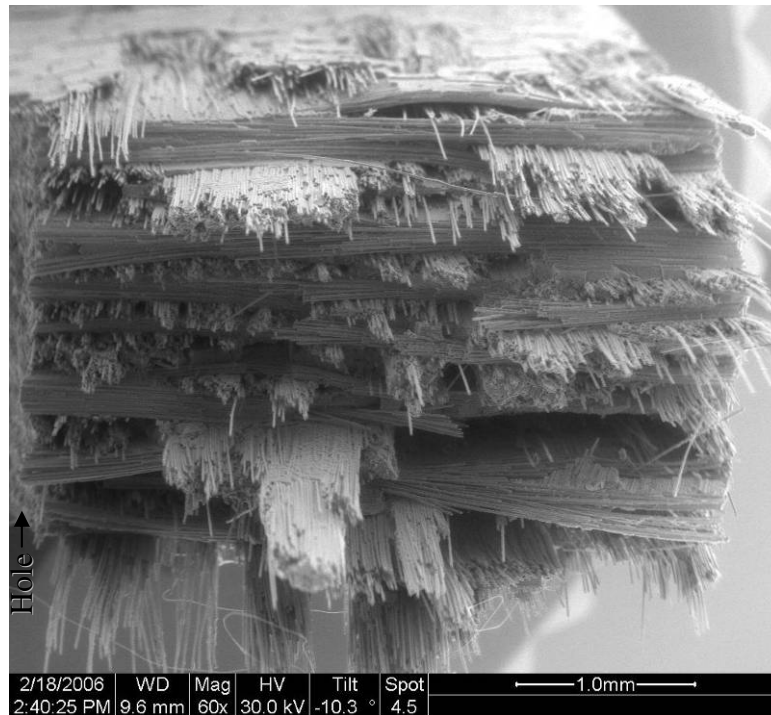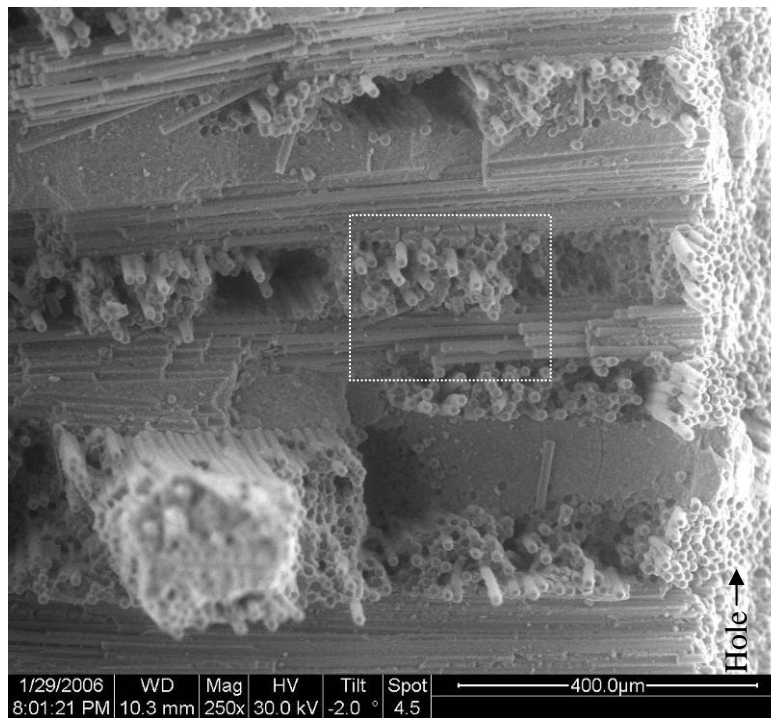**(hole 0.5 mm to right of image)**
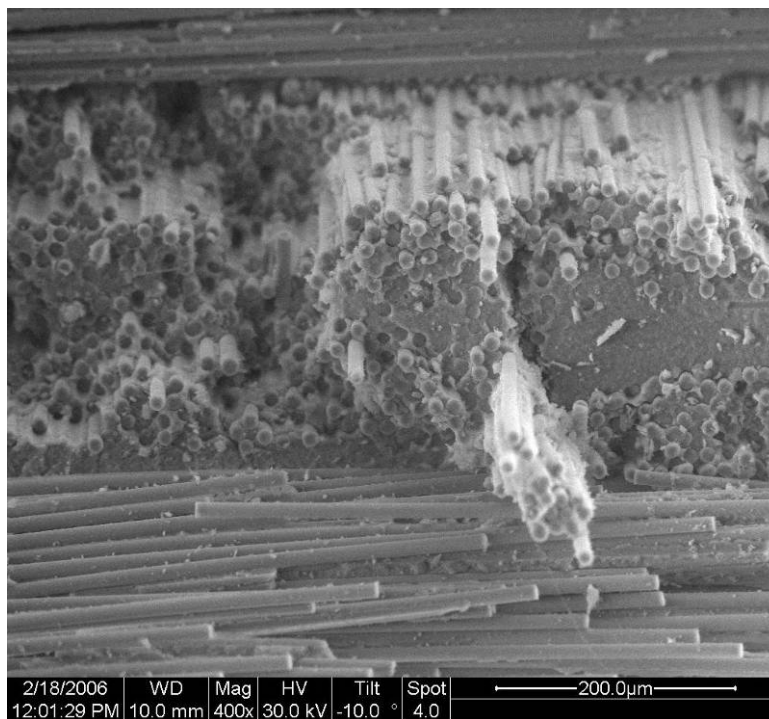
Figure 47. Specimen MH1 (notched, tensile, 1200°C), 400x
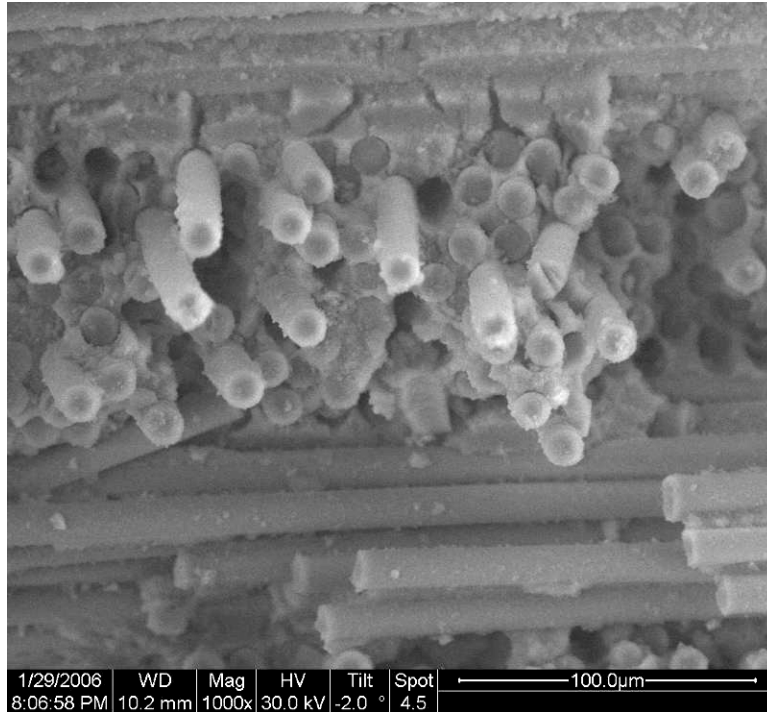**(hole 3.0 mm to left of image)**

Figure 48. Specimen MH1 (notched, tensile, 1200°C), 1600x (hole 0.25 mm to right of image)

Figure 49. Specimen CH1 (notched, 125 MPa creep, 1200°C), 300x, hole surface with visible macroporosity
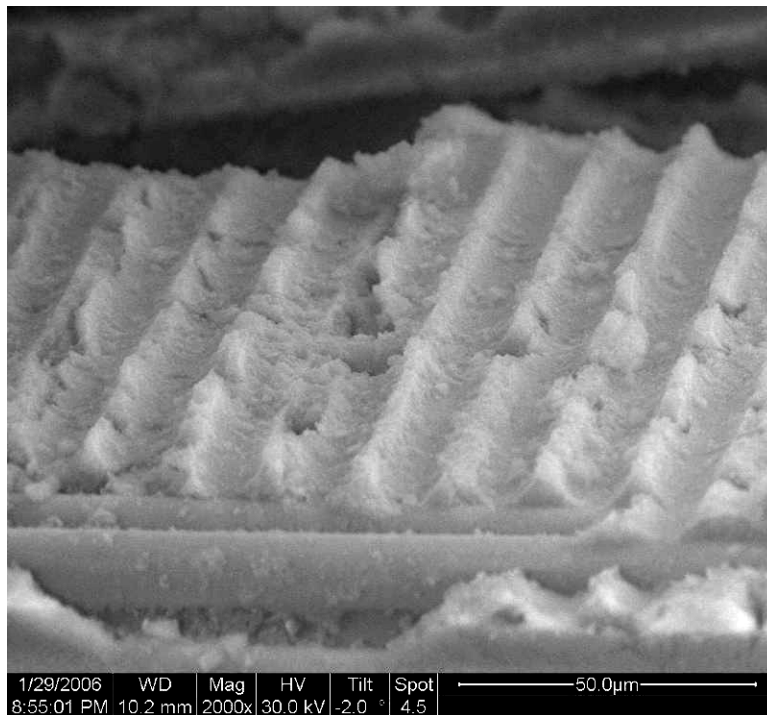
Figure 50. Specimen CH1 (notched, 125 MPa creep, 1200°C), 60x, right side

**Figure 51. Specimen CH1 (notched, 125 MPa creep, 1200°C), 250x
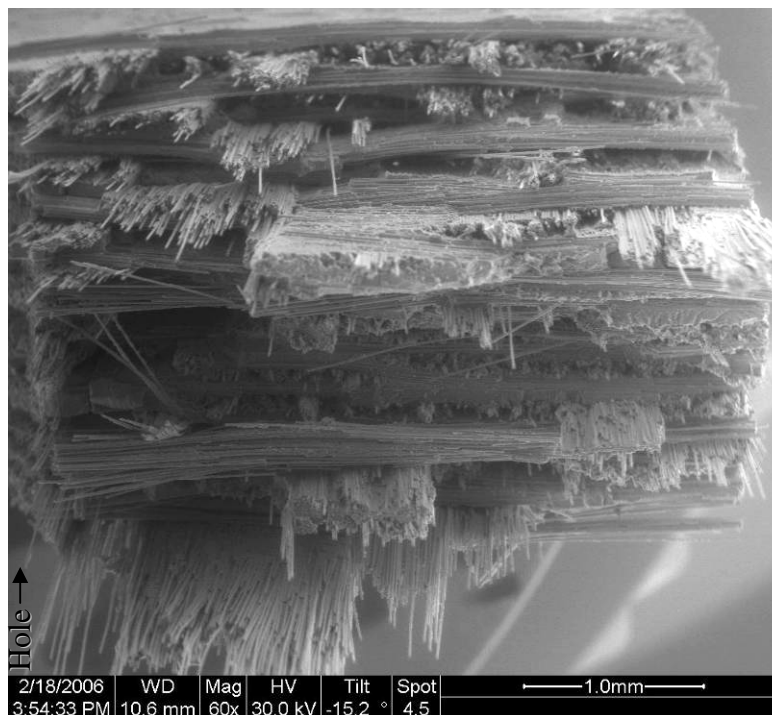(hole at right side of image; boxed region magnified in Figure 52)**

**Figure 52. Specimen CH1 (notched, 125 MPa creep, 1200°C), 1000x
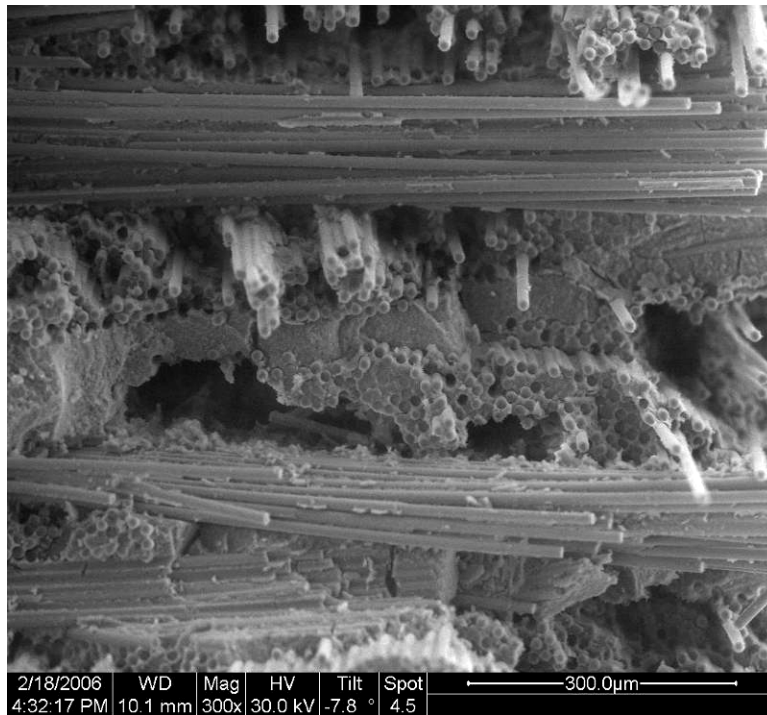(hole 0.4 mm to right of image)**

**Figure 53. Specimen CH1 (notched, 125 MPa creep, 1200°C), 2000x
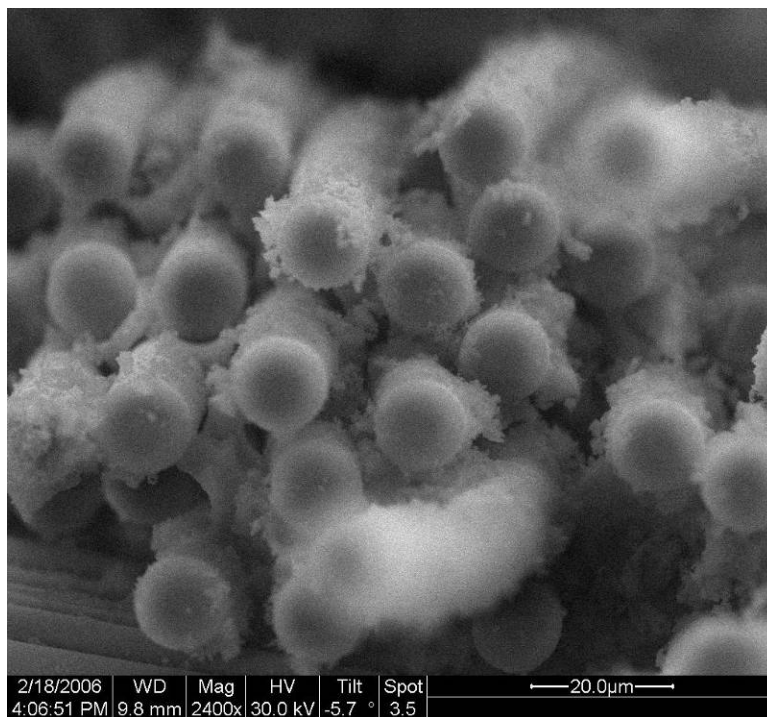(hole 3.5 mm to left of image)**

Figure 54. Specimen CH1 (notched, 125 MPa creep, 1200°C), 250x
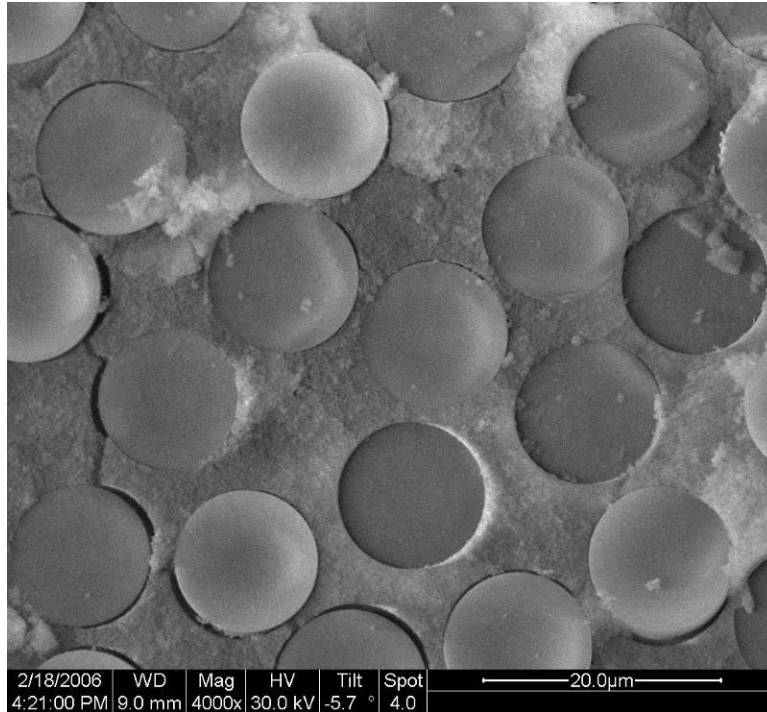**(hole 1.5 mm to left of image)**

Figure 55. Specimen CH2 (notched, 150 MPa creep, 1200°C), 60x
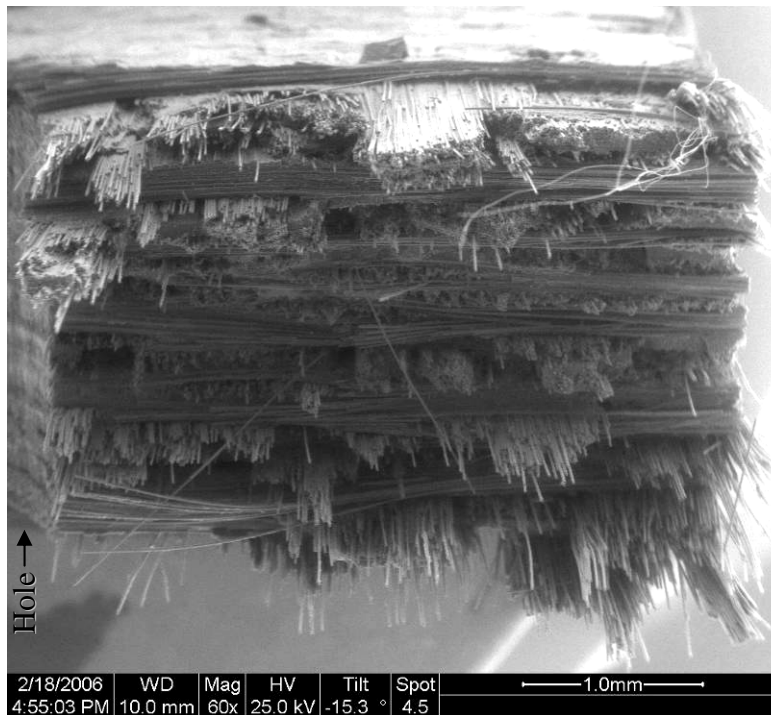**(hole along left edge of image)**

**Figure 56. Specimen CH2 (notched, 150 MPa creep, 1200°C), 300x
(hole 0.5 mm to right of image)**

**Figure 57. Specimen CH2 (notched, 150 MPa creep, 1200°C), 2400x
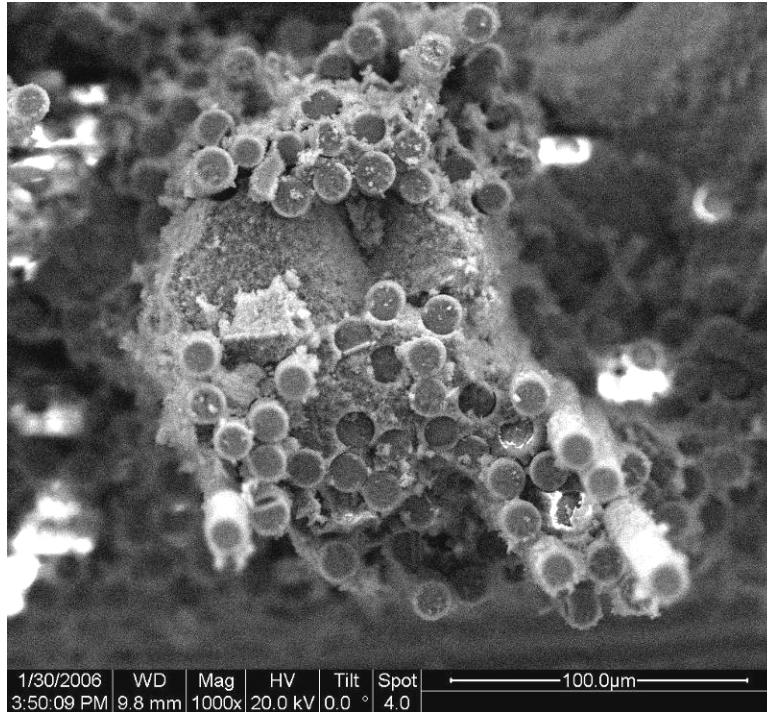(hole 2.5 mm to left of image)**

**Figure 58. Specimen CH2 (notched, 150 MPa creep, 1200°C), 4000x
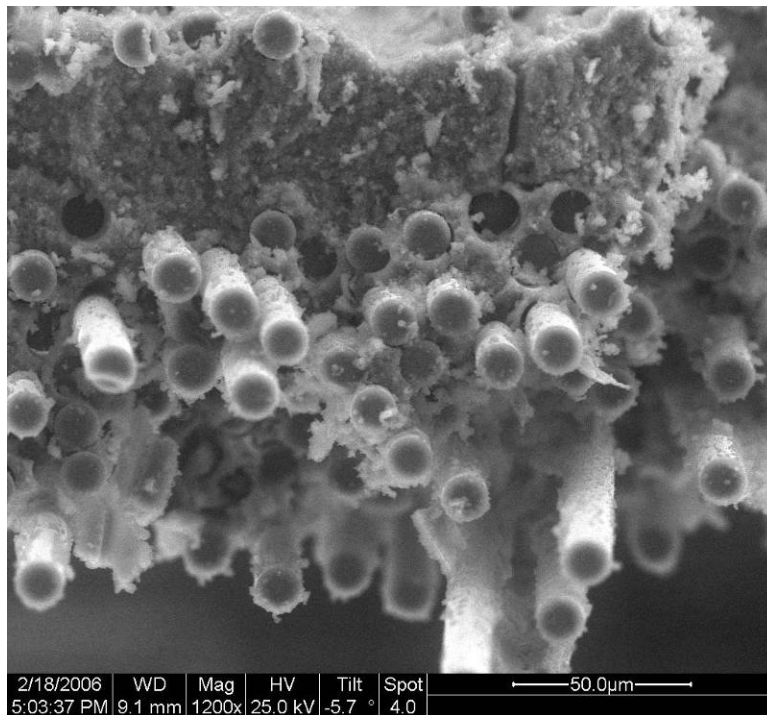(hole 1.5 mm to left of image)**

**Figure 59. Specimen CH5 (notched, 175 MPa creep, 1200°C), 60x
(hole at left edge of image)**

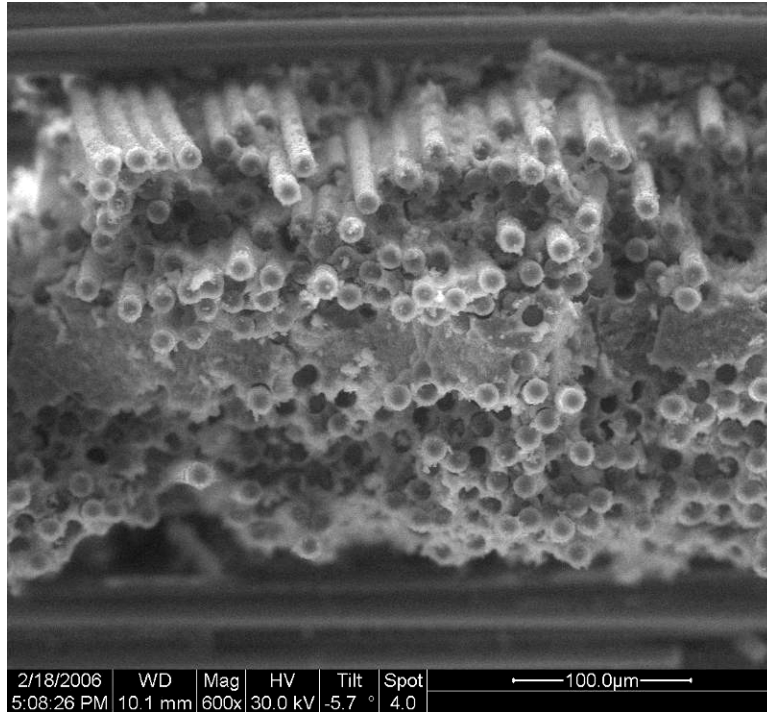**Figure 60. Specimen CH5 (notched, 175 MPa creep, 1200°C), 1000x
(hole 0.75 mm to right of image)**

**Figure 61. Specimen CH5 (notched, 175 MPa creep, 1200°C), 1200x
(hole 0.25 mm to left of image)**

**Figure 62. Specimen CH5 (notched, 175 MPa creep, 1200°C), 600x
(hole 1.0 mm to left of image)**

**Figure 63. Specimen FH4 (notched, 150 MPa fatigue, 1200°C), 60x
(hole along left side of image)**
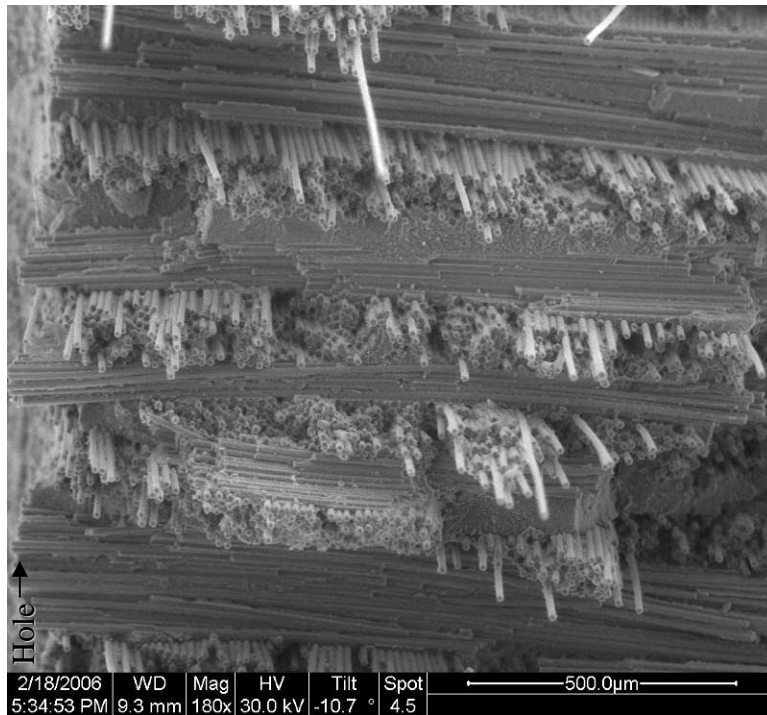
Figure 64. Specimen FH4 (notched, 150 MPa fatigue, 1200°C), 180x (hole along left side of image)
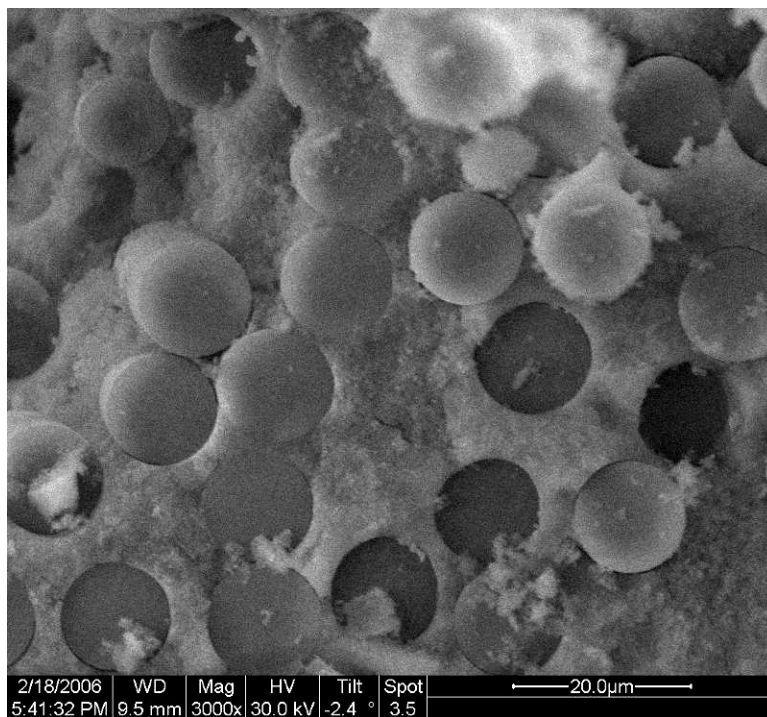
Figure 65. Specimen FH4 (notched, 150 MPa fatigue, 1200°C), 3000x (hole 0.75 mm to left of image)

**Figure 66. Specimen FH4 (notched, 150 MPa fatigue, 1200°C), 150x
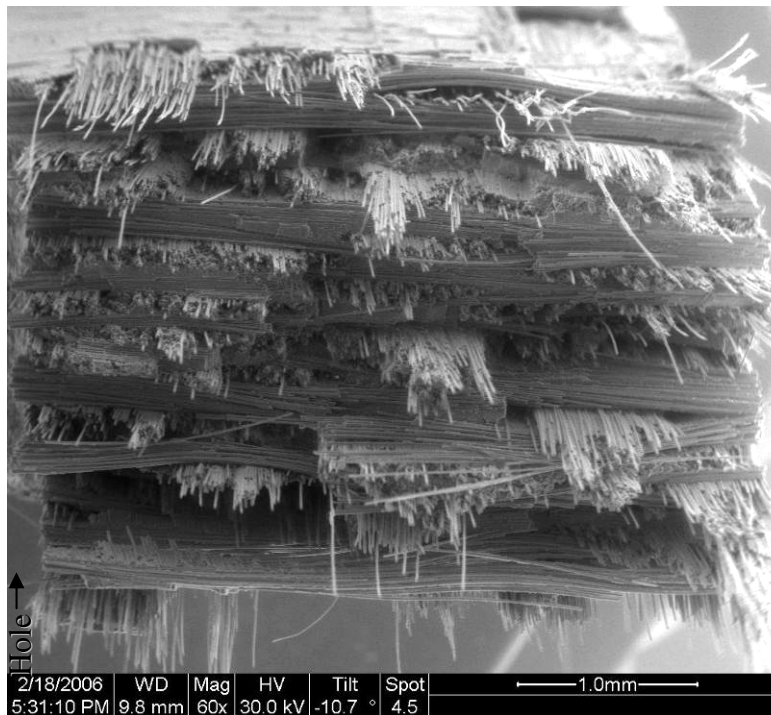(hole along right side of image)**

**Figure 67. Specimen FH4 (notched, 150 MPa fatigue, 1200°C), 1600x
(hole 0.25 mm to right of image)**

**Figure 68. Specimen FH6 (notched, 160 MPa fatigue, 1200°C), 60x
(hole along left side of image)**

**Figure 69. Specimen FH6 (notched, 160 MPa fatigue, 1200°C), 500x
(hole surface composes 25% of right side of image; Box indicates 0° fibers at hole surface;
fiber ends rounded from water jet machining)**

Figure 70. Specimen FH6 (notched, 160 MPa fatigue, 1200°C), 500x
(hole 0.75 mm to right of image; boxed region magnified in Figure 71)

Figure 71. Specimen FH6 (notched, 160 MPa fatigue, 1200°C), 1500x
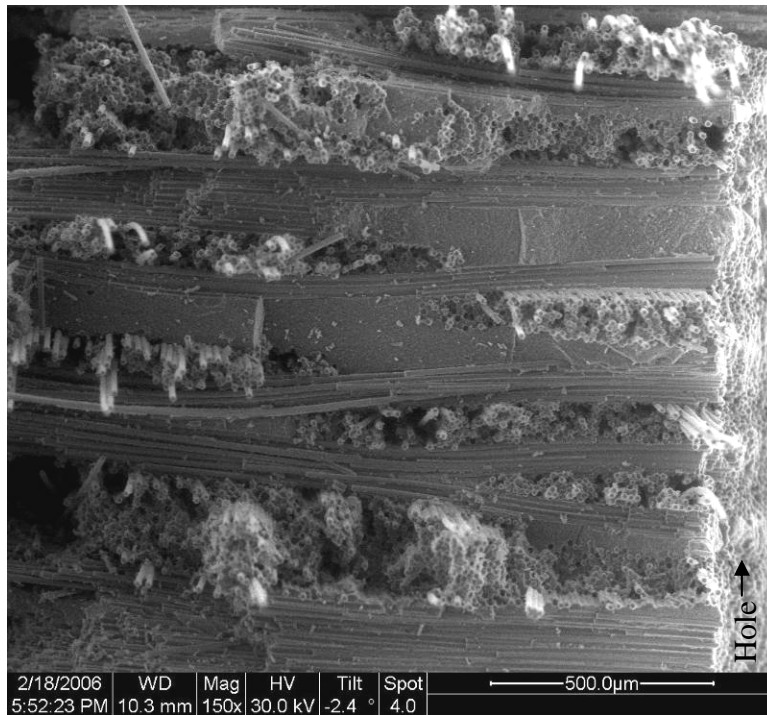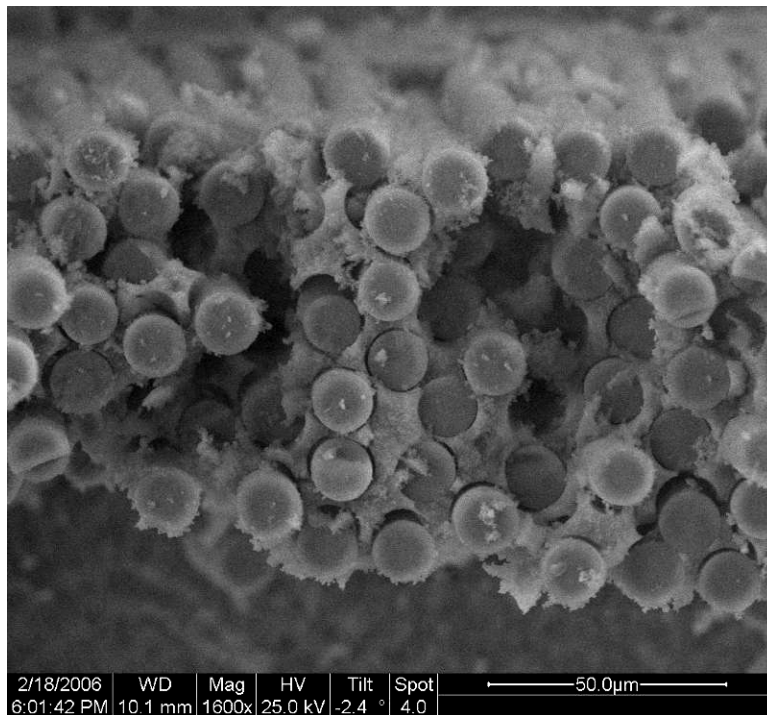**(hole 0.8 mm to right of image)**

**Figure 72. Specimen FH5 (notched, 175 MPa fatigue, 1200°C), 60x
(hole along left edge of image)**
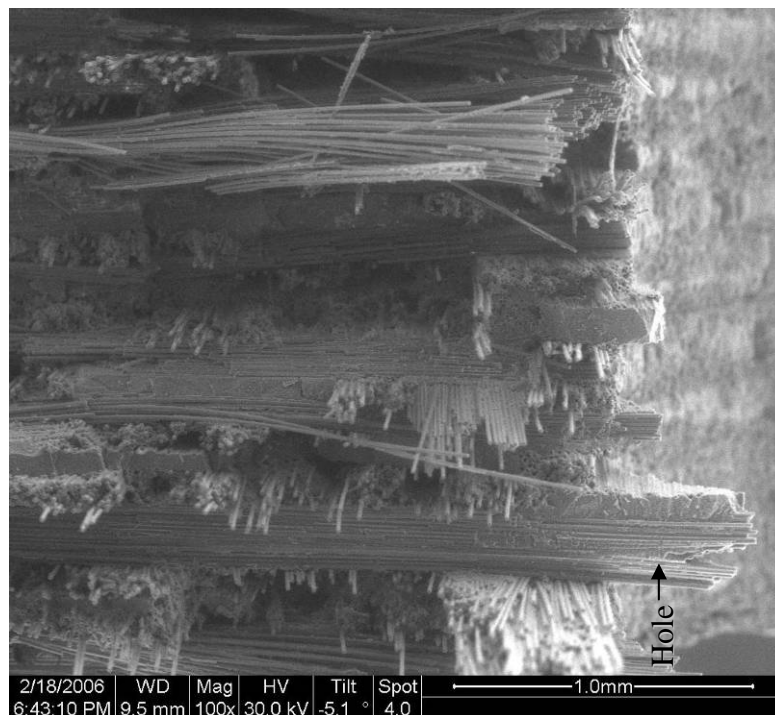
**Figure 73. Specimen FH5 (notched, 175 MPa fatigue, 1200°C), 100x
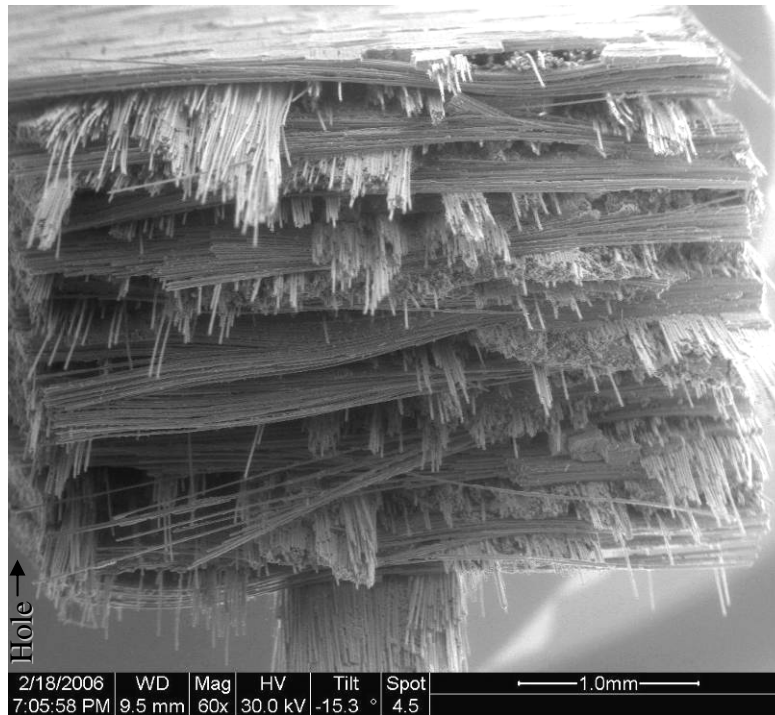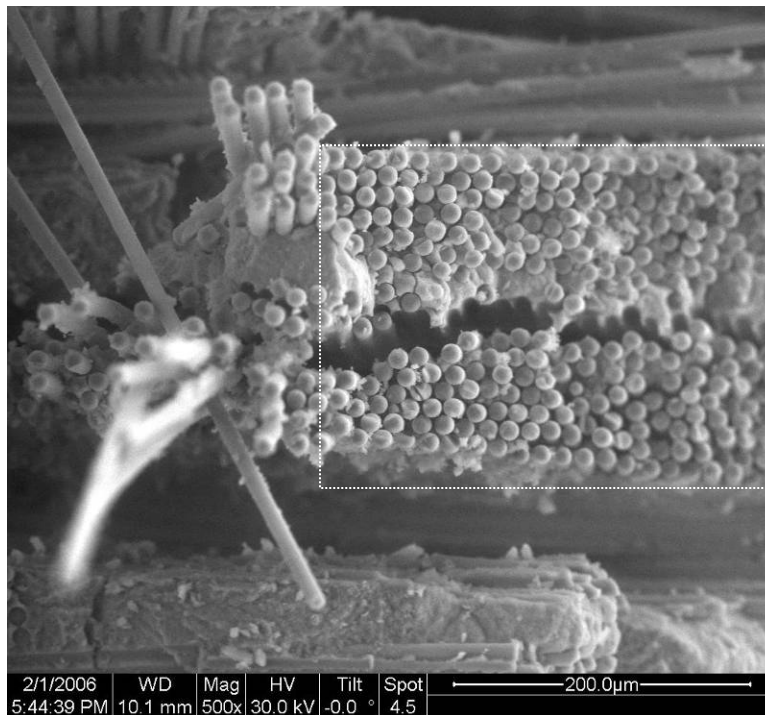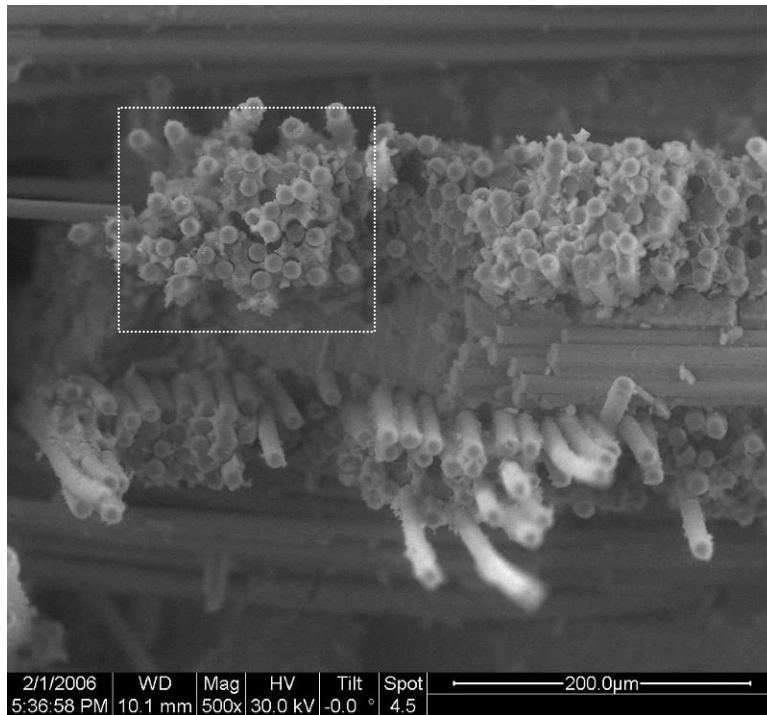(hole along right side of image)**

**Figure 74. Specimen FH5 (notched, 175 MPa fatigue, 1200°C), 600x
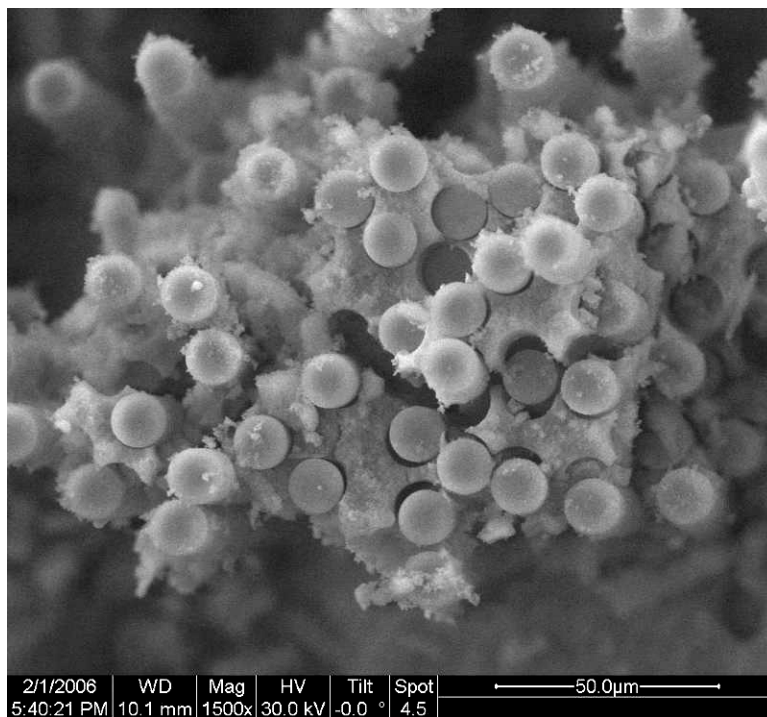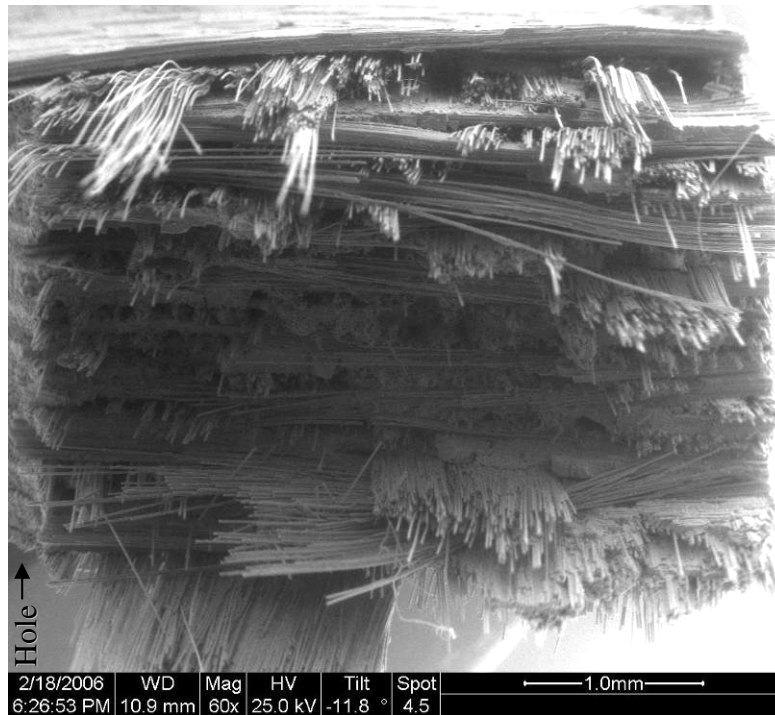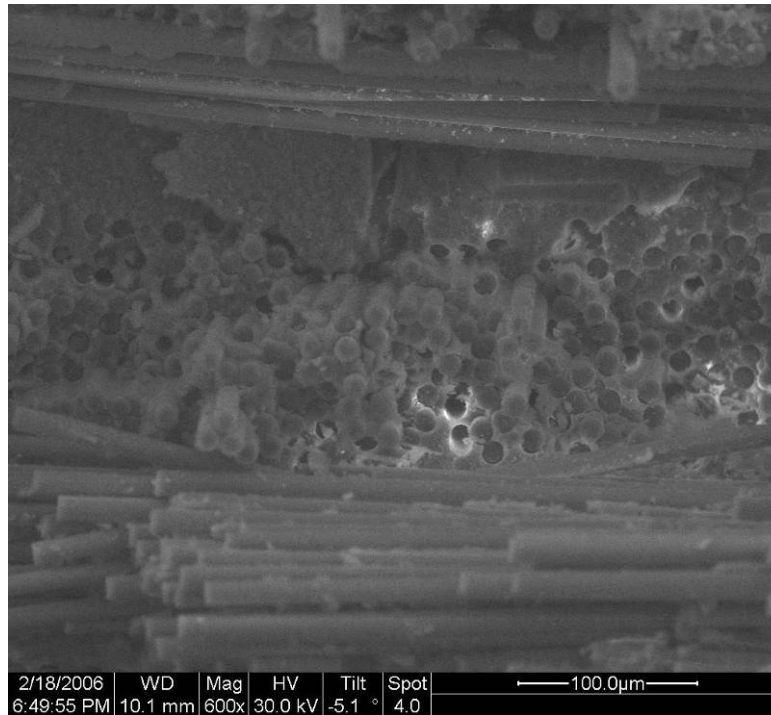(hole 2.0 mm to right of image)**

Bibliography

1. "3M Ceramic Fiber Typical Properties," *Nextel™ Ceramic Textiles Technical Notebook*. Product Brochure. St. Paul MN: 3M Corporation, no date.

2. Antti, M-L. and Edgar Lara-Curzio. "Effect of Notches, Specimen Size, and Fiber Orientation on the Monotonic Tensile Behavior of Composites at Ambient and Elevated Temperatures," *Ceramic Engineering and Science Proceedings*, 22[3], 643-650 (2001).

3. Antti, M.-L., E. Lara Curzio and R. Warren. "Thermal degradation of an oxide fibre (Nextel 720)/aluminosilicate composite," *Journal of the European Ceramic Society*, 24: 565-578 (2004).

4. Barnard, P., M. B. Henderson and N. Rhodes. "CMC Integration and Demonstration for Gas Turbine Engines," *Applied Thermal Engineering*, 24[11-12]: 1755-1764 (2004).

5. Buchanan, Dennis J., Reji John and Larry P. Zawada. "Creep-Rupture Behavior of ±45° Oxide/Oxide Nextel 720/AS Composite," *Ceramic Engineering and Science Proceedings*, 24[4], 451-458 (2003).

6. -----. "Notched Fracture Behavior of Oxide/Oxide Nextel™720/AS Composite," *Ceramic Engineering and Science Proceedings*, 21[3], 581-588 (2000).

7. Buchanan, Dennis J., Victoria A. Kramb, Reji John and Larry P. Zawada. "Effect of Small Effusion Holes on Creep Rupture Behavior of Oxide/Oxide Nextel™720/AS Composite," *Ceramic Engineering and Science Proceedings*, 22[3], 659-666 (2001).

8. Cantor, B., F. P. E. Dunne, I.C. Stone, eds. *Metals and Ceramic Matrix Composites*. Philadelphia: Institute of Physics Publishing, 2004.

9. Carlsson, Leif A. and others. *Experimental Characterization of Advanced Composite Materials* (Second Edition). Lancaster: Technomic, 1997.

10. Chawla, K. K. *Ceramic Matrix Composites*. New York: Chapman & Hall, 1993.

11. Composite Optics Inc. Ceramics. "Oxide-Oxide Overview." Unpublished article. n. pag. http://www.coiceramics.com/cmcdevelopment.htm. 10 May 2005.

12.   Daniel, Isaac M. and Ori Ishai. *Engineering Mechanics of Composite Materials* (Second Edition). New York: Oxford UP, 2006.

13.   Dowling, Norman E. *Mechanical Behavior of Materials: Engineering Methods for Deformation, Fracture, and Fatigue* (Second Edition). New Jersey: Prentice Hall, 1999.

14.   Eber, Chalene A. *Effect of Temperature and Steam Environment on Fatigue Behavior of an Oxide-Oxide Continuous Fiber Ceramic.* MS thesis, AFIT/GA/ENY/05-M09. School of Engineering and Management, Air Force Institute of Technology (AU), Wright-Patterson AFB OH, March 2005.

15.   Generazio, Edward R., ed. *Advanced Ceramic Matrix Composites*. Lancaster PA: Technomic, 1996.

16.   Groner, Daniel J. *Characterization of Fatigue Behavior of 2-D Woven Fabric Reinforced Ceramic Matrix Composite at Elevated Temperature.* MS thesis, AFIT/GAE/ENY/94D-15. School of Engineering, Air Force Institute of Technology (AU), Wright-Patterson AFB OH, December 1994.

17.   Harlan, Lee B. *Creep-Rupture Behavior of an Oxide/Oxide Ceramic Matrix Composite at Elevated Temperatures in Air and Steam Environments.* MS thesis, AFIT/GA/ENY/05-M05. School of Engineering and Management, Air Force Institute of Technology (AU), Wright-Patterson AFB OH, March 2005.

18.   Headrick, William L., Robert E. Moore, Musa Karakus and Xiaoting Liang. "Characterization and Structural Modeling of Magnesiaalumina Spinel Glass Tank Refractories," Excerpt from unpublished article. n. pag. http://www.eere.energy.gov/industry/glass/pdfs/spinel.pdf. U of Missouri-Rolla, (October 2003).

19.   Heredia, Fernando E., et al. "Notch Effects in Carbon Matrix Composites," *Journal of the American Ceramic Society*, 77[11], 2817-2827 (1994).

20.   Mackin, Thomas J., et al. "Notch Sensitivity and Stress Redistribution in Three Ceramic-Matrix Composites," *Journal of the American Ceramic Society*, 78[7], 1719-1728 (1995).

21.   "Integrated High Performance Turbine Engine Technology: A Century of Power for Flight," Excerpt from 2002 brochure, n. pag. http://www.pr.afrl.af.mil/divisions/prt/ihptet/ihptet_brochure.pdf. (Feb 2005).

22. John, Reji, Dennis J. Buchanan, Victoria A. Kramb and Larry P. Zawada. "Creep-Rupture Behavior of Oxide/Oxide Nextel™720/AS and MI SiC/SiC Composites with Effusion Holes," *Ceramic Engineering and Science Proceedings*, 23[3], 617-628 (2002).

23. Kramb, Victoria A., Reji John, David A. Stubbs. "A study of the damage progression from notches in an oxide/oxide ceramic-matrix composite using ultrasonic C-scans," *Composites Science and Technology*, 61[11], 1561-1570 (2001).

24. Kramb, Victoria A., Reji John and Larry P. Zawada. "Notched Fracture Behavior of an Oxide/Oxide Ceramic-Matrix Composite," *Journal of the American Ceramic Society*, 82[11], 3087-96 (1999).

25. Lewinsohn, C. A., C. H. Henager Jr. and R. H. Jones. "Fibers to Bridged Cracks," *Journal of the American Ceramic Society*, 21[3], 415-422 (2000).

26. Mattingly, Jack D., William H. Heiser and David T. Pratt. *Aircraft Engine Design* (Second Edition). Reston VA: American Institute of Aeronautics and Astronautics, 2002.

27. Musil, Sean S. *Creep Behavior of an Oxide/Oxide Composite with Monazite Coating at Elevated Temperatures.* MS thesis, AFIT/GAE/ENY/05-M14. School of Engineering and Management, Air Force Institute of Technology (AU), Wright-Patterson AFB OH, March 2005.

28. Oates, Gordon C. *Aerothermodynamics of Gas Turbine and Rocket Propulsion* (Third Edition). Reston VA: American Institute of Aeronautics and Astronautics, 1997.

29. Robinson, Craig R. "Testing and Characterization of CMC Combustor Liners," *Ceramic Engineering and Science Proceedings*, 24[4], 275-280 (2003).

30. Shigley, Joseph E. and Charles R. Mischke. *Mechanical Engineering Design* (Fifth Edition). New York: McGraw-Hill, 1989.

31. Steel, Steven G. *Monotonic and Fatigue Loading Behavior of an Oxide/Oxide Ceramic Matrix Composite*. MS thesis, AFIT/GMS/ENY/00M-02. School of Engineering and Management, Air Force Institute of Technology (AU), Wright-Patterson AFB OH, March 2000.

32. Stephen, Ralph, et al. *Metal Fatigue in Engineering* (Second Edition). New York: Wiley & Sons, 2001.

33.   Trefilov, V.I., ed. *Ceramic- and Carbon-Matrix Composites*. New York: Chapman & Hall, 1995.

34.   Veitch, Lisa C. and William S. Hong. "Will Pigs Fly Before Ceramics Do?" *Ceramic Engineering and Science Proceedings*, 22[3], 31-42 (2001).

35.   Wilson, D. M., S. L. Lieder and D. C. Lueneburg. "Microstructure and High Temperature Properties of Nextel 720 Fibers," *Ceramic Engineering and Science Proceedings*, 16[5], 1005-1014 (1995).

Vita

  Captain Mark A. Sullivan graduated from Lewis and Clark High School in

Spokane, Washington, in 1996. He entered undergraduate studies at the University of

Idaho in Moscow, Idaho where he graduated with a Bachelor of Science degree in

Mechanical Engineering in May 2001. Following graduation he was commissioned a

Second Lieutenant through Air Force ROTC Detachment 905.

  His first assignment was to the Aeronautical Systems Center at Wright-Patterson

AFB, Ohio where he served as a Mechanical Subsystems Engineer. In August 2004, he

entered the Graduate School of Engineering and Management at the Air Force Institute of

Technology. Upon graduation, he will be assigned to the Air Force Research Laboratory

at Kirtland AFB, New Mexico.

			Form Approved OMB No. 074-0188

REPORT DOCUMENTATION PAGE

Form Approved
OMB No. 074-0188

The public reporting burden for this collection of information is estimated to average 1 hour per response, including the time for reviewing instructions, searching existing data sources, gathering and maintaining the data needed, and completing and reviewing the collection of information. Send comments regarding this burden estimate or any other aspect of the collection of information, including suggestions for reducing this burden to Department of Defense, Washington Headquarters Services, Directorate for Information Operations and Reports (0704-0188), 1215 Jefferson Davis Highway, Suite 1204, Arlington, VA 22202-4302. Respondents should be aware that notwithstanding any other provision of law, no person shall be subject to an penalty for failing to comply with a collection of information if it does not display a currently valid OMB control number.
PLEASE DO NOT RETURN YOUR FORM TO THE ABOVE ADDRESS.

1. REPORT DATE *(DD-MM-YYYY)* 23-03-2006	**2. REPORT TYPE** Master's Thesis	**3. DATES COVERED** *(From – To)* March 2005 – March 2006

4. TITLE AND SUBTITLE Creep-Rupture and Fatigue Behaviors of Notched Oxide/Oxide Ceramic Matrix Composite at Elevated Temperature	**5a. CONTRACT NUMBER**
	5b. GRANT NUMBER
	5c. PROGRAM ELEMENT NUMBER

6. AUTHOR(S) Sullivan, Mark, A., Captain, USAF	**5d. PROJECT NUMBER**
	5e. TASK NUMBER
	5f. WORK UNIT NUMBER

7. PERFORMING ORGANIZATION NAMES(S) AND ADDRESS(S) Air Force Institute of Technology Graduate School of Engineering and Management (AFIT/EN) 2950 Hobson Way WPAFB OH 45433-7765	**8. PERFORMING ORGANIZATION REPORT NUMBER** AFIT/GAE/ENY/06-M30

9. SPONSORING/MONITORING AGENCY NAME(S) AND ADDRESS(ES) AFRL/MLLN Attn: Mr. Larry Zawada 2230 10th Street WPAFB OH 45433-7817 DSN: 785-1352	**10. SPONSOR/MONITOR'S ACRONYM(S)**
	11. SPONSOR/MONITOR'S REPORT NUMBER(S)

12. DISTRIBUTION/AVAILABILITY STATEMENT
      APPROVED FOR PUBLIC RELEASE; DISTRIBUTION UNLIMITED.

13. SUPPLEMENTARY NOTES

14. ABSTRACT

  Oxide/oxide composites are being considered for use in high temperature aerospace applications where their inherent resistance to oxidation provides for better long life properties at high temperature than most other ceramic matrix composites (CMCs). One promising oxide/oxide CMC is Nextel™720/A (N720/A) which uses an 8-harness satin weave (8HSW) of Nextel™720 fibers embedded in a porous alumina matrix. Possible aerospace applications for N720/A will likely require inserting holes into the material for mounting and cooling purposes. The notch characteristics must be understood to ensure designs using the material are sufficient for the desired application. This research effort examined the fatigue and creep-rupture characteristics of N720/A with a 0°/90° fiber orientation and notch to width ratio (2a/w) of 0.33. Specifically, 12.0 mm wide rectangular specimens with a 4.0 mm center hole were subjected to axial fatigue and creep-rupture loads in 1200°C laboratory air. Monotonic tensile tests at 1200°C were performed on unnotched specimens to provide a baseline for comparison with previous research. Fracture surfaces were examined under microscope to observe microstructure and damage mechanisms. Comparisons to previous unnotched research results at 1200°C show N720/A to be primarily insensitive to 0.33 notch ratios.

15. SUBJECT TERMS
   Ceramic Matrix Composites, Notch Sensitivity, Creep, Fatigue, Temperature, Nextel 720

16. SECURITY CLASSIFICATION OF:			**17. LIMITATION OF ABSTRACT**	**18. NUMBER OF PAGES**	**19a. NAME OF RESPONSIBLE PERSON** Dr. Shankar Mall, AFIT/ENY
REPORT U	**ABSTRACT** U	**c. THIS PAGE** U	UU	104	**19b. TELEPHONE NUMBER** *(Include area code)* (937) 255-3636, ext 4587; e-mail: shankar.mall@afit.edu

Standard Form 298 (Rev: 8-98)
Prescribed by ANSI Std. Z39-18